



**Cape Peninsula
University of Technology**

**INFLUENCE OF GEOMETRY AND MATERIAL PROPERTIES
ON THE OPTIMUM PERFORMANCE OF THE C-SHAPE
PIEZO-COMPOSITE ACTUATOR.**

By

ALEXANDER NIKWANDUKA MTAWA

Thesis submitted in fulfilment of the requirements for the

DTech: Mechanical Engineering.

in the Faculty of Engineering

at the

CAPE PENINSULA UNIVERSITY OF TECHNOLOGY

(Bellville)

Supervisor: Prof. Bohua Sun

External supervisor: Prof. Jasson Gryzagoridis

Cape Town

February 2008

DECLARATION

I, Alexander Nikwanduka Mtawa, I declare that the contents of this thesis represent my own unaided work, and that the thesis has not previously been submitted for academic examination towards any qualification. Furthermore, it represents my own opinions and not necessarily those of the Cape Peninsula University of Technology.



Signed

23/07/2007

Date

ABSTRACT

In recent years, due to rapid advances in technology there has been an increasingly high demand for large displacement and large force, precise positioning, fast response, low power consuming miniature piezoelectric actuators.

In certain smart structure applications, the use of curved piezoelectric actuators is necessary. The present work extends the earlier investigations on the C- shape actuator by providing a detailed investigation on the influence of geometric and material properties of the individual layers of the C-shape piezocomposite for its optimal performance as an actuator.

Analytical models have been used to optimize the geometry of the actuator. Experimental and finite element analyses (using general purpose finite element software i.e. CoventorWare and MSC. Marc) have been used for validation.

The present work has established that, by maintaining the thickness of the substrate and piezoceramic layers constant; changing the external radius, for example increasing it, the stiffness of the structure decreases and thus yielding large displacement. This has a negative effect on the force produced by the actuator.

With fixed thickness of the substrate and varying the thickness of the piezoceramic (for fixed external radius) the result is as follows: Increasing the thickness of the piezoceramic layer has the effect of decreasing the displacement while the force increases.

With fixed PZT thickness as well as the external radius, varying the substrate thickness has the following effect: As the thickness of the substrate increases the displacement increases reaching a maximum. Subsequent increase in the thickness of the substrate the displacement is reduced. The force continues increasing at least for the ratios up to 1.0, further increase of the substrate, subsequent decrease of force is also noted. In addition to changing the thickness of the substrate, the choice of different material for the substrate has the following effect: For substrate/PZT ratios of up to 0.6, an actuator with substrate material having higher elastic modulus will produce larger displacement while for ratios beyond this ratio the situation is reversed. The causes for this kind of behaviour have been addressed.

In all cases both force and displacement are found to be directly proportional to applied voltage.

The individual C- shape actuators may be combined in series and parallel to yield accordingly large displacement or force. To demonstrate this, a micro-motor/actuator comprising C-shape piezoelectric actuators (with optimized geometry) combined in series and in parallel has been designed and analyzed.

A Finite Element model that was developed based on the Bernoulli beam theory, to investigate the dynamic behaviour of an individual C-shape piezoelectric actuator yielded results regarding the natural frequency and the corresponding normal modes which agree well with the model developed using the general purpose finite element software MSC. Marc.

The results also show that an increase of both substrate/PZT thickness ratio and the elastic modulus of the substrate contribute to raise the fundamental frequency of the C-shape actuator. The results were compared to those computed using published equations and there is good agreement between them.

It is hoped that some of this work will be a useful tool to designers in selecting the appropriate sizes, and materials of the actuator constituents, depending whether the desired goal is large displacement or large force and/or high bandwidth.

ACKNOWLEDGEMENTS

First and foremost, I would like to thank His Almighty God for blessing me and for providing me with strength during the period of my studies.

I am truly grateful to my supervisor Professor Bohua Sun for accepting me to join his research team and for introducing me to the field of smart materials and structures. I am indebted to him for his advice and assistance during the course and many enlightening discussions especially during the formulation of the problem.

I would like to express my most profound gratitude and sincere appreciation to my external supervisor, Professor Jasson Gryzagoridis for his constructive criticism, guidance, encouragement, and support which he has tirelessly provided throughout the preparation of this work.

I wish to extend my special thanks to Mechanical Engineering staff particularly Mr. T.Z. Ngewana (HOD), Jacob Keith (previous HOD and current Associate Dean – Engineering faculty) and Professor G. Oliver (Postgraduate Programme Coordinator) for making it possible for me to study in the department, Elvina Moosa (the secretary to the HOD) for all assistance rendered. Nicole Titus, thank you for language-editing and proof reading my work. I would also like to thank Dr. F. Utou, N. Mbonde and Liezel Van Zyl for their time to time encouragement and advice.

I also wish to thank W. Mwita for the discussions we had on Finite Elements Analysis and Mechanics.

Much appreciation and love is extended to all of my family and friends for their encouragement and love throughout this journey.

Most importantly, I would like to express my gratitude to my wife, Joyce and my children, Angela, Amos and my new born baby Amani for their love, sacrifice, encouragement and for believing.

Thank you. I love you all.

The financial assistance of the National Research Foundation (NRF) of the Republic of South Africa and The Cape Peninsula University of Technology (CPUT) towards this research is gratefully acknowledged. Opinions expressed in this thesis and the conclusions arrived at, are those of the author, and are not necessarily to be attributed neither to the NRF nor to the CPUT.

Finally, I would like to extend my gratitude and thanks to The Mbeya Institute of Science and Technology (MIST)- Tanzania especially for giving me the opportunity to pursue my studies and for supporting me both morally and materially.

DEDICATION

For My family

My wife: Joyce

My children: Angela, Amos and Amani

For their love, encouragement, understanding and believing.

TABLE OF CONTENTS

DECLARATION.....	II
ABSTRACT.....	III
ACKNOWLEDGEMENTS.....	V
DEDICATION	VI
TABLE OF CONTENTS	VII
LIST OF TABLES.....	X
LIST OF FIGURES.....	X
LIST OF APPENDICES.....	XV
GLOSSARY	XVI
CHAPTER ONE.....	1
INTRODUCTION	1
1.1 Background.....	1
1.2 Overview of Smart Materials and Structures	1
1.3 Application of Smart Structures.....	3
1.4 Problem Statement	3
1.5 Why C- Actuator?.....	4
1.6 Significance of the Research.....	4
1.7 Research Objectives:	4
1.8 Research Methodology	5
1.9 Scope of the Thesis	5
CHAPTER TWO.....	6
LITERATURE REVIEW AND THEORETICAL FRAMEWORK.....	6
2.1 Piezoelectric Phenomena.....	6
2.2 Constitutive Relation	7
2.3 Polarization of Piezoelectric Materials	8
2.4 Piezoelectric Coefficients and Directions	10
2.5 Piezoelectric Actuators.....	12
2.6 Actuator Materials	13
2.7 Development Trend of Piezoelectric Actuators	14
2.8 C-Shape Piezoelectric Actuator	21
CHAPTER THREE.....	23
INFLUENCE OF THE EXTERNAL RADIUS, THICKNESS AND WIDTH OF THE PIEZOCERAMIC LAYER ON THE DISPLACEMENT AND FORCE	23
3.1 Introduction	23
3.2 Individual C- Shape Actuator.....	23
3.3 Displacement and Force Equations:.....	25
3.4 Optimization of the Geometry of the Piezoceramic Layer.	27
3.4.1 Case Study 1: Influence of Maximum External Radius.....	28

3.4.2 Case Study 2: Influence of Piezoceramic Layer Thickness	30
3.4.3 Case Study 3: Influence of Width.....	32
3.5 Numerical Validation Using Coventorware FE Software.....	34
3.5.1 Description of CoventorWare FEA Software.....	34
3.5.2 Finite Element Characterization for Piezoelectric Materials.....	35
3.5.3 Numerical Analysis Results	36
3.6 Discussion of results.....	36
CHAPTER FOUR	38
INFLUENCE OF SUBSTRATE THICKNESS AND MATERIAL PROPERTIES ON THE DISPLACEMENT AND FORCE OF A C – SHAPE ACTUATOR.....	38
4.1 Introduction	38
4.2 Optimization of the Substrate Geometry and Material.....	38
4.2.1 Case Study 4: Influence of Substrate/PZT Thickness Ratio	38
4.2.2 Case Study 5: The Effect of Elastic Properties of the Substrate Material	40
4.2.3: The Coefficient of Unimorph Actuator	42
4.2.4 Determining the Appropriate Location of the Neutral Axis	45
4.2.5 Dependence of the Radius of Neutral Axis on the Substrate Material's Elastic Properties.....	49
4.2.6 Effect of Substrate Material on the Piezoelectric Moment.....	51
4.2.7 Effect of Elastic Modulus of a Substrate Material on the Blocked Force.....	53
4.3 Discussion of results	54
4.4 Finite Element Validation Using MSC Marc.	57
4.4.1 Strain.....	57
4.4.2 Electric Field.....	57
4.4.3 Creating the Finite Element Model.....	58
4.4.4 Boundary Conditions.....	59
4.4.5 Material Properties	59
4.4.6 Load-Cases and Job Parameters	59
4.4.7 Discussion of Simulation Results.....	59
CHAPTER FIVE.....	62
EXPERIMENTAL INVESTIGATION	62
5.1 Introduction	62
5.2 Fabrication of a Unimorph C- Shape Actuator.....	62
5.3 Experimental Procedure.	65
5.3.1 Measurements of the Static Displacement	65
5.3.2 Measurement of Static Force	65
5.3.3 Displacement Measurement Results and Discussion.....	68
5.3.4 Force Measurement Results and Discussion.....	69
5.4 Conclusions	72
CHAPTER SIX.....	73
A MICRO-MOTOR COMPRISED C-SHAPE PIEZOCERAMIC ACTUATORS.....	73
6.1 Introduction	73
6.2 C-Shape Actuators Connected in Series and Parallel Arrays	74

6.3 Selection of Appropriate Substrate Material and Thickness.....	76
6.4 Finite Element Simulation.....	77
6.4.1 Creation of Finite Element Model.....	77
6.4.2 Boundary Conditions.....	77
6.4.3 Load-Cases and Job Parameters.....	78
6.4.4 Numerical Simulation Results.....	78
CHAPTER SEVEN.....	82
FINITE ELEMENT FOR DYNAMIC ANALYSIS OF AN INDIVIDUAL C-SHAPE PIEZOELECTRIC ACTUATOR .	82
7.1 Introduction.....	82
7.2 Finite Element Formulation.....	82
7.2.1 Kinematics.....	83
7.2.2 Actuator Equations.....	85
7.2.3 Strain Energy.....	85
7.2.4 Kinetic Energy.....	87
7.3 Equations of Motion.....	88
7.4 Frequency Response Analysis.....	89
7.4.1 Modal Analysis Method.....	89
7.4.2 Modal Solution.....	90
7.4.3 Eigenvalue Problem.....	91
7.5 Numerical Examples.....	91
7.5.1 Computation of Eigenfrequency with the aid of MATLAB.....	91
7.5.2 Dynamic Analysis Simulation Using MSC Marc.....	97
CHAPTER EIGHT.....	102
CONCLUSIONS AND RECOMMENDATIONS.....	102
8.1 Conclusions.....	102
8.2 Recommendations for Future Work.....	104
REFERENCES.....	105
APPENDICES.....	114

LIST OF TABLES

Table 2.1	Solid- state actuator materials	14
Table 3.1	Material properties	28
Table 3.2	Displacement and force results for the selected geometry	33
Table 4.1	Internal radii for a substrate layer for selected substrate materials and external radii.	47
Table 5.1	Total actuator stiffness for selected substrate materials and Thickness	69
Table 6.1	Materials and dimensional specifications of the micro-motor basic unit	77

LIST OF FIGURES

CHAPTER 1

Figure 1.1	Basic elements forming a smart structure	2
-------------------	--	---

CHAPTER 2

Figure 2.1	Pervoskite structure	7
Figure 2.2	Electric dipole moments in Weiss Domains	9
Figure 2.3	Hysterisis loop of a poled piezoceramic Material	10
Figure 2.4	Representation of axes of deformation of a piezoelectric crystal	11
Figure 2.5	Energy conversion by piezoelectric materials	12
Figure 2.6a	Single Layer Longitudinal (d33) actuator (expanding) getting thicker	13
Figure 2.6b	Single layer transverse (d31) actuator (motor) with sides contracting	13
Figure 2.6c	Longitudinal (d33) sensor (generator) being compressed from the top and bottom	13
Figure 2.6d	Transverse (d31) sensor (generator) being compressed from the sides	13
Figure 2.7a	Piezo-stack	16
Figure 2.7b	Bender actuator	16

Figure 2.8	THUNDER actuator	17
Figure 2.9	Clamshell arrangement of Thunder actuators	18
Figure 2.10	Cymbal flex tensional actuator	19
Figure 2.11	External leverage- mechanical amplification	19
Figures 2.12	Ultrasonic motor by H.V. Barth	20
Figure 2.13	C-block actuators in an array	22
Figure 2.14	A rotor blade cross-section showing C-block actuators	22

CHAPTER 3

Figure 3.1	Unimorph C- shape actuator	24
Figure 3.2	Internal forces and moment at a cross-section cut at an angle θ	25
Figure 3.3	Dependence of actuator displacement on the external radius	29
Figure 3.4	Dependence of actuator force on external radius	30
Figure 3.5	Dependence of displacement on piezoceramic layer thickness	31
Figure 3.6	Actuator force Vs thickness of a piezoceramic layer	31
Figure 3.7	Dependence of displacement on actuator width	32
Figure 3.8	Dependence of force on actuator width	33
Figure 3.9a	Predicted and FEM displacement analysis results for various external radii at 50V input voltage	37
Figure 3.9b	Predicted and FEM force analysis results for various external radii at 50V input voltage	37
Figure 3.9c	Predicted and FEM displacement analysis results for various piezo-thickness at 50V input voltage	37
Figure 3.9d	Predicted and FEM force analysis results for various piezo-thickness at 50V input voltage	37

CHAPTER 4

Figure 4.1.	Displacement for different substrate/PZT thickness ratio	39
Figure 4.2	Actuator force for different substrate/PZT thickness ratio	39

Figure 4.3	Normalized force and displacement versus substrate/PZT thickness ratio	40
Figure 4.4	Displacement for different thickness ratios for Aluminium, Brass and Mild Steel substrate. (For 1mm thick PZT)	41
Figure 4.5	Dependence of the composite stiffness axis on the thickness ratios for different substrate materials	41
Figure 4.6	Radius of neutral axis in respect to substrate/PZT thickness ratio	41
Figure 4.7	The cross section of an actuator from top: piezoceramic and substrate layers respectively	42
Figure 4.8	Relationship between the coefficient of unimorph actuator and the substrate/PZT thickness ratio	45
Figure 4.9	Individual C-shape actuator	46
Figure 4.10	Radius of neutral axis for a range of substrate/PZT thickness ratios for different substrate materials	48
Figure 4.11	Displacement for a range of substrate thickness/PZT thickness ratio for different substrate materials	48
Figure 4.12	Force for a range of substrate thicknesses from different substrate materials	49
Figure 4.13	Dependence of the radius of neutral axis on the elastic constant of substrate material	51
Figure 4.14	Dependence of piezoelectric moment on the elastic properties of the substrate material	53
Figure 4.15	Relationship between blocked force and the elastic modulus of a substrate material	54
Figure 4.16	Recommended Substrate/PZT thickness ratios for engineering use	55
Figure 4.17	Work done of the C- block actuator with respect to thickness ratio (Substrate/PZT) 1mm PZT layer at 50V	56
Figure 4.18	Blocked force versus free displacement for the selected substrate/PZT ratios	56
Figure 4.19	Displacement Vs thickness ratio: Theoretical results compared to numerical analysis at 50V input voltage for brass substrate	60
Figure 4.20	Force vs. thickness ratio: Theoretical results compared to numerical analysis at 50V input voltage for brass substrate	60
Figure 4.21	Contour plot of the actuator force in the X- direction at 0.31	61

thickness ratio

Figure 4.22	Contour plot of displacement in the X-direction at 0.31 substrate/PZT thickness ratio	61
--------------------	---	----

CHAPTER 5

Figure 5.1	C-shape piezoceramic ring	63
Figure 5.2	Substrate rings from Mild Steel, Aluminium and Brass	63
Figure 5.3	C-shape actuator components ready for assembly	64
Figure 5.4	A set of assembled unimorph C-shape actuators with Aluminium, Brass and Mild steel substrates	64
Figure 5.5	Experimental set up for the measurement of displacement	66
Figure 5.6	Experimental setup for the measurement of static force	67
Figure 5.7	Displacement dependence on the applied voltage and substrate thickness of the substrate	68
Figure 5.8	Dependence of actuator displacement on applied voltage and on the elastic properties of the substrate material	68
Figure 5.9	Experimental results compared to finite element analysis for the displacement of an actuator made with a 1mm brass substrate.	70
Figure 5.10	Dependence of force on the applied voltage for selected substrate layer thickness	71
Figure 5.11	Dependence of force over applied voltage for selected substrate layer material	71
Figure 5.12	Comparison of experimental and predicted results of actuator force output for a 1mm brass substrate	71
Figure 5.13	Results for Displacement for PZT/Brass thickness ratio. (1mm PZT thickness, 10mm width, at 50Volts)	72
Figure 5.14	Results for the force for PZT/Brass thickness ratio. (1mm PZT thickness, 10mm width, at 50 Volts)	72

CHAPTER 6

Figure 6.1	A section view of an actuating device showing part of C-element actuator arrays	73
-------------------	---	----

Figure 6.2	Summation of piezoelectric moment from individual elements	74
Figure 6.3	Internal forces and moment at a cross-section cut at an angle θ .	75
Figure 6.4	Parallel array and serial C -actuators and the applied boundary conditions	78
Figure 6.5	Displacement of a single actuator	79
Figure 6.6	Force generated by a single actuator	79
Figure 6.7	Displacement of two units in series	80
Figure 6.8	Force generated two units in series	80
Figure 6.9	Displacement produced by two units in series and two units in parallel	81
Figure 6.10	Two units in series and two units in parallel	81

CHAPTER 7

Figure 7.1a	Straight arc element subjected to both extensional and bending deformations	83
Figure 7.1b	Straight arc element assemblage used to model an arc	83
Figure 7.2:	The laminated beam (from bottom to top: substrate, bond and Piezoceramic layer) with the corresponding straight arc element	84
Figure 7.3	C-shape piezoelectric actuator approximated with four straight arc elements	92
Figure 7.4a	Comparison of values of fundamental frequency for Mild Steel substrate.	93
Figure 7.4b	Comparison of values of fundamental frequency for Brass Substrate.	93
Figure 7.4c	Comparison of values of fundamental frequency for Aluminium substrate.	93
Figure 7.5	Frequency - response curves for Aluminium Substrate at an excitation voltage of 10V, damping Coefficient = 0.707	94
Figure 7.6	Frequency - response curves for a Mild steel Substrate (excitation voltage=10V, damping coefficient =0.7071)	95
Figure 7.7	Frequency - response curves for Brass substrate, (excitation voltage=10V, damping coefficient =0.7071)	96

Figure 7.8	First mode shape for a 0.25mm Aluminium substrate	98
Figure 7.9	Second mode shape for a 0.25mm Aluminium substrate	99
Figure 7.10	Third mode shape for a 0.25mm Aluminium substrate	100

LIST OF APPENDICES

Appendix A	Material Specification	114
	Table 1: Material properties and dimensions	
	Table 2: Electromechanical properties of the PZ6 (Piezoceramic material)	114
APPENDIX B	Matlab Codes	115
APPENDIX B1	Matlab program to find the dynamic response of the C-shape Piezoelectric Actuator	115
APPENDIX B2	Matlab sub-function to calculate some C-shape piezoelectric performance parameters	122
APPENDIX B3	Matlab sub-function program to compute stiffness matrices straight arc element	124
APPENDIX B4	Matlab sub-function program to compute mass matrices of a straight arc element	125
APPENDIX C	Stiffness and Mass Matrices for a Straight Arc Element (four elements)	126
APPENDIX C1	Global stiffness matrix of an element with the boundary conditions taken into account	126
APPENDIX C2	Global consistent mass matrix of an element with the boundary conditions taken into account	129
APPENDIX D	The Three Lowest Eigenfrequencies for Selected Substrate Material and Substrate/PZT Thickness Ratios	132

GLOSSARY

<u>Acronym</u>	<u>Explanation</u>
CERAMBOW	CERAMic Biased Oxide Wafer
ERF	ElectroRheological Fluid
FEA	Finite Element Analysis
FEM	Finite Element Method
FO	Fiber Optics
LaRC-SI™	Amorphous thermoplastic developed at NASA
LIPCA:	L ightweight P iezo- C omposite A ctuator
MEMS	Micro Electro-Mechanical Systems
MRF	MagnetoRheological Fluid
PMN	Lead Magnesium Niobate
PVDF	polyvinylidene fluoride
PZN-PZT	Lead zinc niobium and lead zirconate titanate)
PZT	Lead Zirconite Titanate
RAINBOW	R educed A nd I nternally B iased O xide W afer
SMA	Shape Memory Alloys
THUNDER	T hin U nimorph D river and sensor

CHAPTER ONE

Introduction

1.1 Background

Integration of smart materials in structures is among the most promising technologies for improved reliability of structures and systems. Understanding and controlling the composition and microstructure of any new materials (material properties) and at a device level, control of geometry and improved control algorithms are among the ultimate objectives of research in this field.

The need and expectation of smart materials for engineering applications have increased enormously, and the expectation of the technology to achieve them is promising. The following are some of the expectations:

- High level of reliability, efficiency and sustainability of the structures and systems.
- High security of the infrastructures especially when subjected to extreme and unstructured conditions.
- Continuous health and integrity monitoring.
- Damage detection and self-recovery.
- Intelligent operational management system.

1.2 Overview of Smart Materials and Structures

Smart materials and structures have been drawing the attention of many researchers for the past couple of decades.

Discoveries of a new generation of smart materials and structures that features a network of sensors and actuators with real-time control capabilities and a host structure (figure 1.1) have significantly impacted on the design and manufacture of the current generation of products. Smart structures, some times referred to as intelligent structures, have extraordinary abilities, as they are capable of self-correcting in order to improve and enhance their performance. Sensors and actuators embedded in a structure will detect a problem or a change in its environment, say through a change in variables such as strain, temperature, vibration, cracks etc, identify and analyze the problem, and thereafter initiate an appropriate action via a feedback system to correct or eliminate the problem [1]. In other words, smart structures are such structures and systems that are coupled with suitable control strategies and circuits exhibiting self-monitoring and self-controlling capabilities.

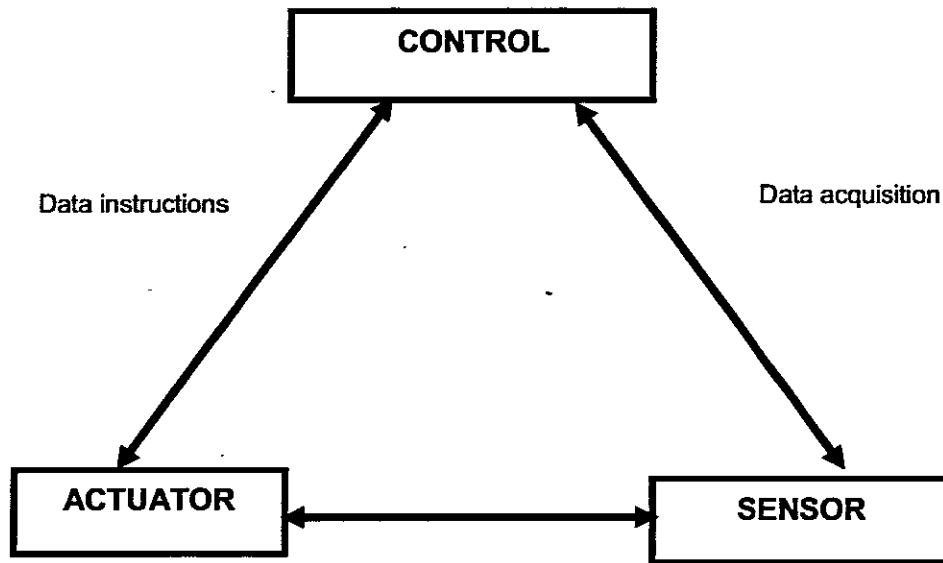


Figure 1.1: Basic elements forming a smart structure

These sensors and actuators are made from smart materials, a group of materials that are known to possess unusual properties. Smart materials produce certain responses upon being subjected to certain types of external stimuli such as electrical and magnetic fields, mechanical, chemical and thermal energy. This group of materials includes: *Piezoelectric* (PZT), which undergo mechanical (dimensional or shape) change when subjected to an electric field and vice versa; *Shape Memory Alloys* (SMA), which undergo phase transformation and hence shape change when subjected to thermal fields; *ElectroRheological* (ER) and *MagnetoRheological* (MR)- these liquids are typically suspensions of micron sized hydrophilic particles suspended in suitable hydrophobic carrier liquids, which undergo significant instantaneous reversible changes in their mechanical properties, such as mass distribution energy dissipation character when subjected to an electric field for the (ER) and when subjected to the magnetic field for (MR). *Fiber Optics* (FO)- they use intensity, phase, frequency or polarization of modulation for measurement of temperature, strain, magnetic or electric fields etc. *Magnetostrictive* materials are smart materials which when subjected to a magnetic field will undergo an induced strain. *Electrostrictive* materials are similar to magnetostrictive materials and they develop mechanical deformation when an external electric field is imposed upon them, the direction of these changes in geometry does not change if the direction of the electric field is reversed. Each of these materials has different performance characteristics with respect to sensing and actuating functions. [1], [2].

1.3 Application of Smart Structures

Examples of potential smart structural systems and some mechanisms that are candidates for smart structure application are air-craft (monitoring the state of strains in key locations and giving warning to prevent development and propagation of cracks), spacecrafts (pointing accuracy of large antennas maintained through an elaborate network of sensors and actuators), buildings (earthquake damage resistance, smart windows, electronic windows that sense weather changes and human activity and automatically adjust light and heat), bridges (monitoring of strains, deflections and vibration characteristics in order to warn of impending failures), ships (hulls and propulsion systems that detect and remove turbulence and prevent deflection), machinery (tools chatter suppression, rotor critical speed control), jet engines (fan, compressors, turbine blades that exploit asymmetry arising out of non uniformity in structural or aerodynamic properties), pipelines (monitoring of leakage and damage in underground pipes of water, oil and gas), medical devices (blood sugar sensors, insulin delivery pumps, micro-motor capsules that unclog arteries, filters that expand after insertion into vessels to trap blood clots)[1].

1.4 Problem Statement

Actuators are a vital part of the smart structure network and therefore need to be technologically matched. Improvement of actuator performance such as displacement, force generation, hysteresis, response time and bandwidth etc are the most significant parameters. Earlier PZT actuators were mostly used in static operations such as precision positioning or adjustments (i.e. involving movement from one point to another), but recently PZT actuators are increasingly being in demand for more complicated operations. Dynamically actuated components such as valves and fuel injection devices, together with applications in adaptive smart structures such as shape tuning, vibration excitation, cancellation, and mode shape tuning etc, are a few examples cited. For these operations, fast response, large displacement, variation of force and energy conversion are issues of concern. In certain applications, particularly in vibration control, small actuators with minimum power consumption, large displacement and force capable of operating both at low and high frequencies are increasingly under demand [3] [4] [5].

From this perspective, the motivation behind this research is to determine the optimum geometry and material properties for high performance-actuating device, which to a good extent will fulfil some of the aforementioned requirements and expectations.

This work entails the solution to the main problem, which is titled: *"Influence of geometry and material properties on the optimum performance of the C-shape piezocomposite actuator"*.

The solution comprises the collection of the solutions to the following sub-problems:

Sub Problems

1. The optimization of an actuating device capable of large displacement and large force.
2. Linear-elastic quasi- static analysis:
 - Force and displacement analysis of an individual piezoelectric actuator.
 - Force and displacement analysis of a piezoelectric actuator arrays
3. Dynamic analysis:
 - Frequency- amplitude analysis of the individual actuator.
 - Modal analysis- determination of mode shapes and natural frequencies.

1.5 Why C- Actuator?

The reasons for pursuing the study on a C-shape element are from the fact that recently there has been an increased use of curved shape actuators in various industrial applications. The C-shape actuator covers a wide mid-range of applications where most of applications fall due to the fact that it offers mid range of performance in terms of displacement and force.

1.6 Significance of the Research

It should be obvious that piezoelectric actuators are now in demand in complex applications where not only precision positioning ability is desired, but also other issues such as variation of force and/or generation of mechanical energy, the speed of response etc. All these facts underscore the significance and the need for improving actuator performance through optimization of actuator geometry and material properties. The optimized actuating device is expected to cater for applications that require large displacement and force as well as vibration control at a wider range of frequency. Static and dynamic analysis results will provide reliable information to designers concerning the influence of various design parameters such as geometry and material properties on the performance of the actuator.

1.7 Research Objectives:

The objective of this research was to perform theoretical, experimental and finite element analyses in order to optimize the performance of the C-shape piezoelectric actuator. There are four major components to the work being presented here:

- i. To perform quasi-static analyses of the C-shape actuator.
- ii. To manufacture a prototype.
- iii. To conduct experiments on the prototype to validate quasi-static analysis results.
- iv. To perform finite element formulation and simulation of the dynamic performance of the C-shape actuator.

1.8 Research Methodology

The methodology adopted for the preparation, implementation and reporting of the study is detailed as follows: A literature survey has been performed with regard to curved shape piezoelectric actuators i.e. past research findings in the related field. The qualitative nature of the research included assessment of the performance of selected types of piezoelectric actuators in terms of displacement and force, together with identification of parameters influencing the actuator performance. Theoretical, experimental and numerical simulation tools have been used to analyze and validate the findings.

1.9 Scope of the Thesis

The rest of the chapters of this thesis are organized as follows: Chapter 2 presents a literature survey on the theoretical overview of piezoelectric materials, the actuation methodologies and development trend of piezoelectric actuator technologies.

An investigation on the influences of the geometry and the inherent piezoelectric properties of the piezoceramic layer, the size and elastic properties of the substrate layer as well as the role of the ratio between substrate and PZT thicknesses on the performance of the C-shape piezo-composite actuator in terms of displacement and force are explored in chapters 3 and 4 respectively. Chapter 5 reports on the results from the experimental investigations performed on the piezo-composite unimorph actuators made from three different substrate materials (aluminium, brass and mild steel) with different thicknesses. Chapter 6 demonstrates the selection and use of the optimized geometry and material properties on the proposed design of the micro-motor comprising C-shape piezoelectric actuators. The Finite Element Method for the dynamic analysis of an individual C-shape actuator is discussed in chapter seven. Chapter eight presents the conclusions and recommendations for future work.

CHAPTER TWO

Literature review and theoretical framework

2.1 Piezoelectric Phenomena

Many polymers and ceramics are permanently polarized i.e. some parts of their molecules are positively charged, while other parts of their molecules are negatively charged. These materials will produce an electric field when the material changes dimensions as a result of an imposed mechanical force. These materials were named piezoelectric, and the phenomenon is known as the piezoelectric effect. Conversely, if an electric field is applied to these materials it will cause their dimensions to change. This phenomenon is known as electrostriction, or the reverse of piezoelectric effect (converse effect). A related property known as pyroelectricity is the ability of certain crystals to generate electrical charge when heated (David Brewster, in 1824) [6]. These are polycrystalline ferroelectric materials with a perovskite crystal structure i.e. a tetragonal/rhombohedral structure very close to the cubic crystal structure, figure 2.1a. Ferroelectricity is the presence of a spontaneous electric moment in a crystal which can be changed in its orientation between two or more distinct crystallographic directions by applying an external electric field [7].

An individual crystal is made up of positively and negatively charged atoms taking specific positions in a repeating elementary cell or unit. The possession of piezoelectric properties in a crystal is determined by specific symmetry of the unit cell i.e. when the structure of a crystal is centro-symmetric, with its positive and negative charge sites coinciding, there will be no dipoles present in the material, this is known as paraelectric behavior. Piezoceramics are noncentrosymmetric unit cells below a Curie temperature; above this temperature these ceramics are centro-symmetric and therefore have no piezoelectric characteristics. Lack of center of symmetry implies that the net movement of the negative and positive ions with respect to each other as a result of stress, produces an electric dipole [8].

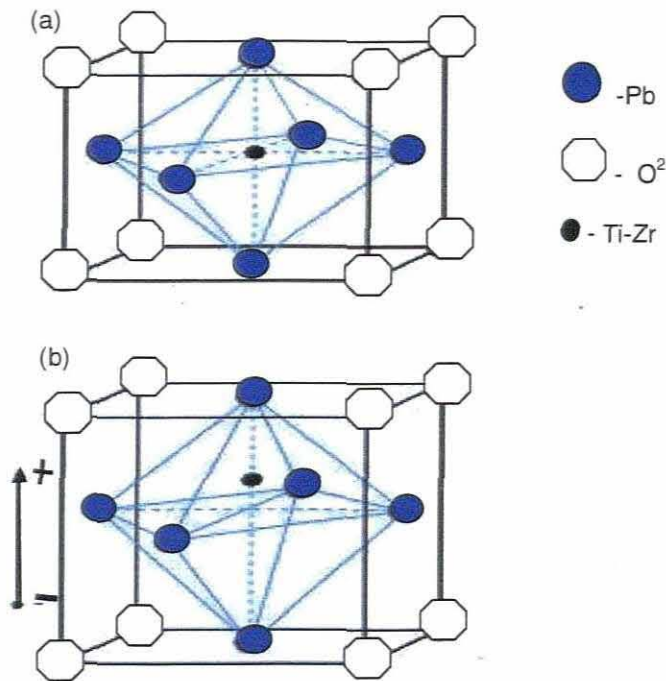


Figure 2.1: Pervoskite structure

(a) Lead zirconate titanate (PZT) unit cell in the symmetric cubic state above the Curie temperature.

(b) Tetragonally distorted unit cell below the Curie temperature.

2.2 Constitutive Relation

Individual crystals/dipoles in piezoelectric materials are randomly oriented with respect to each other; in this state the material is said to possess isotropic properties and therefore does not exhibit a piezoelectric effect since individual crystals cancel one another and hence produce no gross change of dimensions of the PZT element. The piezoelectric effect may be described mathematically using the following constitutive relations [9]:

Strain-Charge form

$$\begin{aligned} \epsilon &= s^E \sigma + d^T E \\ D &= d \sigma + \xi^\sigma E \end{aligned} \tag{2.1}$$

Strain - Voltage form

$$\begin{aligned}\varepsilon &= s^D \sigma + g^T D \\ E &= -g\sigma + \frac{1}{\varepsilon^D} D\end{aligned}\tag{2.2}$$

Stress -charge form

$$\begin{aligned}\sigma &= Q^E \varepsilon - e^T E \\ D &= -q\varepsilon + \xi^E E\end{aligned}\tag{2.3}$$

Stress-voltage form

$$\begin{aligned}\sigma &= Q^E \varepsilon - e^T E \\ E &= -g\sigma + \frac{1}{\varepsilon^\sigma} D\end{aligned}\tag{2.4}$$

Where

ε = Strain

σ = Mechanical stress

d = piezoelectric coupling coefficients for strain- charge form

s^E and s^D = Compliance at fixed electric field, and fixed electric displacement respectively

Q^E = Elastic modulus at fixed electric field

g = Piezoelectric coupling coefficients for strain-voltage form.

e = piezoelectric coupling coefficients for stress-charge form

D = Dielectric displacement (charge density)

E = Applied electric field

ξ^E and ξ^σ = Dielectric (permittivity) constant of the material at fixed strain and fixed stress respectively.

q = Piezoelectric coupling coefficients for stress-voltage form.

NB. Superscript T implies matrix transpose

2.3 Polarization of Piezoelectric Materials

The anisotropic nature of the constants ' d ' and ' s ' in equation 2.1 and 2.2 determine the degree of symmetry [9]. When manufactured, a piezoelectric material has electric dipoles arranged in random directions although neighboring dipoles align with each other to form regions of local alignment known as 'Weiss domains' (figure 2.2a-c). Within a Weiss domain, therefore, all the dipoles are aligned, giving a net dipole moment to the domain, and hence a net polarization (dipole moment per unit volume). So as to have a useful macroscopic response, the dipoles are permanently oriented with one another through a process called polling. This is done by heating the piezoceramic to above Curie temperature while a strong electric field is applied (usually a DC voltage). The direction of the applied field determines

the direction of final polarization, and thus the dipoles shift and aligns with it (figure 2.2b). The material is then cooled to below its Curie temperature while holding the poling field. Upon removal of the poling field, the ceramic returns to its un-poled dimensions, but the dipoles remain aligned in the poling direction, which is what gives the ceramic its piezoelectric properties i.e. the material will have a permanent remnant (residual) polarization. The magnitude of the piezoelectric properties thus depends on the polarization level. On the other hand the level of polarization is determined by the material composition [8].

In the poled state the piezoceramic material acquires anisotropic properties.

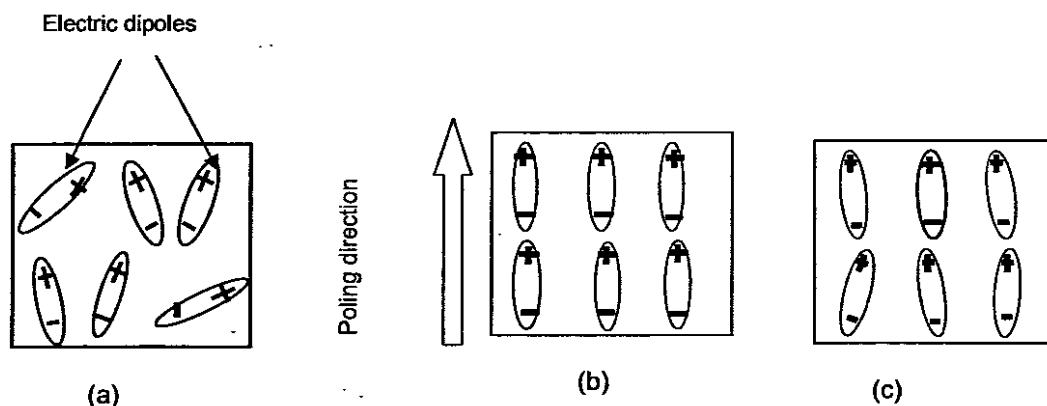


Figure 2.2: Electric dipole moments in Weiss domains.
(a) Before polarization;
(b) During polarization;
(c) After polarization

The hysteresis loop (Fig. 2.3) of the polarisation plays an important role in the analysis of actuator behaviour under a large mechanical loading and high electric field. [10][11][12][13][14][15]. The hysteresis curve provides information about, for example, coercive electric field and remnant polarisation which are crucial in the determination of suitable poling conditions. Stress state in actuators changes the remnant polarisation and coercive electric field [15]. The coercive electric field (E_c) is the electric field where polarisation of an actuator is zero while P_r is the value of the polarization when the electric field is zero.

The coercive electric field determines how high an electric field is required to negate the charge of an actuator due to polarization of domains in the material. It also provides information about the minimal poling field which should be applied in order to change polarization, and it determines the maximal usable electric field during excitation of the actuators. The net polarization can be effected if the mechanical stress, thermal and electrical field limits of the material are exceeded during its application.

If excitation exceeds the coercive electric field, depoling or re-poling occurs which effects the properties and performance of actuators.

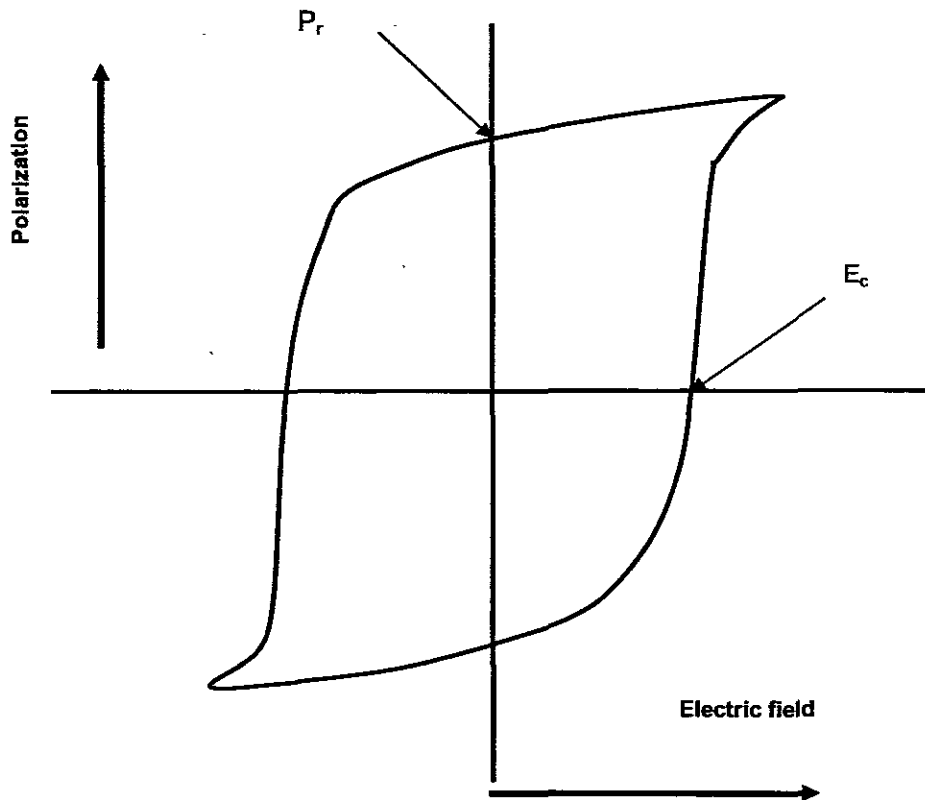


Figure 2.3: Hysterisis loop of a poled piezoceramic material

2.4 Piezoelectric Coefficients and Directions

Because of the anisotropic nature of piezoceramics, piezoelectric effects are dependent on direction. To identify the directions in a piezoelectric element, three axes are used i.e. 1, 2 and 3. The direction of positive polarization is usually assumed to coincide with the 3-axis (polar axis). The shear planes 4, 5 and 6 are perpendicular to the axes 1, 2 and 3 respectively (figure 2.4). The axes 1, 2 and 3 are analogous to the X, Y and Z axes of the Cartesian coordinate system. The properties of the piezoelectric material depend upon their orientation with respect to the poling axis. This orientation determines the direction of the action and response i.e. the direction of application of electric field/mechanical strain to the direction of deformation/electric charge obtained.

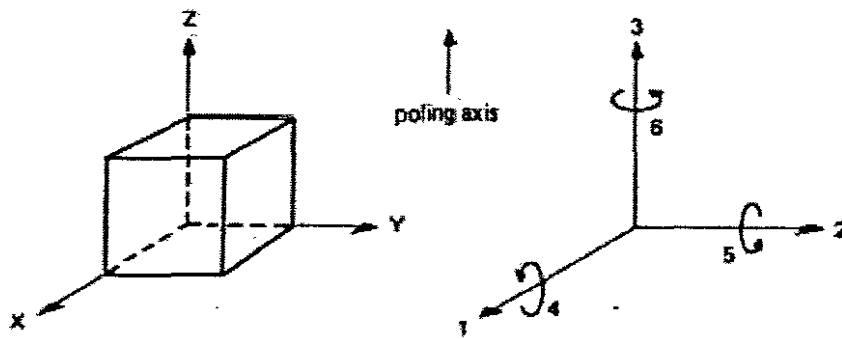


Figure 2.4: Representation of axes of deformation of a piezoelectric crystal.

The direction of polarization (axis 3) is established during the poling process.

Piezoelectric materials are characterized by several coefficients, some of which are:

d_{ij} - Strain coefficients [m/V] or charge output coefficients [C/N]:

Strain developed [m/m] per unit of electric field strength applied [V/m] or (due to the sensor / actuator properties of PZT material) charge density developed [C/m²] per given stress [N/m²].

g_{ij} - Voltage coefficients or field output coefficients [Vm/N]:

Open-circuit electric field developed [V/m] per applied mechanical stress [N/m²] or (due to the sensor / actuator properties of PZT material) strain developed [m/m] per applied charge density [C/m²].

k_{ij} - Coupling coefficients [dimensionless]:

Describe the conversion from mechanical to electrical energy or vice versa. k^2 is the ratio of energy stored (mechanical or electrical) to energy (mechanical or electrical) applied.

Double subscripts, such as in d_{ij} are used to describe the relationships between mechanical and electrical parameters. The first index indicates the direction of the application of excitement (stimulus), the second shows the direction of the response of the system.

Other important parameters are the Young's modulus ' Q_E ' (which describes the elastic properties of the piezoelectric material) and the dielectric constant ' K ' which is the ratio between the charge stored in an electroded slab material subjected to a certain voltage and the charge on a set of identical electrodes separated by vacuum.

When the electric field is applied parallel to the poling direction (thickness) of the piezoelectric actuator, the thickness of the actuator increases while the length of the actuator decreases (Poisson's effect). A reverse of polarity will produce the opposite behavior. The piezoelectric coefficients are specified by the material manufacturer under prescribed

conditions such as, stress-free conditions, low electric fields, constant frequency and at a specified working temperature.

The piezoelectric coefficients d_{33} , dielectric constant k_{33} as well as upper temperature limit : of electro-ceramic in technical applications change their magnitudes depending on the amount of pre-stress applied. This behaviour on the other hand depends on material composition [13][16][17].

2.5 Piezoelectric Actuators

The piezoceramic materials develop very specific and uniquely combined properties. These place piezoceramic components in a position to:

- Convert mechanical energy such as pressure, expansion or acceleration into electrical energy.
- Convert electrical energy into mechanical movement or force (figure 2.5).

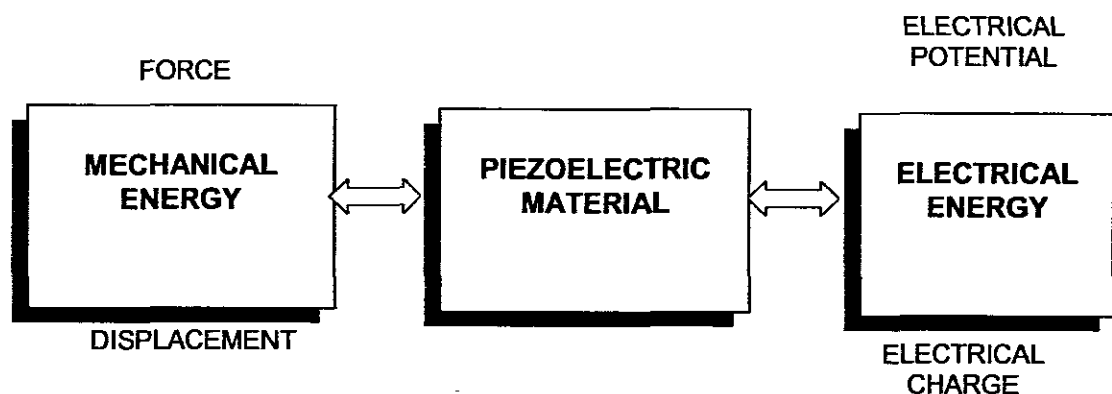


Figure 2.5: Energy conversion by piezoelectric materials

Piezoelectricity is an effect that is related to the microscopic structure of the solid i.e. displacement of ionic charges within a crystal structure. Normally structures, which do not have a centre of symmetry, are more likely to exhibit the piezoelectric effect. Applying stress to such a crystal will cause the distance between the dipole moments to change (i.e. positive and negative charge sites in each unit cell) leading to a net polarization at the crystal surface. This polarization is directly proportional to the applied stress and it is also dependent on the direction of application of stress e.g. voltages of opposite polarities will be generated from compressive or tensile stresses. The same applies to the converse effect; if the crystal is exposed to an electric field, it will experience an elastic strain causing its dimensions to change that is, to increase or decrease depending on the polarity of the electric field.

These two phenomena form a basis for the development of sensors and actuators, while the direct effect is suitable for sensors (fig. 2.6c-2.6d), and the converse effect is employed for actuators (fig. 2.6a-2.6b).

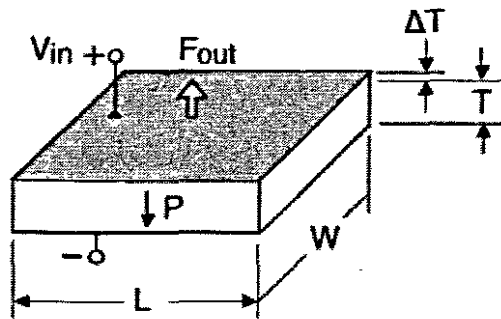


Figure 2.6a: Single Layer Longitudinal (d33) actuator (expanding) getting thicker

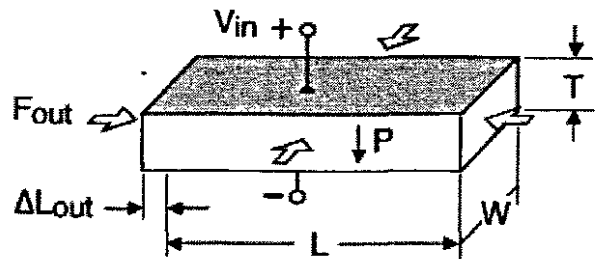


Figure 2.6b: Single layer transverse (d31) actuator (motor) with sides contracting

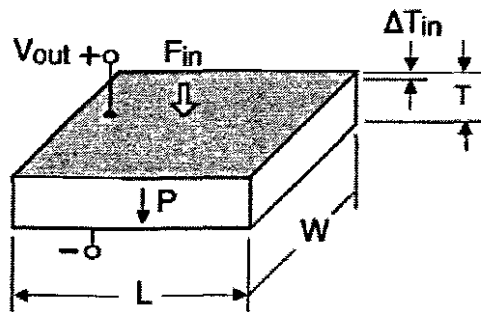


Figure 2.6c: Longitudinal (d33) sensor (generator) being compressed from the top and bottom

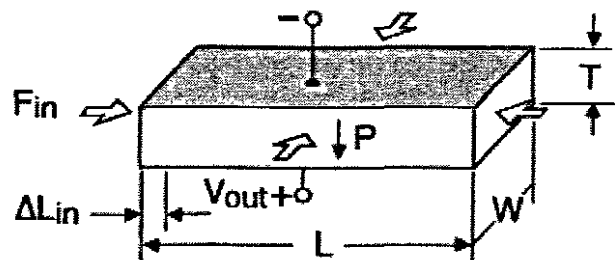


Figure 2.6d: Transverse (d31) sensor (generator) being compressed from the sides

2.6 Actuator Materials

Lead Zirconite Titanate (PZT) is widely used as a piezoceramic smart material due to its high piezoelectric, dielectric and elasticity coefficients [18]. They have high stiffness which gives adequate energy densities, and their fast response times make them suitable for high bandwidth compared to other solid-state actuation materials (See table 2.1)[19]. Piezopolymer films (PVdF) are strong against damage, but they have low stiffness. Shape Memory

Alloys (Nitinol) are capable of providing very high strains, but are limited to ultra-low bandwidth applications (< 5 Hz) due to the time needed for heat transfer to take place. Electrostrictive materials (PMN) exhibit less hysteresis losses and have high stiffness compared to piezoceramics, but have poor temperature stability; they feature a nonlinear constitutional relationship, which requires some biasing so as to obtain a linear behaviour. Also, due to their high material dielectric they require high currents to operate. Magnetostrictive actuators (Terfenol-D) are capable of providing high actuation energy density and bandwidth as piezoceramics, but they are very heavy when the coils and flux path materials are accounted for [15].

Table 2.1: Solid- state actuator materials [21]

Property	Piezoceramic	Piezofilm	Electro- strictive	Magneto- strictive	Shape memory alloy
	PZT5H	PVDF	PMN	Terfenol D	Nitinol
Max. Strain	0.13%	0.07%	0.1%	0.2%	2% - 8%
Modulus [GPa]	60.6	2	64.5	29.7	75(high temp) 28(low- temp)
Density [Kg/m ³]	7500	1780	7800	9250	7100
Temperature range [°C]	-20 to 200	Low	0 to 40	High	-
Useful Frequency Range [Hz]	0 -10E+08	0 – 10E+07	10E+05	10E+04	5
Energy Density [J/Kg]	6.83	0.28	4.13	6.42	252-4032

2.7 Development Trend of Piezoelectric Actuators

The history of a piezoelectric effect (i.e. producing charge when stressed) in some single crystalline materials started way back in 1880 when Pierre and Paul Jacques Curie

discovered this effect in quartz crystals. Later in 1881, G. Lippman discovered a converse effect i.e. developing strain when voltage is applied [6].

One of the first commercial applications of this technology was in 1916, when a quartz piezoelectric element was developed (quartz transmitter and receiver for underwater sound - the first SONAR) for submarine detection (by Frenchman, Langevin) and later in 1918 as frequency vibration controllers (Walter Cady, University of Wesleyan). The Piezoelectric effect provided by these natural piezoelectric materials was small and could only be used for certain applications. Since then a number of studies have been conducted to seek higher performance of the piezoelectric materials. In 1946, researchers such as Arthur Von Hippel and others at MIT (Massachusetts Institute of Technology) discovered that polycrystalline ferroelectric ceramic materials such Barium Titanate $BaTiO_3$ and Lead Metaniobate ($PbNb_2O_6$), if subjected to a high polarizing voltage, are able to exhibit higher levels of the piezoelectric effect than natural quartz, Rochelle salt and tourmaline can provide. Later in 1954 a very strong and stable piezoelectric effect was discovered in Lead Zirconite Titanate ($Pb(TiZr)O_3$), popularly known as PZT [2]. In the 1960's, a weak piezoelectric effect in whale bone and tendon was discovered. In 1969, Kawai [20] found a very high piezoelectric effect in the polarized fluoropolymer, polyvinylidene fluoride (PVDF). The piezoelectricity phenomenon has been successfully applied in the development of sensing and actuating devices. Over a hundred years since their discovery there has been an increasing pace of development and advances in terms of actuator technology. Actuators using the piezo effect have transformed the world of precision positioning and motion control. New trends to overcome limitations of actuator performance through the use of piezoelectric actuating design or structural geometry have become evident. Three popular methods in use for amplification of actuator displacement as well as force include: external leverage, internal leverage, and frequency leverage [3]. In the internally leveraged group of actuators, amplification is obtained through the optimization of the internal structure of an actuator. Some of the outcomes of extensive research on this scheme are the following actuator designs:

- **Stacks** (figure 2.7a), whereby maximum displacement for a given voltage can be increased by lamination of the ceramics [21].

- **Simple straight benders** piezoelectric actuators, (figure 2.7b), used in the hybrid position/force control of a parallel two fingered gripper [22].
- **CRESCENT**: Chandran et al[23], in their work, developed the CRESCENT :

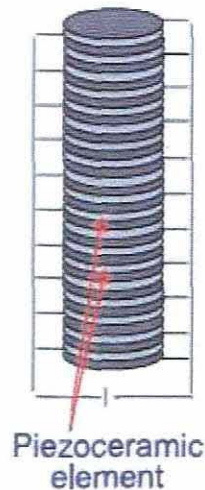


Figure 2.7a: Piezo-stack

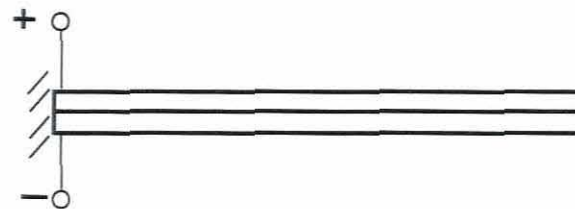


Figure 2.7b: Bender actuator

piezoelectric bending actuator. CRESCENT is a stress-biased ceramic-metal composite actuator, which involves the use of the difference in thermal contraction between the ceramic and the metal plates bonded together at a high temperature by a polymeric agent to produce a stress-biased curved structure. The device fabricated at optimum temperature exhibits large tip displacement and blocking force and possesses superior electromechanical characteristics to conventional unimorph actuator.

- **RAINBOW** (Reduced And Internally Biased Oxide Wafer), it is also a stress-biased solid-state actuator with one surface of the wafer chemically reduced, to give a stress-biased dome-like structure [24].

In their work, Pearce and Button [25] introduced an alternative method for fabricating RAINBOW-type devices, in which the necessary shape and internal electrode structure were created during sintering. The small difference in sintering shrinkage between low and high silver content compositions was utilized in laminated structures to produce as-fired curvatures and hence pre-stress.

- **CERAMBOW** (developed in 1996)- CERAMBOW technology is based on a thermal contraction mismatch between two bonded layers which results in a stress-biased structure. Displacement of a CERAMBOW actuator is a function of temperature under both loaded and unloaded conditions [26].
- **THUNDER** actuator -(**T**hin **U**nimorph **D**riv**E**R and sensor) [24][25],(developed in 1994), is a multilayer actuator composed of stainless steel, aluminum and PZT

piezoceramic, bonded together to form a sandwich like package by using a high temperature adhesive called LaRCTM -SI,(figure 2.8). Mismatch of thin layers laminated together causes pre-stress which is the reason behind the large displacement.

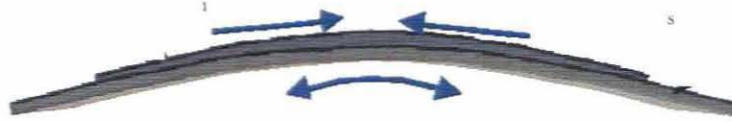


Figure 2.8: THUNDER ACTUATOR
 Courtesy of Face International Corp, (2002),
 [28]

- **LIPCA:** (Lightweight Piezo-Composite Actuator) K. Joon et al [29]. LIPCA has a 3-layer configuration of which the top layer contains a fiber-composite of a high modulus of elasticity and of a low coefficient of thermal expansion (carbon/epoxy) and a middle layer composed of a PZT ceramic wafer. The base layer is made up of a material with a low modulus of elasticity and high coefficient of thermal expansion (glass/epoxy). This technique differs slightly to that used in the THUNDER actuator in that the heavy metals (stainless steel and aluminium) used in THUNDER are replaced by lightweight fiber-composite materials. Better results for LIPCA2 in terms of actuation displacement compared to the THUNDER were reported.

J.X. Gao et al [30] designed an actuator assembly in which two THUNDER actuators are put in a clamshell configuration (Figure 2.9). It is observed that the design has overcome the drawbacks of a single THUNDER actuator i.e. by providing larger displacement. However, it was indicated that the new actuator was suitable only for low frequency active vibration control, in which the basic requirement is larger displacement. In vibration control, apart from large displacement it requires large force as well.

Li et al [31], examined the static axial displacement of a ceramic d_{31} -gradient flextensional transducer of two lead zirconate titanate systems, (PZT)/PZT and PZT/ZnO. The transducers consisted of two PZT layers of different d_{31} coefficients. The transducers axial displacement varied with the thickness ratio of the constituent layers. The measured axial displacements were about twice the calculated values, suggesting an enhanced d_{31} value because of the tensile bending stress in the PZT layer.

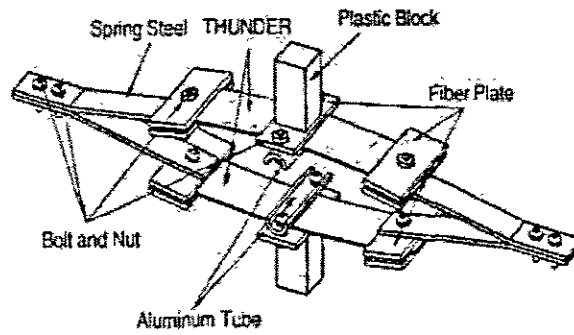


Figure 2.9: Clamshell arrangement of Thunder actuators [30]

A two-layered flextensional actuator, composed of a piezoelectric layer and a conducting layer, Yoon et al [32] and later a multilayer flextensional bender-type actuator Chang et al [33], which was composed of five piezoelectric layers and one passive conducting layer, were fabricated using a co-extrusion process. The method utilizes a co-fired composite of PZN-PZT (lead zinc niobium and lead zirconate titanate) and dispersed silver particles to introduce the initial pre-stress state due to the mismatch of coefficients of thermal expansion. Telescopic actuator (developed in 1999) is another example of an internal leverage scheme - Consists of interconnected concentric, cascaded cylinders that telescope out when activated [34], [35].

External leveraged actuators use external component for mechanical amplification. This group includes flexure-hinged actuators such as:

- **Moonie** actuator (developed in 1992) - a poled lead zirconate titanate (PZT) ceramic sandwiched between two specially designed metal end caps. Piezoelectric coefficients of an order of magnitude larger than PZT itself are obtained [36].
- **Cymbal** transducers (developed in 1996; figure 2.10) consist of a cylindrical ceramic element sandwiched between two truncated conical metal end caps and can be used as both sensors and actuators. The cymbal actuator exhibits almost 40 times higher displacement than the same size ceramic element [37].

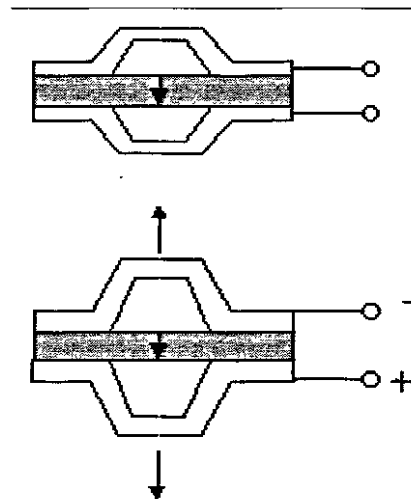


Figure 2.10: Cymbal flex-tensional actuator[37]

Dhananjay Samak et al [38] provide another example of externally leveraged amplifications. They developed an electromechanical actuator based on the concept of mechanical amplification with piezo and electrostrictive stacks as drivers to achieve high force and high displacement actuation (figure 2.11).

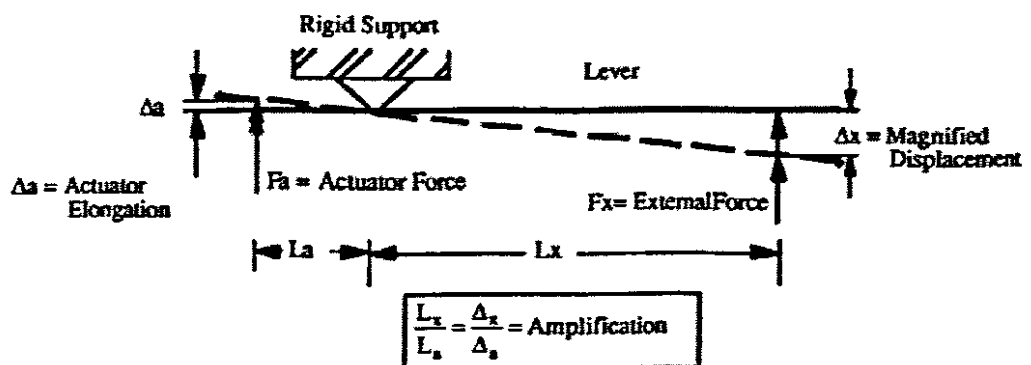
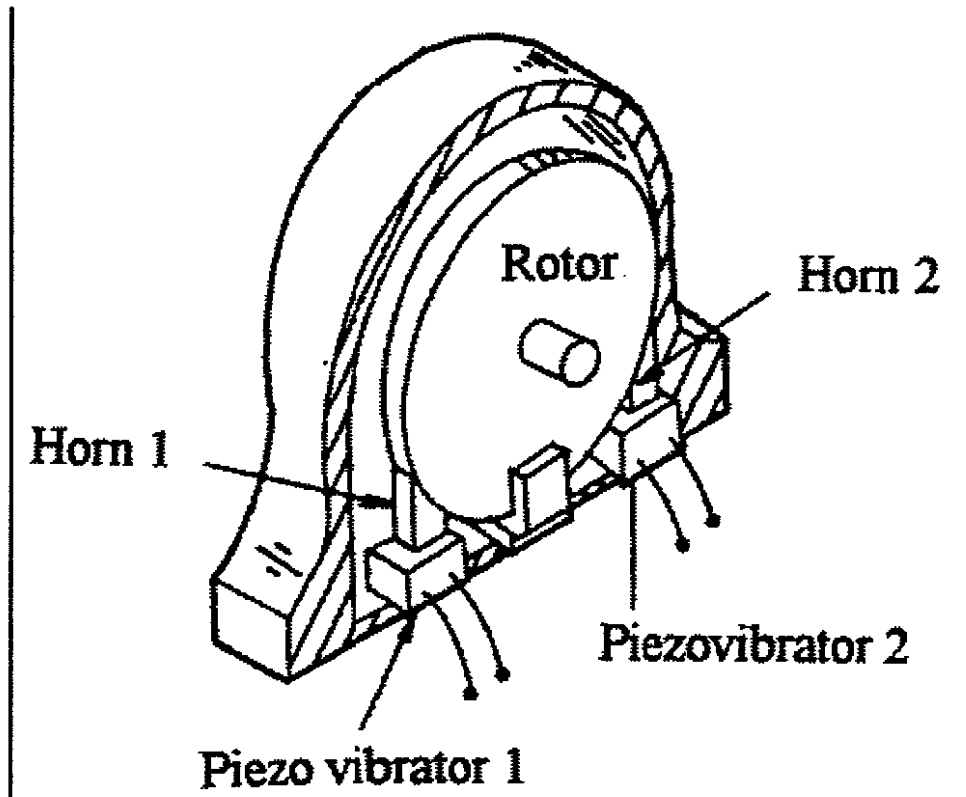


Figure 2.11: External leverage- mechanical amplification [38]

Frequency leveraged actuators mainly depend on the alternating control signal to generate motion. Actuators such as inchworm and ultrasonic motors fall under this category. For an inchworm actuator, frequency performance of the piezoelectric material is used to move the actuator in one direction in a series of small steps, this action results in an increase of strain [3]. The resonant displacement in the ultrasonic motor for example is proportional to the drive frequency [39]. Very high speed of motion due to high frequency will be achieved. The schematic of the first ultrasonic motor proposed by H.V. Barth (developed in 1973) is shown

in figure 2.12). When one of the horns is excited, the rotor rotates in one direction, and by exciting the other horn, the rotation direction will be reversed.



Figures 2.12: Ultrasonic motor by H.V. Barth [36]

As far as internal leverage actuators are concerned it can be said that control of the stresses in a piezoelectric actuator is vital in order to get better performance characteristics.

Pre-loading a piezoceramic actuator has proven to cause substantial changes in the electromechanical coupling factors (that is, piezoelectric coefficients, dielectric constant, and elastic compliance) due to nonlinear effects and stress depoling effects. A DC bias electric field can be applied parallel to the original poling direction, to maintain the ceramic poling state so that the ceramic can be used at high stress without losing its piezoelectric properties. This can also be achieved by regulating the initial compressive stress in the piezoceramic material [40].

Studies show that a suitable stress state will change the initial domain configuration and electromechanical characteristics, especially at high electric fields, as a result of the d_{31} coefficient having increased[41],[42], [43],[44],[45][46].

Generally in the internally leveraged actuators the displacement is mainly produced by bending through the d_{31} coefficient. Benders are typically thin but long so that the displacement produced by d_{31} is much larger than that produced by d_{33} [47].

Displacement of the actuator depends on its structure, materials, actuation mode and clamping [48].

Contraction and expansion of the piezoceramic layer in the lateral direction is resisted by the non piezoceramic material (substrate) or a piezoceramic layer with a lower d_{31} coefficient consequently the structure is forced to bend under electrical excitation due to stresses developed between the neighbouring layers.

Bending of the actuator can produce significant axial displacement through amplification of the lateral displacement. The amplification depends on the size and shape of the actuator, Young's modulus and the material thicknesses of the passive and active materials [49], [50], [51], [42] [53][54].

2.8 C-Shape Piezoelectric Actuator

For certain smart structures applications, the use of curved piezoelectric actuators is necessary, for example active controls of satellite dishes or mirrors etc [55], [56].

The C-Block piezoelectric actuator was developed in 1996 by A.J. Moskalik and Diann Brei [57]. –It is a mid-range solid-state piezoelectric actuator, made of semicircular laminated layers.

When individual actuators are combined in series or parallel, they (figure 2.13) can respectively generate larger displacement and more force than a comparable straight bender. The force produced by an array of actuators is proportional to the number of individual actuators in a parallel arrangement. The resulting displacement equals the sum of displacements of individual actuators in a series arrangement [58]. One of the first C shape actuator applications was by Chattopadhyay et al [59]. A number of curved polymeric piezoelectric C- shape actuator arrays were designed to drive a “smart” flap for individual helicopter blade control (figure 2.14).

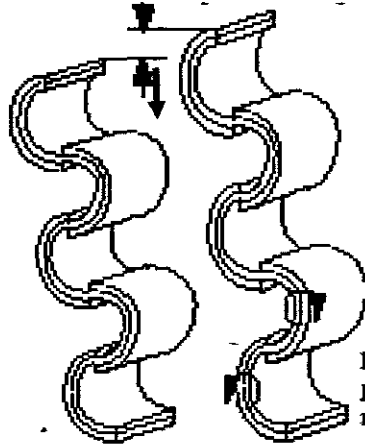


Figure 2.13: C-block individual actuators in an array, Reference [58]

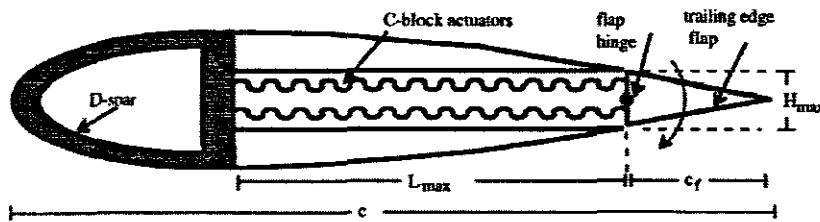


Figure 2.14: A rotor blade cross-section showing C-block actuators [59]

The present work related to the C –actuator is based on previous work by J.Moskalik and D. Brei (57) who proposed a linear model for the quasi-static case. The models were experimentally verified in the unimorph and bimorph configurations for PZT5 and PZT8 piezoceramic materials and multimorph configuration for the PVDF material. They also proposed models that predicted and validated the force-deflection behaviour of C-block actuator arrays [58].

Finally, J.Moskalik and D. Brei proposed a model for the dynamic performance of individual C-block and C-block array architectures [60] [61]. These models were used for the identification of natural frequencies and the amplitude across a frequency spectrum.

CHAPTER THREE

Influence of the External Radius, Thickness and Width of the Piezoceramic Layer on the Displacement and Force

3.1 Introduction

This chapter covers the quasi-static analysis of a C-shape piezoelectric actuator. As mentioned earlier in chapter 2, energy conversion is a key feature in the assessment of any actuator performance. Energy conversion mainly depends upon the applied voltage, piezoelectric material properties and the geometrical configuration of an actuator. In this chapter more focus has been put on the optimization of the geometry of a C-shape actuator (particularly of the piezoceramic layer). An analytical model is used to optimise the geometry of an individual C-actuator. The influence of parameters such as external radius, total thickness and width of the piezoceramic layer on the displacement and force of the C-actuator have been investigated.

The information gathered from the parametric analytical and experimental work is a useful guide to a designer, enabling the selection of appropriate material and geometry of a basic C-shape actuator, depending on whether the primary requirement is large force or large displacement, or for that matter a suitable combination. The information is also useful in deciding on the required number of individual elements in series and/or parallel depending of course on overall dimensional limitations.

3.2 Individual C- Shape Actuator

As mentioned earlier when individual C-block actuators are combined in series and/or parallel it is possible to generate displacement and force larger than a comparable straight bender. The force produced by an array of C- block actuators is proportional to the number of individual C-blocks in a parallel arrangement, while the resulting displacement equals the sum of displacements of individual blocks in a series arrangement [58].

A unimorph C- shape piezoelectric actuator (figure 3.1) consists of three layers laminated together to form a semicircular shell i.e. one active layer (piezoceramic) and passive layers (bonding and substrate). The PZT layer is pre-plated with electrode layers on its inner and outer surfaces.

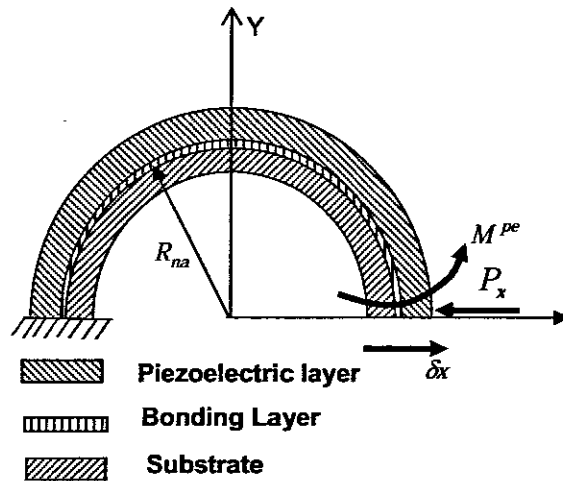


Figure 3.1: Unimorph C- shape actuator

The inner surface of the piezo-ceramic element that has been preplated with an electrode layer is bonded on the outer surface of a substrate. Epoxy is used as the bonding agent and a strong bond is created between the piezo element and the substrate. This ensures that all loads applied by the active element are transmitted fully to the substrate. With unimorph actuators, when the piezoelectric element expands/contracts in the radial direction the strain in the plane normal to the poling direction undergoes a contraction/expansion.

The “perfect bond” between the piezoceramic element and the substrate leads to a concentrated couple or moment M^{pe} at the edges of the piezoelectric actuator layer once a voltage is applied [18]. The concentrated moment will eventually cause the whole structure to flex. The assumption of “perfect bond” also implies continuity of displacement/strain between the interfaces of the laminate. For the PZT material, the unimorph configuration is preferred particularly when the actuating device is to be subjected to both tensile and compressive loads (especially under large dynamic loads). PZT materials are weak in tension; therefore for an actuator to perform safely it is important that when determining the stacking sequence of the layers in the laminate, the piezoceramic element must be positioned on one side of the neutral axis. This will ensure that the PZT experiences only compressive stresses during its operation. In addition, by locating the active element as far as possible from the neutral axis a larger moment arm will be obtained and hence larger bending moment. The location of the neutral axis is normally achieved by the introduction of passive layers (i.e. substrate) of appropriate thickness and elastic modulus.

3.3 Displacement and Force Equations:

To obtain C shape actuator equations, the following assumptions are made:

1. The piezoelectric actuator layers are perfectly bonded together.
 - continuous strain across the bond
 - Shear stresses in the interfaces are ignored.
2. Small displacements and strains
 - Material behaviour is limited within the linear elastic range
3. The actuator is thin
 - the effect of transverse shear forces is neglected, cross-sections remain plane and normal, the rotational deformation is due to bending alone

Since the C-block element is considered to have a thin cross-section it is reasonable to consider a unidirectional state of loading. The radial displacement and force at the tip of the free end can be defined by the force-displacement equation obtained using Castigliano method for thin piezoelectric curved beams [8] [62].

The internal moment ' M ' at any angular position (figure 3.2) is the sum of moment due to externally applied force and the piezoelectric moment

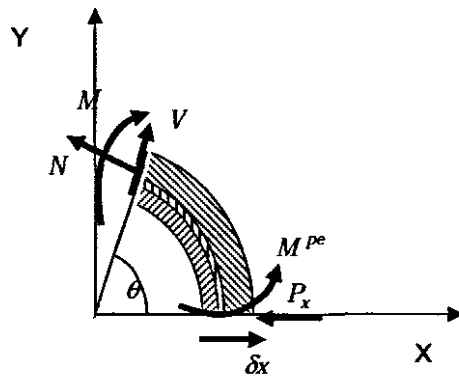


Figure 3.2: Internal forces and moment at a cross-section cut at an angle θ

$$M = -P_x R_{na} \sin\theta + M^{pe} \quad (3.1)$$

Where

P_x = Available force at the free end tip.

M^{pe} = Piezoelectric moment

R_{na} = Radius from the origin of the semi-circle to the neutral axis (figure (3.1)).

$$\frac{\partial M}{\partial P_x} = -R_{na} \sin\theta \quad (3.2)$$

The complementary energy of an individual actuator (figure 3.2) is obtained by the equation

$$U_c = \frac{1}{2QI_z} \int_0^\pi M^2 R_{na} d\theta \quad (3.3)$$

Where:

Q = Young's modulus of elasticity of the material.

I_z = Moment of inertia of cross-section of the actuator about the neutral axis.

The displacement of the free end can be obtained using complementary energy as follows [62]:

$$\begin{aligned} \delta_x &= \frac{\partial U_c}{\partial P_x} = \frac{1}{QI_z} \int_0^\pi M \frac{\partial M}{\partial P_x} R_{na} d\theta \\ &= \frac{1}{QI_z} \int_0^\pi (M^{pe} - P_x) R_{na}^2 \sin \theta d\theta \\ \delta_x &= \frac{2M^{pe} R_{na}^2}{D} - \frac{P_x \pi R_{na}^3}{2D} \end{aligned} \quad (3.4)$$

Where δ_x is the radial displacement at the free end.

Expressing the available force in terms of the piezoelectric moment and radial displacement from equation 3.4, we obtain the net force at the tip of the free end:

$$P_x = \frac{4M^{pe}}{\pi R_{na}} - \frac{2D\delta_x}{\pi R_{na}^3} \quad (3.5)$$

Where:

$D = QI_z$ = Composite bending stiffness

The composite bending stiffness can be obtained by [63]

$$\begin{aligned} D &= \sum_{j=1}^n Q_j I_{zj} = \sum Q_j \frac{b_j (h_j - h_{j-1})^3}{12} + b_j (h_j - h_{j-1}) \frac{(h_j + h_{j-1})^2}{4} \\ D &= \left(\frac{1}{3} \sum_{j=1}^n b_j Q_j (h_j^3 - h_{j-1}^3) \right) \end{aligned} \quad (3.6)$$

The piezoelectric moment, M^{pe} can be obtained from [8] [57]

$$M^{pe} = \frac{1}{2} \sum_{j=1}^n b_j Q_j (h_j^2 - h_{j-1}^2) \times (d_{31} E_3)_j \quad (3.7)$$

Where:

b_j = The width of the j^{th} layer

Q_j = Young's modulus of elasticity of the material of the j^{th} layer in the laminate

h_j = Coordinate of the outer surface of the j^{th} layer

h_{j-1} = Coordinate of the inner surface of the j^{th} layer

$h_j = r_j - R_{na}$

d_{31} = Piezoelectric strain constant

E_3 = Electric field

For a thin piezoelectric actuator it is sufficient to assume that an electric field is equal to the change of voltage between the electrodes 'V' divided by the thickness t of the piezoceramic layer concerned, i.e. $t = h_j - h_{j-1}$, hence

$$E_3 = \frac{V}{h_j - h_{j-1}} \quad (3.8)$$

Using equation 3.8 into equation 3.7 the bending moment for composite layer becomes:

$$M^{pe} = \frac{1}{2} \sum_{j=1}^n b_j Q_j (h_j + h_{j-1}) \times (d_{31} V)_j \quad (3.9)$$

And the radius to the neutral axis of the composite circular beam is given by:

$$R_{na} = \frac{\sum_{j=1}^n 0.5 Q_j b_j (r_j^2 - r_{j-1}^2)}{\sum_{j=1}^n Q_j b_j (r_j - r_{j-1})} \quad (3.10)$$

Where r_j and r_{j-1} are the radii from the origin to the inner and outer surfaces of the j^{th} layer respectively.

The piezoelectric "blocked force" (the force obtained when the displacement of the tip of the free end is equal to zero, (equation 3.5):

$$F_b = \frac{4M^{pe}}{\pi R_{na}^2} \quad (3.11)$$

Free-displacement at the tip of the free end (i.e. when the piezoelectric forcing term is not resisted externally in any way, (equation 3.4)) becomes:

$$\delta_{free} = \frac{2M^{pe} R_{na}^2}{D} \quad (3.12)$$

3.4 Optimization of the Geometry of the Piezoceramic Layer.

The prime objective of this work is to obtain a compact, low powered, high performance-actuating device using C- shape actuating actuator. Energy conversion is an important issue to be considered in the design of an actuating device. For actuators, materials with a high piezoelectric strain coefficient are preferred, for which piezoceramic materials are appropriate candidates. Moderately hard piezoceramic material will be suitable if one is

seeking a high performance-actuating device in terms of both displacement and force. A PZT material with larger transverse piezoelectric strain coefficient i.e. ' d_{31} ' is preferred. The materials and their properties chosen for the purpose of this part of the study are shown in table 3.1.

As mentioned earlier the geometric features of an actuator such as thickness, curvature, the

Table 3.1: Material Properties

Material name	Young's [Gpa]	Modulus	Piezoelectric constant- d_{31} [m/V]	Density [g/cm ³]
Piezo-ceramic (PZT-5H)		6.3E+10	-274E-12	7.8
Epoxy		1.9E+09	0	1.3
Mild- Steel		1.90E+11	0	7.854

number of passive layers and their arrangement have a great influence on the performance of an actuator. An actuator made with a relatively thicker piezoceramic element will be able to produce a larger force but yields lesser displacement; it can operate at higher frequencies than a thinner component of comparable electromechanical and material properties, however, it consumes more voltage to drive it. The effect of change in the geometry such as the maximum interface radius, thickness of individual layers and width, that have on the displacement or force of an individual C-shape element over a range of voltages is analyzed and the results are shown in figures 3.3 to 3.8.

A Matlab code for computing the blocked force and free displacement values was developed based on equations 3.5 to 3.8 and is found in appendix C.

The materials and specifications used in the study are drawn from commercially available standard sizes of piezoceramic tubes i.e. PI Ceramic [64], Morgan Eletro-ceramics [65] and Staveley NDT Technologies [66].

3.4.1 Case Study 1: Influence of Maximum External Radius

The influence of external radius on displacement and force is displayed in figures 3.3 and 3.4 respectively.

Eight different radii were used for this analysis.

Radii [mm]: 9.53, 10.0, 10.8, 11.0, 12.70, 15.88, 19.05 and 20.0.

The width = 22.0mm

Total thickness of 1.480mm that is,

$$t_{pzt} = 0.84\text{mm, (fixed)}$$

$$t_{epoxy} = 0.18\text{mm},$$

$$t_{substrate} = 0.46\text{mm}$$

Figures 3.3 and 3.4 show that by increasing the external radius of the actuator the displacement of the free end tip increases while the force is decreased. This can be justified by the fact that increasing an interface radius, the radius to thickness ratio increases which makes the beam to be more flexible. This also increases the radius of neutral axis (equation 3.9) which in turn increases displacement quadratically (equation 3.11) On the other hand the radius of neutral axis has an inverse effect on the force (equation 3.10). Both displacement and force increase with increasing voltage.

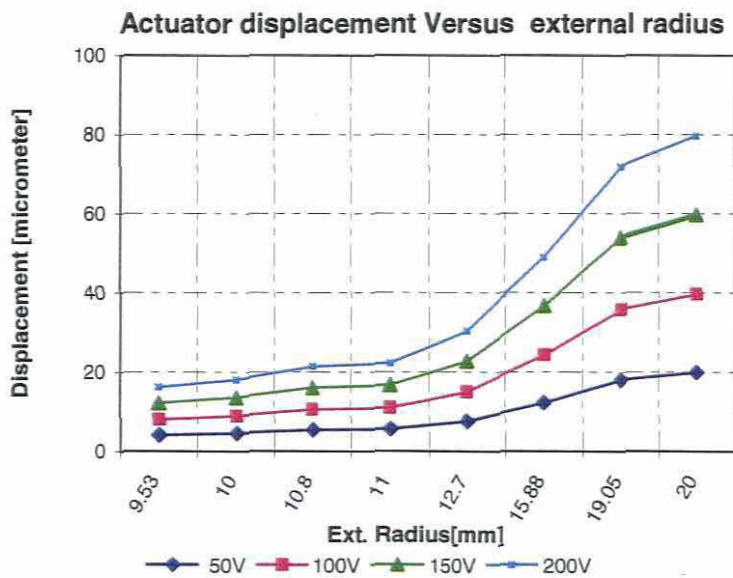


Figure 3.3: Dependence of actuator displacement on the external radius

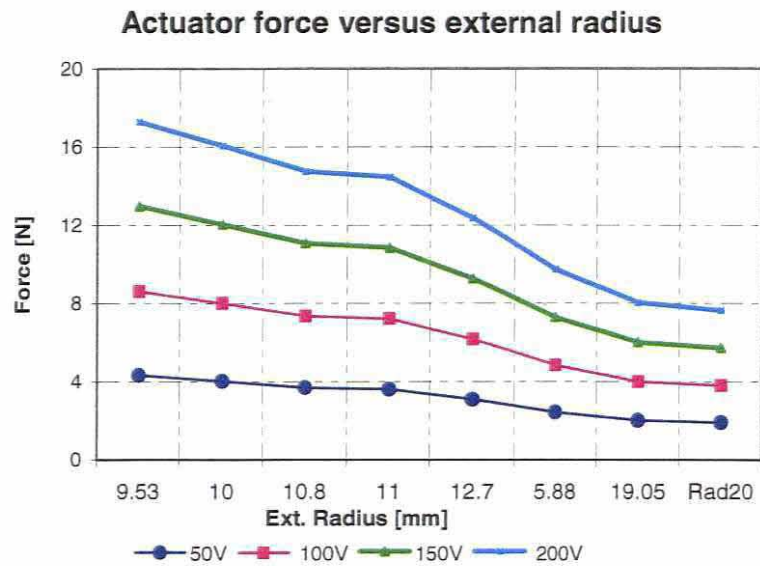


Figure 3.4: Dependence of actuator force on external radius

3.4.2 Case Study 2: Influence of Piezoceramic Layer Thickness

The influence of the thickness of piezoceramic layer on displacement and force output from the actuator is shown in figures 3.5 and 3.6 respectively. The thickness of the substrate and the bonding layers were kept constant while changing the thickness of the piezoceramic layer. The width and the external radius used were 22.0mm and 10.0mm respectively.

The following PZT thicknesses were investigated: 0.75, 0.84, 1.0, 1.5, 2.0 [mm].

Total thickness of 1.480mm i.e. ($t_{pzt} = 0.84\text{mm} = t_{epoxy} 0.18\text{mm}$)

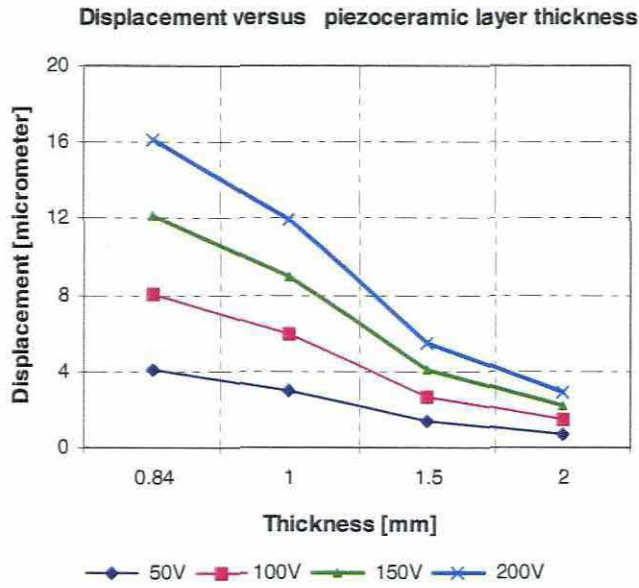


Figure 3.5: Dependence of displacement on piezoceramic layer thickness

$t_{substrate} = 0.46\text{mm}$). Figure 3.5 shows that by increasing piezo-layer thickness the displacement is reduced while the force is increased (figure 3.6). A simple explanation for this is that the generated force, apart from the applied voltage it also depends on the amount of piezoelectric material in (this case the PZT thickness). The thickness also affects the stiffness of the actuator. While force requires stiff material, displacement requires flexible material..

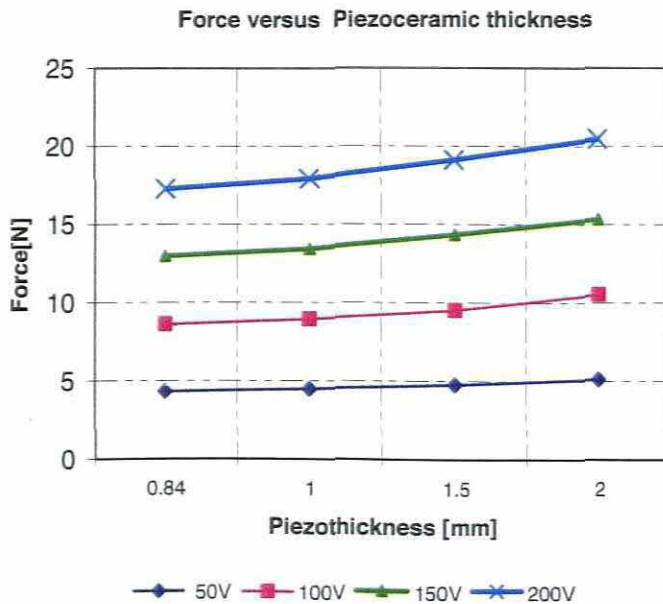


Figure 3.6: Actuator force Vs thickness of a piezoceramic layer

3.4.3 Case Study 3: Influence of Width

Given a total thickness of 1.480mm e.g. $t_{pzt} = 0.84\text{mm}$, bonding and substrate thickness $t_{epoxy} = 0.18$ and $t_{substrate} = 0.46\text{mm}$ respectively, the external radius of 10.0mm, five different widths i.e. 12.7, 16.8, 22, 30 and 38.1 [mm] were used for the analysis. Results show that the width does not affect the displacement in any way (Figure 3.7), while the force increases with increased width (Figure 3.10). This behaviour occurs when the width is increased while other features are kept constant, which results from the piezoelectric moment and the composite stiffness increasing simultaneously in equal proportions (this is analogous to having actuators placed in parallel array). Increase of stiffness will directly increase the force output (equation 3.11), hence from equation 3.12 it is evident that there will not be any change in displacement due to proportional increase in both piezoelectric moment and composite bending stiffness.

In figures 3.3 through 3.8 it can be observed, that to obtain large displacement it requires a large radius, appropriate width and a relatively thin piezoceramic layer while on the other hand in order to obtain large force it needs a relatively smaller radius, a thicker and wider (stiff), actuator.

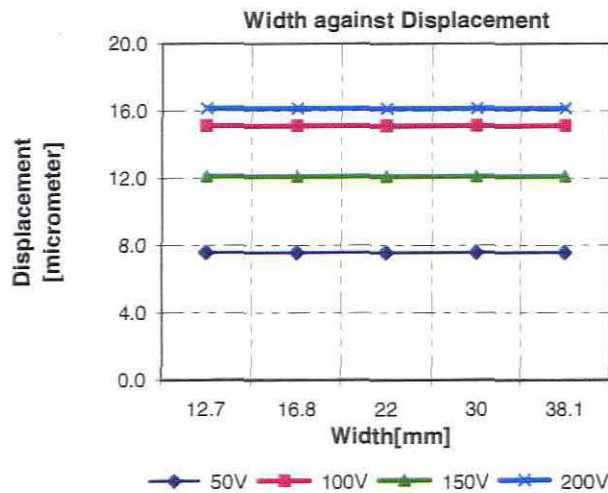


Figure 3.7: Dependence of Displacement on actuator width

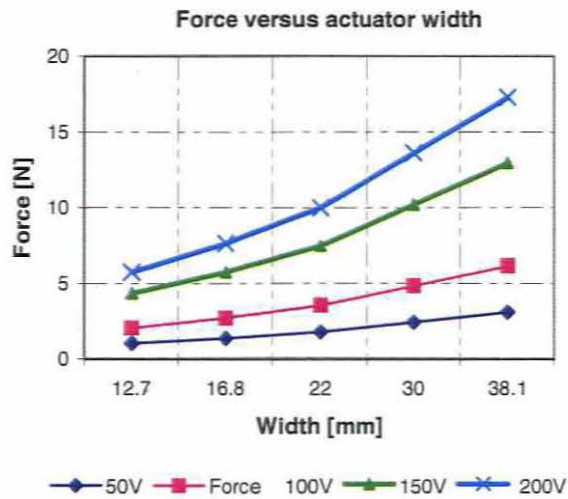


Figure 3.8: Dependence of force on actuator width

Obviously, these requirements are contradictory, which makes it necessary to seek an optimum geometry, which will provide us with most favourable values of force as well as displacement.

To illustrate this idea we can refer to results from case studies (1-3) for the range of external radii, thickness and width tested, where the following set of dimensions was found to provide favourable values of displacement and force for the basic actuator element, see table 3.2.

1. External radius = 10mm,
2. Width = 22mm,
3. Total thickness $t_{pcr} = 1.480\text{mm}$ i.e.
 - (a) Piezoceramic layer thickness = 0.84mm,
 - (b) Bonding material $t_{epoxy} = 0.18$,
 - (c) Substrate $t_{substrate} = 0.46\text{mm}$

Table 3.2: Displacement and force results for the selected geometry

External Radius [mm]	Displacement [μm]	Force [N]
10.0	2.68	1.38

3.5 Numerical Validation Using Coventorware FE Software

In order to validate the analytical model, a general-purpose finite element analysis software (CoventorWare) [67] was used. The displacement and force of an individual C shape actuator was analysed.

3.5.1 Description of CoventorWare FEA Software

CoventorWare is a Finite Element Analysis software which is meant for the design and analysis of MEMS (Micro ElectroMechanical Systems), fluidic components and subsystems. CoventorWare consists of four main modules that may be used either as stand-alone analysis tools or integrated into a complete design flow:

ARCHITECT – This module is used to quickly explore design alternatives and optimize performance.

DESIGNER – is a physical design tool that contains a 2-D layout editor, materials property editor and database, as well as an automatic 3-D model generator.

ANALYZER – is a multi-physics numerical analysis framework. The analyzer is used to support the physics required to design any device and is used with **DESIGNER** to verify designs.

INTEGRATOR - creates non-linear complex reduced-order MEMS models from detailed models created in **ANALYZER** that run in system simulation tools [67].

3.4.4.2 Analysis Procedure

Material properties were selected and set in the material properties database settings as per material data (table 2 in appendix A). This was followed by creating a process flow for the layers i.e. piezoceramic, bonding and substrate layer this is necessary for the construction of a 3-D model from a 2-D layout. In CoventorWare, material layers are constructed in a deposit and etch sequence that emulates the actual fabrication process. The 2-D layout (model) was then created. Based on the information from the 2-D layout, the 3-D model was created ready for meshing and solving. The structure was then subdivided into smaller, simpler finite elements mesh with the following characteristics:

Mesh type – tetrahedrons,

Element order: Parabolic

Element size: 1500.

The information was then posted for solver simulation. The MechMech solver was used for the analysis of the piezoelectric physics. The surface boundary conditions were set; the left end tip was fixed, while the right end one was left free to displace. A 50 volts potential was applied across the two surfaces of the PZT material.

3.5.2 Finite Element Characterization for Piezoelectric Materials

The basic constitutive equations which describe the electromechanical behaviour of piezoelectric materials can be summarized in a strain format as follows:

$$\begin{aligned}\varepsilon &= s^E \sigma + d^t E \\ D &= d\sigma + \xi^\sigma E\end{aligned}\quad (\text{repeated equation 2.1})$$

Where ε = Strain vector (6x1), σ = Stress tensor (6x1), s = compliance matrix (6x6), D = Electric displacement vector (3x1), E = Electric field vector (3x1), ξ = permittivity matrix (3x3) and d = piezoelectric strain-coupling constant matrix (3x6). The superscripts ' σ ' and ' E ' imply that the permittivity data and the elastic coefficient data are measured under at least constant stress field and constant electric field respectively, while ' t ' stands for matrix-transpose.

The polarization and the voltage application were assumed to be in a radial direction i.e. along the thickness of the laminates.

Due to symmetry, the matrices describing the electromechanical behaviour of piezoelectric materials, assuming orthotropic behaviour of PZT material are represented as follows:

$$[s^E] = \begin{bmatrix} s_{11}^E & s_{12}^E & s_{13}^E & 0 & 0 & 0 \\ s_{12}^E & s_{11}^E & s_{13}^E & 0 & 0 & 0 \\ s_{13}^E & s_{13}^E & s_{33}^E & 0 & 0 & 0 \\ 0 & 0 & 0 & s_{44}^E & 0 & 0 \\ 0 & 0 & 0 & 0 & s_{44}^E & 0 \\ 0 & 0 & 0 & 0 & 0 & s_{66}^E \end{bmatrix} \quad (3.12)$$

$$[d] = \begin{bmatrix} 0 & 0 & 0 & 0 & d_{15} & 0 \\ 0 & 0 & 0 & d_{15} & 0 & 0 \\ d_{31} & d_{31} & d_{33} & 0 & 0 & 0 \end{bmatrix} \quad (3.13)$$

$$\xi^s = \begin{bmatrix} \xi_{11}^\sigma & 0 & 0 \\ 0 & \xi_{11}^\sigma & 0 \\ 0 & 0 & \xi_{22}^\sigma \end{bmatrix} \quad (3.14)$$

The piezoelectric material constants assigned to the model are shown in table 2 in appendix A. The piezoelectric constant data were assigned through piezo-strain option. The tetrahedral elements were used to create a 3D mesh model for all the layers. This type of element was chosen due to the fact that they can easily be applied to create models with more complex shapes.

3.5.3 Numerical Analysis Results

The numerical analysis results for the displacement output when compared to predicted results are shown in figures 3.9a to 3.9d.

3.6 Discussion of results

The results obtained using the general purpose CoventorWare finite element software are in reasonable agreement with the theoretical results.

A slight difference in results figures 3.9a to 3.9d can be justified by the following reasons. In the theoretical model, contrary to the 2-D, plain stress numerical analysis, the following assumptions were made:

The actuator is thin, and a one-dimensional state of the actuating device, in which shear and Poisson's effect were ignored.

Isotropic elastic properties for the piezoceramic material were assumed.

Generally, it is evident that in order to obtain an actuator capable of certain performance, optimization of the materials selected and the geometry of the basic building element is necessary. The results are a useful guide for the selection of PZT material and geometry when optimizing the design of an individual C-shape actuator coupled to the primary requirement of whether the large force or large displacement is being sought.

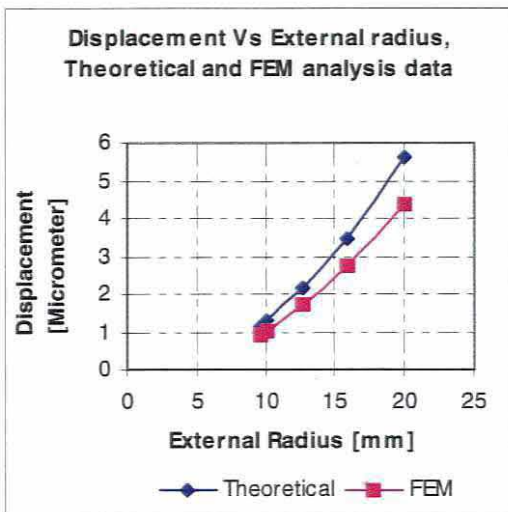


Figure 3.9a: Predicted and FEM (CoventorWare) Displacement analysis results for various external radii, at 50V input voltage.

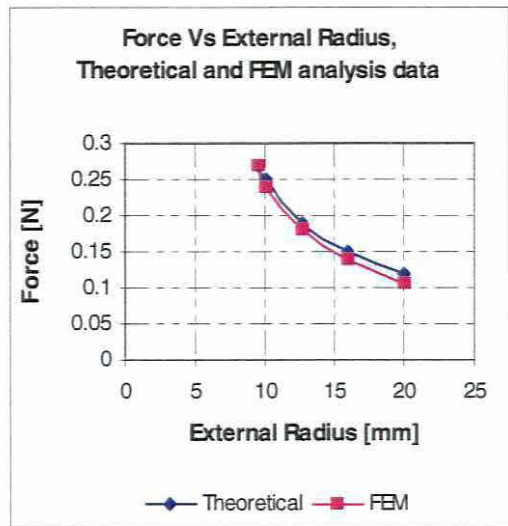


Figure 3.9b: Predicted and FEM (CoventorWare) force analysis results for various external radii, at 50V input voltage

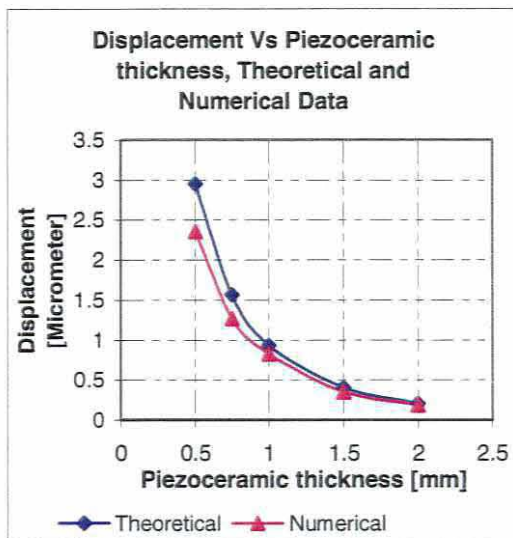


Figure 3.9c: Predicted and FEM (CoventorWare) displacement analysis results for various piezothickness, at 50V input voltage.

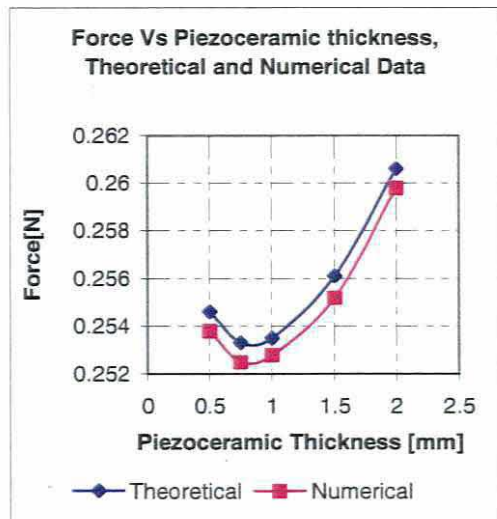


Figure 3.9d: Predicted and FEM force (CoventorWare) analysis results various piezothickness, at 50V input voltage.

CHAPTER FOUR

Influence of Substrate Thickness and Material Properties on the Displacement and Force of a C – Shape Actuator.

4.1 Introduction

It has been established that the geometry and obviously the electromechanical properties of the piezoceramic material are of paramount importance in determining the performance of any piezoelectric actuator. In many cases when the piezoceramic material is used in conjunction with the substrate (particularly in flexural mode), the influence of the substrate geometry to the actuator performance has been overlooked.

This chapter focuses on an investigation of the contribution of the substrate on the performance of the C-shape actuator. Influence of parameters such as Young's modulus, substrate/PZT thickness ratio on the displacement and force of the element were investigated. The information obtained is useful for determining the appropriate or optimized geometry for a given set of elastic properties of a substrate.

4.2 Optimization of the Substrate Geometry and Material

4.2.1 Case Study 4: Influence of Substrate/PZT Thickness Ratio

At first, the free displacement and blocked force were investigated for a PZT layer alone (i.e. without substrate) for which it was found that the values for displacement and force were negligibly small (i.e. almost zero). This is easily explainable by the fact that the neutral axis of the element coincides with the midline of the PZT layer resulting in zero moment arm, and hence zero piezoelectric moment (equations 3.9, 3.11 and 3.12). By introducing a passive/substrate layer to the PZT layer/element, thus forming a composite, an increase of both displacement and force was noted. Further increase of thickness of passive layers, unlike the force, which kept on increasing (figure 4.2), the free displacement, reached a certain maximum value after which it started to decrease (figure 4.1).

An investigation was conducted for various thickness of the piezo-ceramic layer (0.75mm, 0.84mm, 1.0mm, and 1.35mm and 1.5mm). The thickness for the bonding layer (epoxy) was fixed at 0.18mm and the substrate thickness was varied for each PZT thickness as indicated above. In this manner the substrate to the PZT ratio ranged from 0.1 to 1.0. It can be concluded from figure 4.1 that for a given PZT thickness of a C-shaped actuator there is a substrate thickness that yields the highest value of displacement.

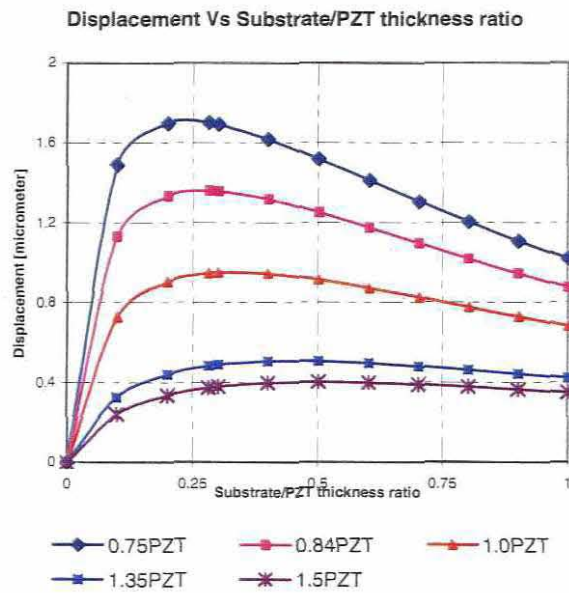


Figure (4.1). Actuator displacement from different substrate thickness for a 10mm width brass substrate, 50 volts

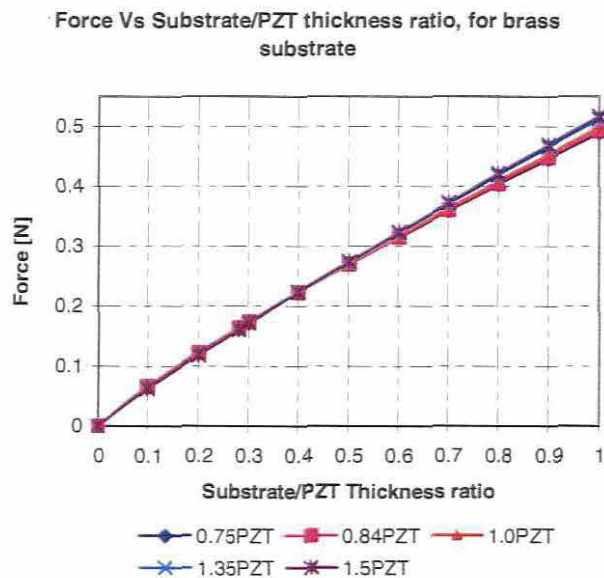


Figure 4.2: Actuator displacement from different substrate thickness for a 10mm width brass substrate, 50 volts

A similar observation was reported by Xiaoping Li et al [68] when examining the electromechanical behaviour of PZT-Brass unimorphs for straight bender actuators. The normalized force and displacement response in respect to thickness ratio are shown in figure 4.3.

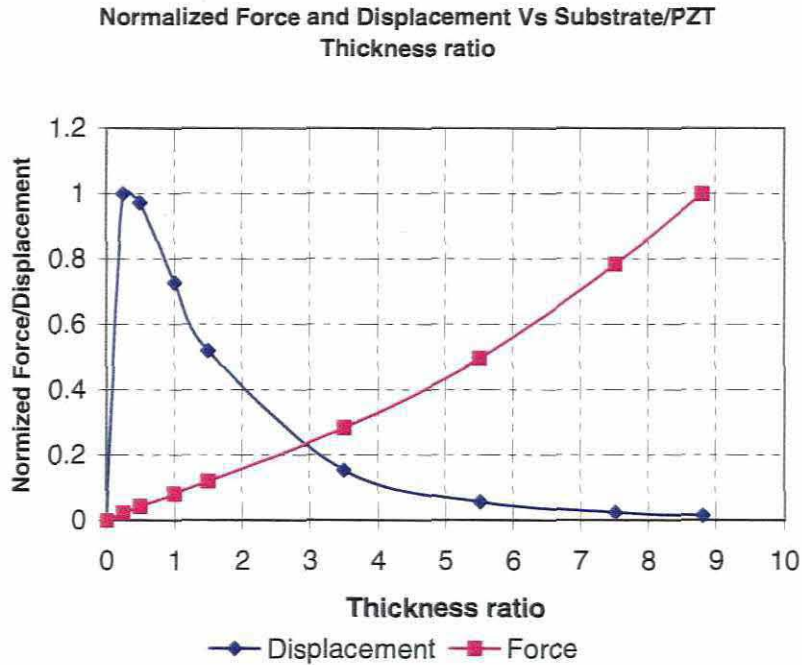


Figure 4.3: Normalized force and displacement versus substrate/PZT thickness ratio for a 1mm thickness of PZT layer at 50V

4.2.2 Case Study 5: The Effect of Elastic Properties of the Substrate Material

Further investigations were conducted to find the effect of the elastic properties of the substrate material on the actuator displacement. Three different substrate materials were compared, that is aluminium, brass and mild steel. Figure 4.4 shows that for the ratios of up to 0.6 the substrate with higher elastic modulus (mild steel in this case) gives larger displacement while beyond this ratio the situation is the other way round. At lower ratios a substrate with larger elastic modulus tends to increase the moment arm¹ (i.e. by shifting the location of neutral axis) hence larger piezoelectric moment which in turn produces larger displacement (equation 3.12). At this range of ratios the bending stiffness is relatively small. At higher thickness ratios the displacement is small for the substrate with higher Young's modulus, this is because of the rapid increase of the composite bending stiffness. This behaviour can also be explained by comparing the rates of change of both the composite stiffness and the radius of neutral axis in respect to the change in the thickness ratio. It can be seen that the rate of increase of composite stiffness at lower ratios is smaller compared to the rate of increase of the same at higher thickness ratios. The situation is different for the

¹ This is due to the fact that the radius of the neutral axis decreases.

radius of neutral axis; the rate of decrease is larger in the lower ratio zone than in the higher ratio zone (see figures 4.5, 4.6).

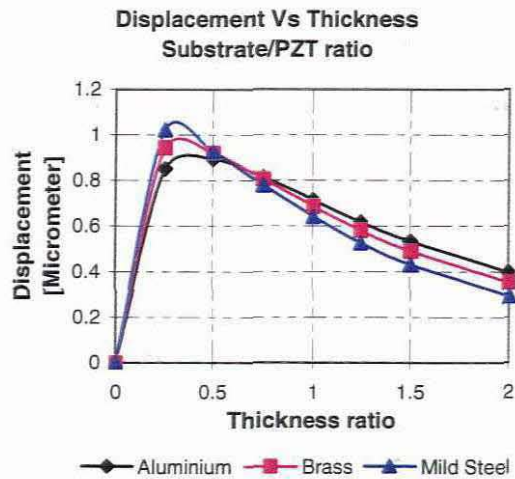


Figure 4.4: Displacement for different thickness ratios for Aluminium, Brass and Mild Steel substrate. (For 1mm thick PZT)

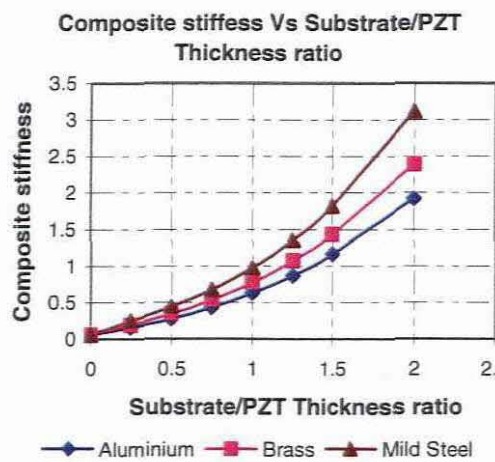


Figure 4.5: Dependence of the composite stiffness axis on the thickness ratios for different substrate materials

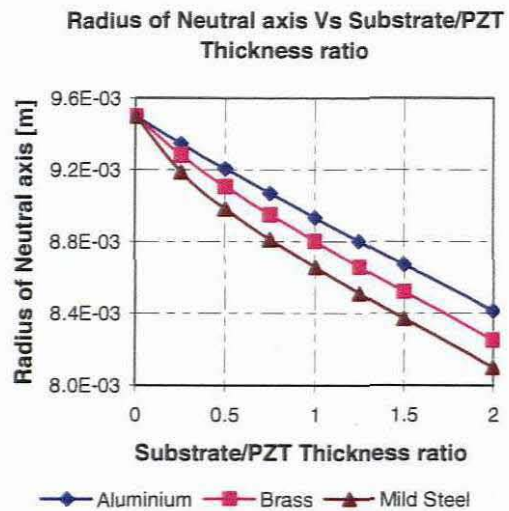


Figure 4.6: Radius of neutral axis in respect to substrate/PZT thickness ratio

4.2.3: The Coefficient of Unimorph Actuator

It was found that when the thickness of the substrate is increased the displacement was increased to a maximum value after which it started decreasing.

From elementary mechanics it is known that the deflection of the beam is determined by change of the radius of curvature of the neutral surface which depends on the change of applied bending moment and the flexural rigidity of the structure, that is:

$$\Delta \frac{1}{R} = \frac{\Delta M}{D} \quad (4.1)$$

Where R is the radius of curvature and

$D = \sum_{i=1}^n Q_i I_i$ is the flexural rigidity (bending stiffness) of the actuator layers.

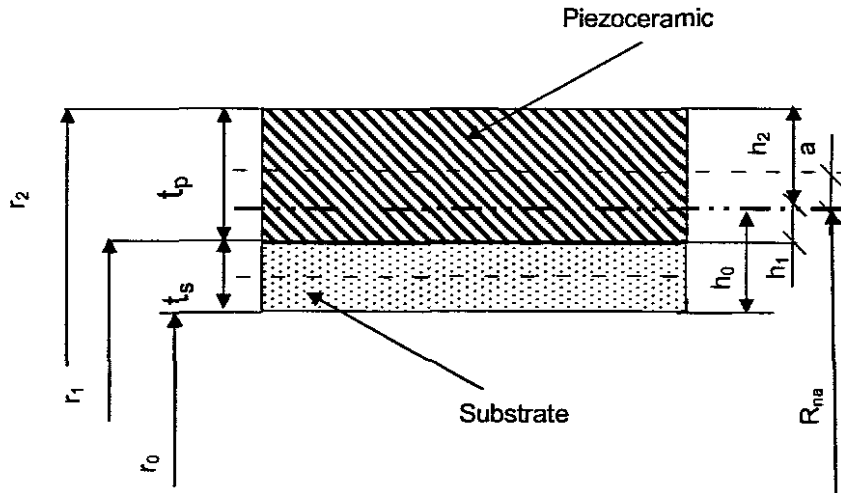


Figure 4.7: A cross section of the C-actuator

If pure bending is assumed and that the bending moment is only due to induced piezoelectric strain of the actuator then we can rewrite equation 3.7 as follows:

$$\Delta M = \Delta M^{pe} = Q_p b (h_2 - h_1) \frac{(h_1 + h_2)}{2} d_{31} \frac{\Delta V}{t_p} \quad (4.2)$$

Using figure 4.7 we can substitute $t_p = (h_2 - h_1)$, $h_1 = r_1 - R_{na}$ and $h_2 = r_2 - R_{na}$ in equation 4.2 and we obtain:

$$M^{pe} = Q_p t_p b \frac{(r_1 - R_{na} + r_2 - R_{na})}{2} d_{31} \frac{\Delta V}{t_p}$$

$$M^{pe} = Q_p b t_p \left\{ \frac{r_1 + r_2}{2} - R_{na} \right\} d_{31} \frac{\Delta V}{t_p} \quad (4.3)$$

The expression in the bracket represents the moment arm a , that is

$$a = \frac{r_1 + r_2}{2} - R_{na} \quad (4.4)$$

Substituting equation 4.3 into equation 4.1 and after rearrangement we obtain

$$\Delta \frac{1}{R} = \frac{a}{\sum_{i=1}^n Q_i I_i} Q_p b t_p d_{31} \frac{\Delta V}{t_p}$$

$$\Delta \frac{1}{R} = \frac{a}{D} Q_p b t_p d_{31} \frac{\Delta V}{t_p} \quad (4.5)$$

In equation 4.5 it is observed that irrespective of the magnitude of the applied voltage, the change of curvature will depend on the ratio of the moment arm a to the bending stiffness D of the actuator. An increase in the moment arm and a decrease in the bending stiffness yields larger displacement.

It was established earlier that by changing the substrate/PZT thickness ratio i.e. by increasing the substrate thickness, the moment arm and the flexural rigidity change simultaneously.

The ratio between the moment arm (equation 4.6) and the bending stiffness has been defined as the coefficient of unimorph actuator c_{ua} [29] [69]. It is obvious that an optimum value of c_{ua} should indicate the optimum displacement.

$$c_{ua} = \frac{a}{D} \quad (4.6)$$

Thus it becomes important that we establish the relationship between the coefficient of the unimorph actuator with the substrate/PZT thickness ratio.

Equation 4.6, may be rewritten as:

$$\frac{a}{D} = \frac{r_1 + r_2 - 2R_{na}}{2 \sum_{i=1}^n Q_i I_i} \quad (4.7)$$

For a fixed piezoelectric thickness, the coefficient of unimorph actuator will only depend on the radius of the neutral axis and the second moment of area about the neutral axis. Substituting the expressions for second moment of areas for the PZT and the substrate in equation 4.7 we have:

$$c_{ua} = \frac{r_1 + r_2 - 2R_{na}}{2 \left\{ Q_p \left(\frac{b t_p^3}{12} + b t_p h_p^2 \right) + Q_s \left(\frac{b t_s^3}{12} + b t_s h_s^2 \right) \right\}} \quad (4.8)$$

The first and the second terms in the denominator of equation 4.8 represent the bending stiffness of the piezoceramic and the substrate layers respectively while the expressions in

the respective brackets represent their corresponding second moments of area about the neutral axis.

Where h_p and h_s are the distances from the mid-surfaces of the PZT layer and the substrate layer respectively to the neutral axis.

By varying the substrate thickness t_s it is obvious that the radius of the neutral axis and the parameters h_p and h_s will vary accordingly. This makes the process of establishing the equation which describes the relationship between the coefficient of the unimorph actuator and the thickness ratio rather complicated. To be able to obtain the mathematical relationship between the two quantities the following approach was adopted:

1. Using equations 4.4 and 3.10 different values of a were obtained for a selected number of substrate/PZT thickness ratios.
2. Equation 3.6 was used to obtain different values of D for the same thickness ratios as in 1 above.
3. Equation 4.6 was then used to calculate different values of the coefficient of unimorph actuator.
4. The c_{ua} versus substrate/PZT thickness ratio graph was plotted using Ms excel software using data from step 3.
5. The trend line tool was used to estimate the equation. The polynomial equation of fifth order was found to give accurate estimation (i.e. regression coefficient of 0.9966)

$$c_{ua} = 0.0017\chi^5 - 0.0095\chi^4 + 0.0199\chi^3 - 0.0192\chi^2 + 0.008\chi + 4E - 08 \quad (4.9)$$

Where $\chi = \frac{t_s}{t_p}$, is the ratio between the thickness of the substrate layer to the thickness of piezoceramic layer.

6. Based on equation 4.9 the coefficient of unimorph actuator versus the substrate/PZT thickness ratio was plotted with the aid of MATLAB (see figure 4.8).

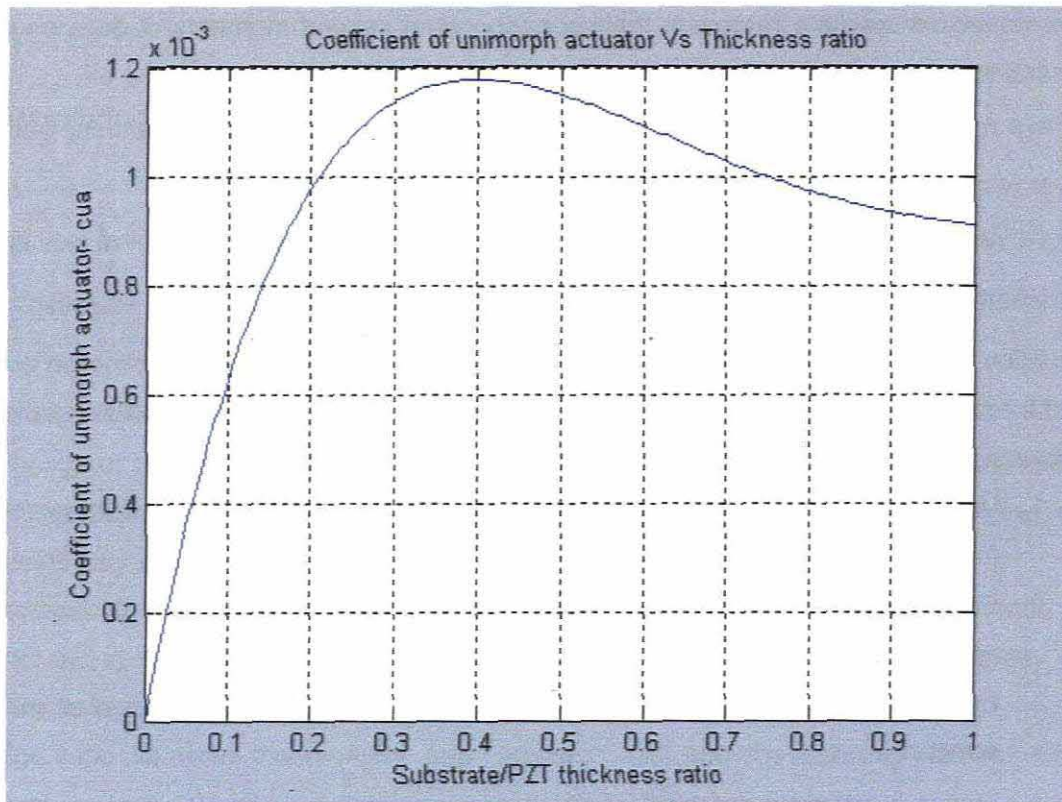


Figure 4.8: Relationship between the coefficient of unimorph actuator and the substrate/PZT thickness ratio

The procedure described in this section 4.2.3 has demonstrated what has been defined as the coefficient of unimorph actuator which depends on the thickness ratio between the substrate and PZT (figure 4.8).

- There is a similarity between the c_{ua} - thickness ratio relationship to that of the displacement – thickness ratio that has been obtained in section 4.2.1 (figure 4.1). However it is not apparent that the ratio between the moment arm and the composite bending stiffness (c_{ua}) can be used to determine the optimum value of displacement.

4.2.4 Determining the Appropriate Location of the Neutral Axis

The investigation on the influence of geometry (i.e. thickness ratio of actuator layers) on displacement and force has shown that maximum displacement is obtained at a substrate/PZT thickness ratio of approximately 0.35, however, for a unimorph C-shape actuator this ratio locates the neutral axis somewhere inside the PZT layer. This situation is suitable for static operations where the working motion is a unidirectional. Regarding to the safety of the piezoceramic material, especially when the actuator is to operate under large external dynamic loading (or high frequency) the neutral axis is recommended to be located out of the piezoceramic layer. It is important therefore, to determine from the given substrate and piezoceramic elastic properties, and given geometry of the piezoceramic layer the

suitable substrate thickness, which will locate the neutral axis outside the PZT layer. This approach is chosen based on the fact that the location of the neutral axis of a laminated structure is determined by both the geometry and the elastic properties of its members. Piezoceramic materials are relatively expensive and difficult to manufacture and because it is a core determinant of the electromechanical coupling effect its characteristics are normally predefined. The simplest and cheaper approach would be to adjust the substrate geometry. This is done by simply optimizing the internal radius of the substrate. Substrate materials in most cases are cheap, readily available and easy to fabricate.

The main task here is to determine the inner radius of the substrate layer, which will locate the radius of the neutral axis out of the PZT layer.

In equation 3.10 the radius of neutral axis will be out of the PZT layer if the following condition is fulfilled:

$$R_{na} \leq (r_1) \tag{4.10}$$

Where r_1 is the internal radius of the PZT layer (figure 4.11).

$$(r_{j-1})_{pzt} \geq \frac{\sum_{j=1}^n 0.5Q_{Ej} b_j (r_j^2 - r_{j-1}^2)}{\sum_{j=1}^n Q_{Ej} b_j (r_j - r_{j-1})} \tag{4.11}$$

If we ignore the thickness of the bonding material (for simplicity), assuming equal width of layers and that the substrate layer conforms into the inner surface of the PZT layer (figure 4.9), the above equation in an expanded form becomes:

$$r_1 \geq \frac{0.5Q_{sub} (r_1^2 - r_0^2)_{sub} + 0.5Q_{pzt} (r_2^2 - r_1^2)_{pzt}}{Q_{sub} (r_1 - r_0)_{sub} + Q_{pzt} (r_2 - r_1)_{pzt}}$$

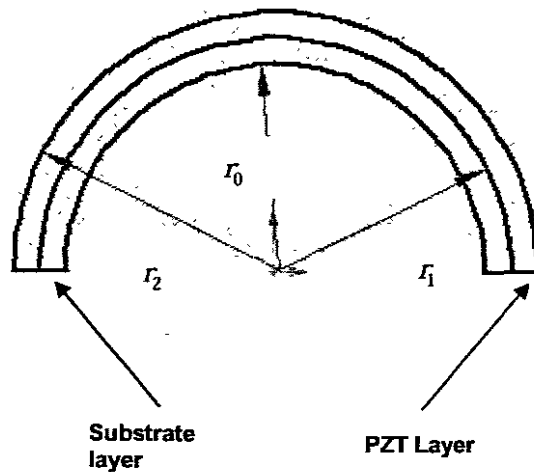


Figure 4.9: Individual C-shape actuator

Cross-multiplying and collecting like terms we obtain:

$$Q_{sub} r_1^2 - Q_{pzt} r_1^2 - 2Q_{sub} r_1 r_0 + 2Q_{pzt} r_1 r_2 + Q_{sub} r_0^2 + Q_{pzt} r_2^2 \geq 0$$

$$(Q_{sub} - Q_{pzt}) r_1^2 + Q_{pzt} (2r_1 r_2 - r_2^2) + Q_{sub} (-2r_1 r_0 + r_0^2) \geq 0$$

Letting γ be the ratio of the elastic modulus of the PZT to substrate layers:

$$\gamma = \frac{Q_{pzt}}{Q_{sub}} . \text{ And the ratio}$$

$$\beta = \frac{Q_{sub} - Q_{pzt}}{Q_{sub}}$$

We have:

$$r_0^2 - 2r_1 r_0 + \beta r_1^2 + \gamma (2r_1 r_2 - r_2^2) \geq 0 \quad (4.12)$$

Solving the quadratic equation in terms of r_0

$$r_0 = r_1 \pm \sqrt{r_1^2 - (\beta r_1^2 + \gamma (2r_1 r_2 - r_2^2))}$$

From the condition given by equation 4.10, the only valid value for r_0 will be

$$r_0 = r_1 - \sqrt{r_1^2 - (\beta r_1^2 + \gamma (2r_1 r_2 - r_2^2))}$$

Hence

$$r_0 \leq r_1 - \sqrt{r_1^2 - (\beta r_1^2 + \gamma (2r_1 r_2 - r_2^2))} \quad (4.13)$$

Equation 4.6 yields values of internal radius of the substrate in terms of elastic moduli and the geometry of the PZT layer which will locate the neutral axis outside the PZT layer. The values for internal radii for selected substrate materials are shown in table 4.2 and the corresponding radii of neutral axis are shown in figure 4.10.

As it was mentioned earlier, in order to obtain a large displacement output, flexible actuator is required while for large force, a considerable stiff actuator will be appropriate. Displacement and force output for the out -of- PZT layer neutral axes for the selected substrate materials are shown in figures 4.11 and 4.12 respectively.

Table 4.2: Internal radii for a substrate layer for selected substrate materials and external radii.

Material	Young's Modulus [Gpa]	r_1 [m]	r_2 [m]	γ [m]	β [m]	r_0 [m]
Aluminium	70	9.00E-03	1.00E-02	1.086	-8.60E-02	7.96E-03
Brass	130	9.00E-03	1.00E-02	5.85E-01	4.15E-01	8.24E-03
Stainless Steel	210	9.00E-03	1.00E-02	3.60E-01	6.40E-01	8.40E-03

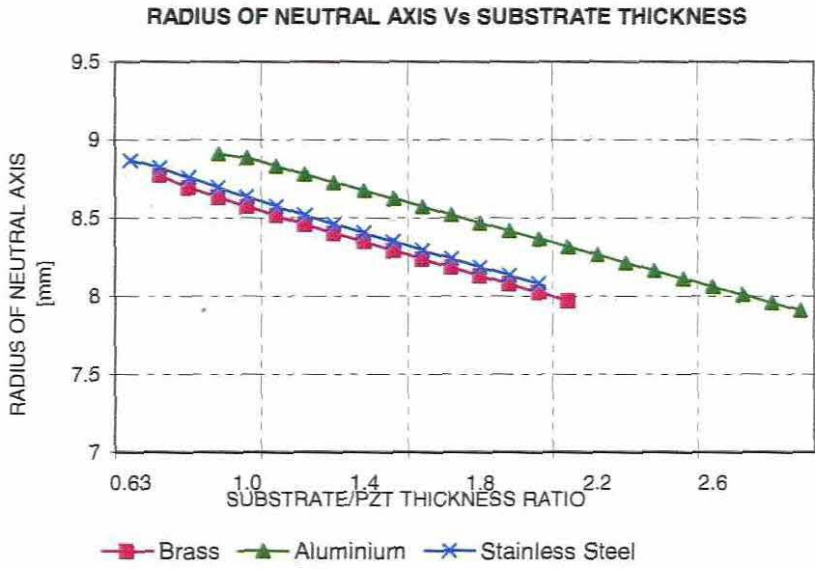


Figure 4.10: Radius of neutral axis for a range of substrate/PZT thickness ratios for different substrate materials

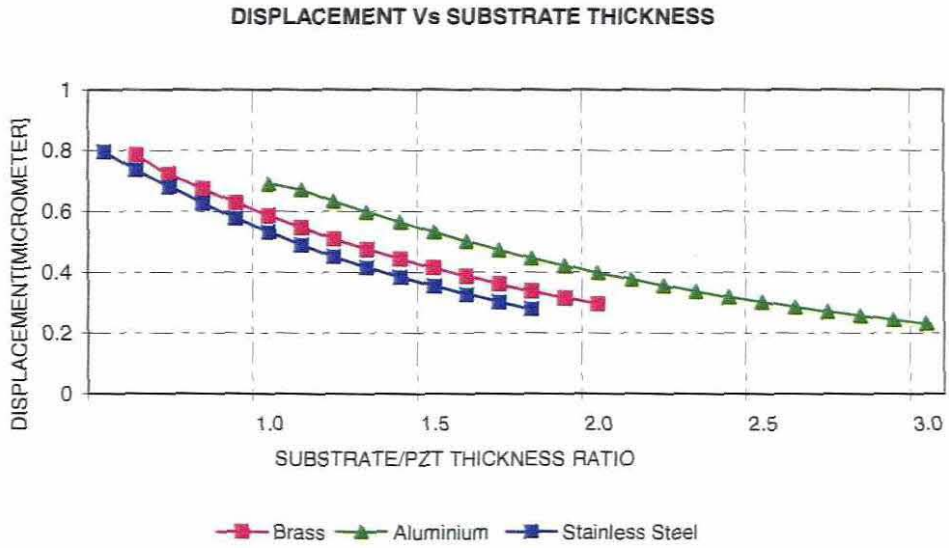


Figure 4.11: Displacement for a range of substrate thickness/PZT thickness ratios for different substrate materials

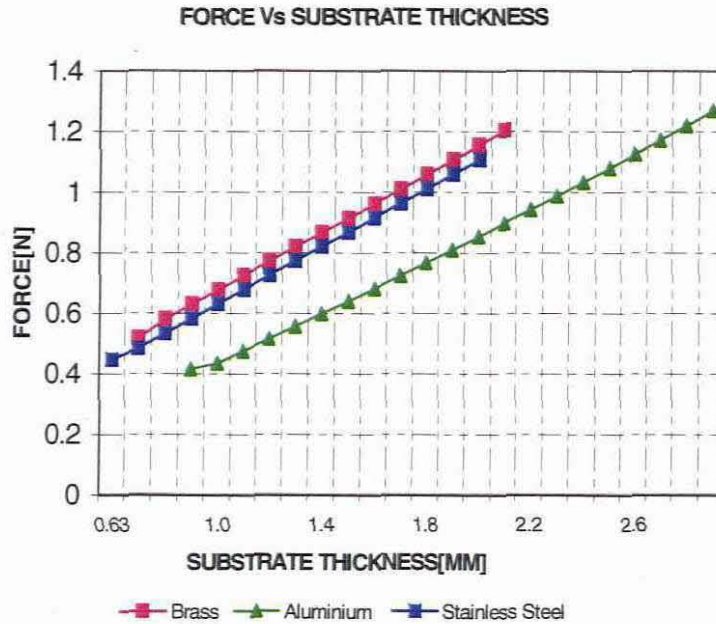


Figure 4.12: Force for a range of substrate thicknesses from different substrate materials

4.2.5 Dependence of the Radius of Neutral Axis on the Substrate Material's Elastic Properties

The main objective of this study is to establish the effect of the substrate material's elastic properties on the location of the neutral axis of the C-shape unimorph piezoelectric actuator. The radius of the neutral axis for the curved shape composite beam is given by equation 3.10 that is:

$$R_{na} = \frac{\sum_{j=1}^n 0.5Q_j E_j b_j (r_j^2 - r_{j-1}^2)}{\sum_{j=1}^n Q_j E_j b_j (r_j - r_{j-1})} \quad \text{(Repeated equation 3.10)}$$

Assumptions

- (1) Actuator is of a unimorph configuration
- (2) Bonding layer is neglected
- (3) Both layers are of equal width

Subscripts 0 and 1 indicate the inner and outer radii of the substrate material respectively and subscripts 1 and 2 are for the inner and outer radii of the PZT layer respectively (figure 4.9). This implies that the substrate layer conforms into inner surface of the PZT layer. Taking into consideration the above assumptions, equation 3.10 in an expanded form becomes:

$$R_{na} = \frac{0.5Q_{sub} (r_1^2 - r_0^2) + 0.5Q_{pzt} (r_2^2 - r_1^2)}{Q_{sub} (r_1 - r_0) + Q_{pzt} (r_2 - r_1)} \quad :$$

$$R_{na} = \frac{0.5Q_{sub} (r_1 - r_0)(r_1 + r_0) + 0.5Q_{pzt} (r_2 - r_1)(r_2 + r_1)}{Q_{sub} (r_1 - r_0) + Q_{pzt} (r_2 - r_1)} \quad (4.14)$$

Taking

$t_{sub} = (r_1 - r_0)$ = Substrate layer thickness

$t_{pzt} = (r_2 - r_1)$ = PZT layer thickness

$2r_{m(sub)} = (r_1 + r_0)$ = Mean radius for substrate layer and

$2r_{m(pzt)} = (r_2 + r_1)$ = Mean radius for PZT layer

Equation 4.14 becomes:

$$\begin{aligned} R_{na} &= \frac{Q_{sub} t_{sub} r_{m(sub)} + Q_{pzt} t_{pzt} r_{m(pzt)}}{Q_{sub} t_{sub} + Q_{pzt} t_{pzt}} \\ &= \frac{Q_{sub} r_{m(sub)} + Q_{pzt} \frac{t_{pzt}}{t_{sub}} r_{m(pzt)}}{Q_{sub} + Q_{pzt} \frac{t_{pzt}}{t_{sub}}} \end{aligned} \quad (4.15)$$

Taking $\alpha = Q_{pzt}^E \frac{t_{pzt}}{t_{sub}}$, equation 4.15 becomes:

$$R_{na} = \frac{Q_{sub} r_{m(sub)} + \alpha r_{m(pzt)}}{Q_{sub} + \alpha} \quad (4.16)$$

The effect of the Young's modulus of the substrate material on the location of the neutral axis is shown in figure 4.13

Radius of Neutral axis Vs Young's Modulus of elasticity of Substrate material

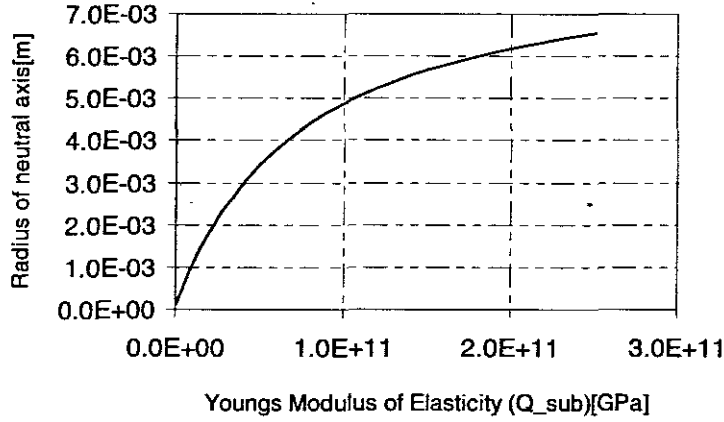


Figure 4.13: Dependence of the radius of neutral axis on the elastic constant of substrate material.

From equation 4.16, if we assume that the actuator element is made up of only PZT layer i.e. $Q_{sub}^E = 0$, then the radius of neutral axis will coincide with the mean radius, but when the substrate is introduced (figure 4.13) shows that the radius of the neutral axis increases quadratically with an increase of modulus of elasticity of the substrate.

4.2.6 Effect of Substrate Material on the Piezoelectric Moment

From equation 3.7 for the piezoelectric moment:

$$M^{pe} = \frac{1}{2} \sum_{j=1}^n b_j Q_j^E (h_j + h_{j-1}) \times (d_{31} V)_j \quad (\text{Repeated equation (3.7)})$$

Expanding equation 4.3 we have:

$$M^{pe} = \frac{1}{2} b Q_{sub} (h_1 + h_0) \times (d_{31} V)_1 + \frac{1}{2} b Q_{pzt} (h_2 + h_1) \times (d_{31} V)_2 \quad (4.17)$$

Since the electric field is applied to the piezoceramic layer only and also due to the fact that the piezoelectric strain coefficient for non-piezoceramic material is zero then the first term in equation 4.17 becomes zero, hence

$$M^{pe} = \frac{1}{2} b Q_{pzt} (h_2 + h_1) \times (d_{31} V)_2 \quad (4.18)$$

From equation 4.18 it implies that the substrate material has no direct effect on the piezoelectric moment instead as it was established in equation 4.16 it has an influence on the location of the neutral axis, hence the moment arm i.e.

$$h_j = r_j - R_{na} \quad (4.19)$$

Substituting equation 4.16 of the neutral axis into equations 4.19 we have:

$$h_j = r_j - \frac{Q_{sub} r_{m(sub)} + \alpha r_{m(pzt)}}{Q_{sub} + \alpha} \quad (4.20a)$$

$$h_1 = \frac{\left(r_1 - r_{m(sub)}\right) Q_{sub} + \left(r_1 - r_{m(pzt)}\right) \alpha}{Q_{sub} + \alpha} \quad (4.20b)$$

And

$$h_2 = \frac{\left(r_2 - r_{m(sub)}\right) Q_{sub} + \left(r_2 - r_{m(pzt)}\right) \alpha}{Q_{sub} + \alpha} \quad (4.20c)$$

Substituting equations 4.20b and 4.20c into equation 14.18 we obtain

$$M^{pe} = \frac{1}{2} b Q_{pzt} \left(\frac{\left(r_2 - r_{m(sub)}\right) Q_{sub} + \left(r_2 - r_{m(pzt)}\right) \alpha + \left(r_1 - r_{m(sub)}\right) Q_{sub} + \left(r_1 - r_{m(pzt)}\right) \alpha}{Q_{sub} + \alpha} \right) \times (d_{31} V)$$

Taking $2r_{m(pzt)} = r_2 + r_1$ then

$$M^{pe} = b Q_{pzt} (d_{31} V) \left(\frac{\left(r_{m(pzt)} - r_{m(sub)}\right) Q_{sub}^E}{Q_{sub}^E + \alpha} \right)$$

Taking

$$K = b Q_{pzt}^E (d_{31} V) \left(r_{m(pzt)} - r_{m(sub)} \right) \text{ we obtain:}$$

$$M^{pe} = \frac{K Q_{sub}}{Q_{sub} + \alpha} \quad (4.21)$$

The effect of the Young's modulus of the substrate material on magnitude of piezoelectric moment is shown in figure 4.14

Figures 4.13 and 4.14, reveal that the radius of neutral axis and the piezoelectric moment are influenced more or less in a similar manner by the elastic moduli of the substrate material.

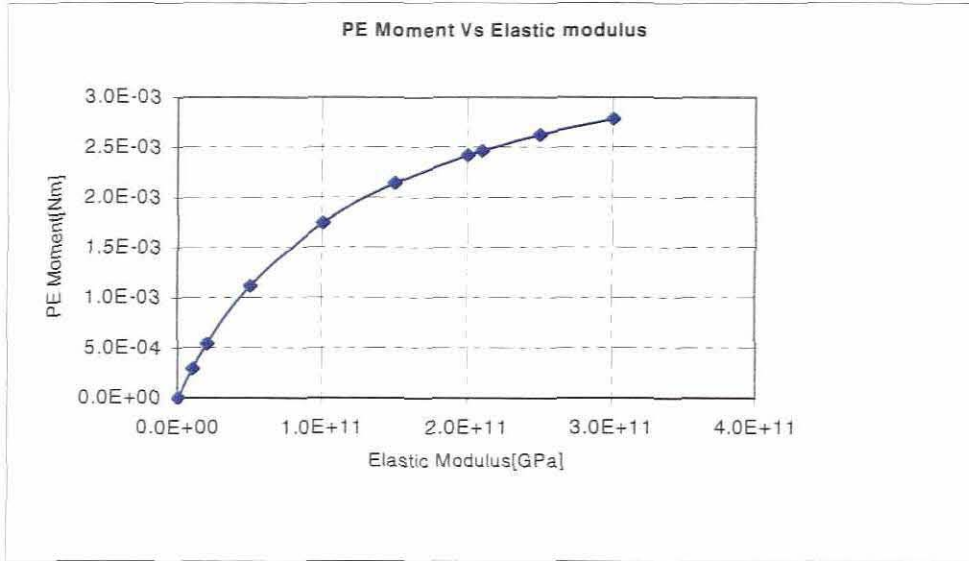


Figure 4.14: Dependence of piezoelectric moment on the elastic properties of the substrate material

4.2.7 Effect of Elastic Modulus of a Substrate Material on the Blocked Force.

In order to establish the direct relationship between the elastic modulus of the substrate material and the blocked force, equations 4.16 and 4.21 are substituted in equation 3.7 and we obtain:

$$P_b = \frac{4KQ_{sub}}{\pi(Q_{sub}r_{m(sub)} + \alpha r_{m(pzt)})}$$

$$P_b = \frac{K^1 Q_{sub}}{(Q_{sub}r_{m(sub)} + \alpha^1 r_{m(pzt)})} \quad (4.22)$$

Where

$$K^1 = \frac{4K}{\pi} \quad \text{and} \quad \alpha^1 = \alpha r_{m(pzt)}$$

The manner in which the elastic modulus influences the actuator force is shown in figure 4.15

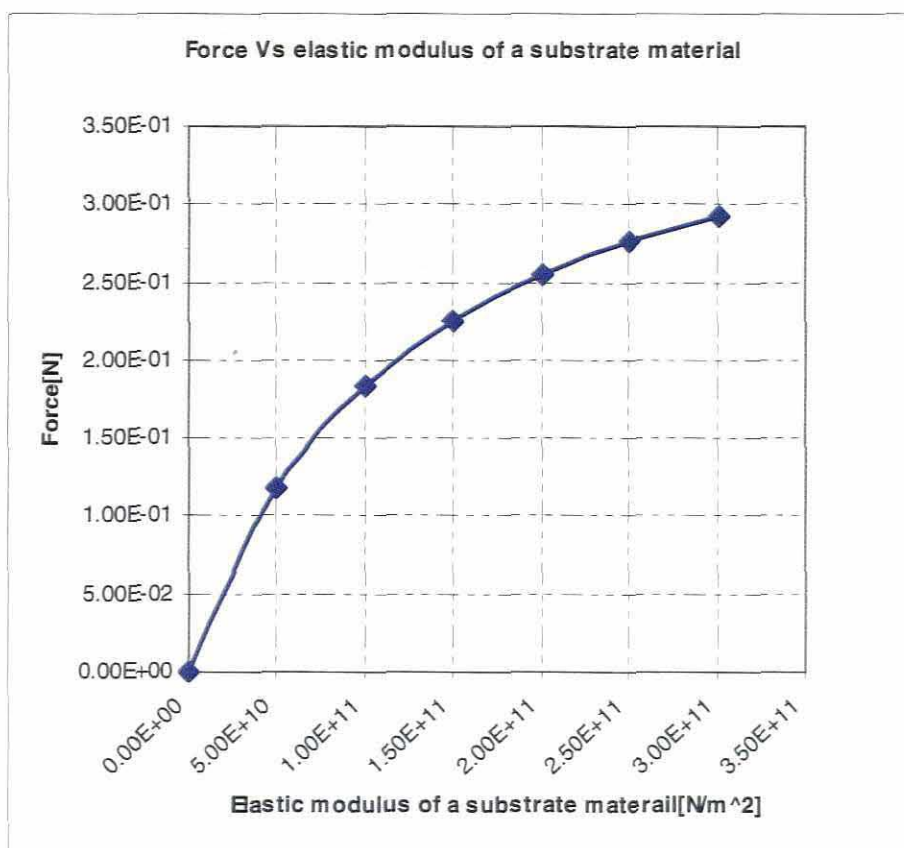


Figure 4.15: Relationship between blocked force and the elastic modulus of a substrate material

4.3 Discussion of results

The substrate/PZT thickness ratio as well the substrate's Young's modulus have a major role in determining the position of the neutral axis (N.A) and thus the moment arm which is defined as the distance between the midline of the PZT layer² to the neutral axis. The position of the neutral axis also determines the portion/part of the cross-section of the PZT layer which will be subjected to compression/tension load during the forward and backward strokes of the actuator especially when subjected to an alternating electric field. The farther the neutral axis goes away from the midline of the structure the larger the moment arm and hence the larger the piezoelectric moment

At the ratio of 1:1 the whole PZT layer will more likely be loaded by a compressive load during the inward stroke and vice versa.

For the thickness ratio which gives the peak displacement, low voltages can be used to produce the same amount of displacement which would have demanded higher voltages if a much thicker actuator was used. From this study it was concluded, that total actuator thickness alone is not enough to determine the actuator performance. It was found that

² The position where the piezoelectric force is assumed to act

thickness ratios between (0.25 – 0.35) produce maximum displacement and relatively small force. For ratios beyond this range the displacement decreases while the force increases. The recommended substrate/PZT thickness ratios which will yield optimum displacement values and thus obviously useful for engineering purposes are shown by the dotted line (Figure 4.16).

The results should be of interest to designers wishing to establish how much force will be sacrificed by choosing to have a certain amount of displacement and vice versa. The results also help to determine the appropriate geometry (i.e. thickness ratio) as well as the suitable substrate material if one aims for large displacement and/or large force. In the case where two quantities are to have reasonable compromise between them perhaps the maximum work done

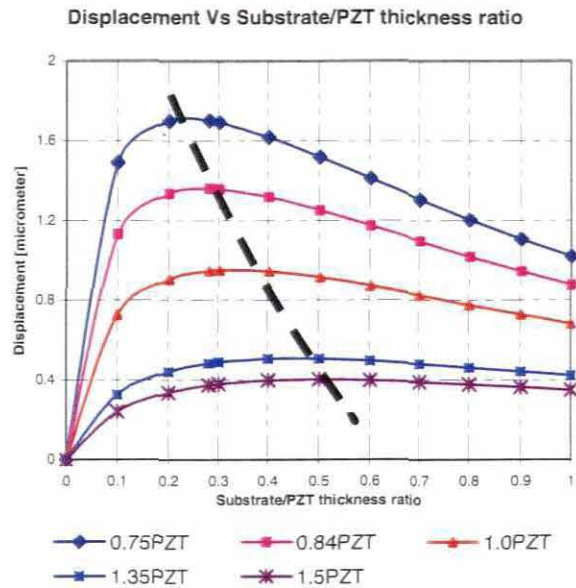


Figure 4.16: Recommended Substrate/PZT thickness ratios for engineering use

will be the best criterion for the selection of the appropriate substrate/PZT thickness. For the given PZT thickness and substrate material, it is indicated that the thickness ratio of 1.5 will produce maximum work output figure 4.17. This can also be shown from figure 4.18 that the maximum work output will be produced from the Force-displacement curve which has a slope of approximate forty five degrees.

In addition, the results obtained from this study assist the designer while making a decision on an appropriate number of C- actuators in series and/or parallel depending on the desired values of force and displacement

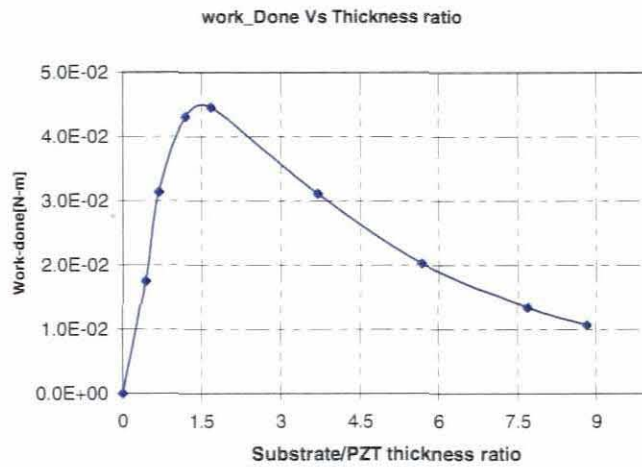


Figure 4.17: Work done of the C- block actuator with respect to thickness ratio (Substrate/PZT), 1mm PZT layer, at 50

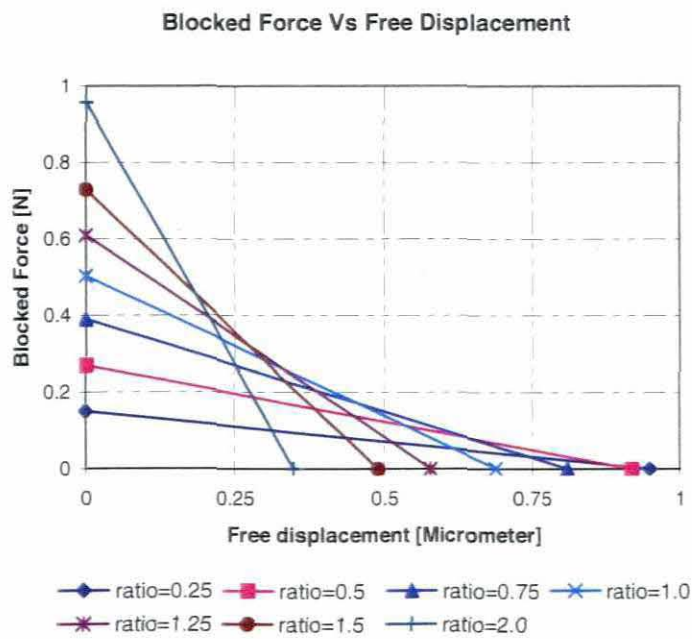


Figure 4.18: Blocked force versus free displacement for selected substrate/PZT ratios for a 1mm thickness of PZT layer at 50V

4.4 Finite Element Validation Using MSC Marc.

A finite element simulation was used in order to validate the results of the analytical study on the influence of substrate/PZT thickness ratio on the actuator performance. For this purpose general-purpose finite element analysis software (MSC Marc) was used. MSC. Marc contains a fully coupled implementation of piezoelectric analysis, which enables simultaneous solving for the nodal displacements and electrical potential.

As mentioned before (in section 3.4.4.3), finite element formulation is based on the general constitutive equations that describe the electromechanical behaviour of piezoelectric materials equation 2.1

$$\begin{aligned} \varepsilon &= s^E \sigma + d^T E \\ D &= d \sigma + \xi^\sigma E \end{aligned} \quad \text{(repeated equation (2.1))}$$

4.4.1 Strain

Strain in terms of displacements for each element may be expressed:

$$\varepsilon^{(e)} = [B_u] \{u\}^{(e)} \quad (4.23)$$

Where: $\{u\}^{(e)}$ is an elemental vector of displacement, and

$[B_u]$ is the matrix containing derivatives of shape functions for the displacements.

4.4.2 Electric Field

In an element, the electric field can be expressed in terms of potential

$$\{E\} = -[B_\varphi] \{\varphi\} \quad (4.24)$$

Where $[B_\varphi]$ is a matrix containing derivatives of shape functions for potential

φ = Nodal potential.

Substituting equations 4.23 and 4.24 into equation 2.1 we obtain:

$$\begin{aligned} \{\sigma\} &= [Q_E] [B_u] \{u\} + [d]^T [B_\varphi] \{\varphi\} \\ \{D\} &= [d] [B_u] \{u\} + [\xi] [B_\varphi] \{\varphi\} \end{aligned} \quad (4.25)$$

But on the other side the general force equilibrium equation in the elasticity problem according to Hellinger –Reissner principle is:

$$\begin{aligned} \int_v \left(\{\delta \varepsilon\}^T \{\sigma\} \right) dv &= \{\delta u\}^T \{F\} \\ - \int_v \left(\{\delta E\}^T \{D\} \right) dv &= \{\delta u\}^T [Q^E] \end{aligned} \quad (4.26)$$

And

$$\begin{aligned} \{\delta \varepsilon\}^T &= \{\delta u\}^T [B_u]^T \\ \{\delta E\}^T &= \{\delta \varphi\}^T [B_\varphi]^T \end{aligned} \quad (4.27)$$

Where

$\delta \varepsilon$ and δu are virtual strain and virtual displacement vectors respectively, and δE is the virtual electric field vector.

Substituting equations 4.25 and 4.27 into equation 4.26 we have:

$$\begin{aligned} \{\delta u\}^T \int_v \left[[B_u]^T [Q_E] [B_u] \{u\} + [B_u]^T [d]^T [B_\varphi] \{\varphi\} \right] dv &= \{\delta u\}^T \{F\} \\ \{\delta \varphi\}^T \int_v \left[[B_\varphi]^T [d] [B_u] \{u\} - [B_\varphi]^T [\xi] [B_\varphi] \{\varphi\} \right] dv &= \{\delta \varphi\}^T [Q_E] \end{aligned} \quad (4.28)$$

Simplifying equation 4.28 we obtain the elemental finite element equations as:

$$\begin{bmatrix} [K_{uu}] & [K_{u\varphi}] \\ [K_{\varphi u}] & [K_{\varphi\varphi}] \end{bmatrix} \begin{Bmatrix} u \\ \varphi \end{Bmatrix} = \begin{Bmatrix} F \\ Q_C \end{Bmatrix} \quad (4.29)$$

Where:

$$[K_{uu}] = \int_v \left([B_u]^T [Q_E] [B_u] \right) dv \quad (4.30)$$

$$[K_{\varphi u}] = [K_{\varphi u}]^T = \int_v \left([B_\varphi]^T [d]^T [B_u] \right) dv \quad (4.31)$$

$$[K_{\varphi\varphi}] = - \int_v \left([B_\varphi]^T [\xi] [B_\varphi] \right) dv \quad (4.32)$$

Where $[K_{uu}]$ represents global stiffness matrix, $[K_{\varphi u}] = [K_{u\varphi}]$ are global piezoelectric coupling matrices and $[K_{\varphi\varphi}]$ is the element dielectric stiffness matrix, Q_C represent global charge, and F is the global surface force.

To obtain the global finite element equations, expressions for each element (equation 4.29) had to be assembled using finite element solver and hence estimation of actuator displacement and force in respect to various thickness ratios.

4.4.3 Creating the Finite Element Model

MSC Marc Mentat was used to create the geometrical and finite element analysis model.

Mentat is a Graphic User Interface program used along with Marc to create an analysis model [70].

For each layer two semi-circular curves were created, from which ruled surfaces were defined, followed by converting them into finite element models. Mesh density was varied according to the thickness ratio.

4.4.4 Boundary Conditions

The potential of the nodes where the piezoceramic elements are connected with the bonding elements (inner surface nodes) were set to zero. The voltage of 50V is applied to the nodes on the outer surface of the piezoceramic layer. One end tip was completely constrained from translation and rotation and the other end is left free to move for displacement analysis while for force analysis one node on the free end tip was constrained in x-direction. Reaction force displayed by this node is taken to be the output force of the structure, (blocked force).

4.4.5 Material Properties

Brass was used as a substrate material while an epoxy bonding layer was assumed. The data for the piezoceramic layer were entered by giving mechanical data for (anisotropic properties), and non-mechanical data (electrostatic for dielectric constants, and piezoelectric for the coupling constants). In order to account for direction dependence constants for piezoelectric material and also the polarization of the piezoceramic elements, an orientation option was used as follows: Poling was along Z -axis (thickness direction) and X and Y are respectively in radial and circumferential directions.

4.4.6 Load-Cases and Job Parameters

The objective of the analysis was to obtain displacement and force values for the actuator at different substrate to PZT thickness ratios (i.e. 0.0; 0.25; 0.5; 0.75; 1.0; 1.25; 1.5; 2.0), for a fixed input voltage under quasi-static conditions.

Element type 160 was used for the piezoelectric analysis. Element type 160 is a four-node, isoparametric, arbitrary quadrilateral for plane stress piezoelectric applications. The mechanical part of this element is based on element type 3, which was used for the substrate and bonding materials. The electrical part of this element was added as the third degree of freedom [71]. To improve bending behaviour assumed strain was selected.

4.4.7 Discussion of Simulation Results.

Results from the finite element analysis are compared to the predicted ones. In figure 4.19 it is shown that there is a close agreement in behaviour in terms of the shape of the curves, the

ratio for maximum displacement which falls between 0.25 to 0.35 thickness ratios. As far as magnitudes are concerned, the difference is due to the fact that the theoretical model was simplified to one dimensional state and isotropic properties of piezoelectric material and the width remaining constant were assumed while in the numerical model, the piezoceramic material was considered to have anisotropic properties and plain stress state of loading were assumed where the Poisson's effect

was also taken into account. In the case of results for the force (figure 4.20), it is seen that at higher thickness ratios there is a big difference between the predicted and the finite element analysis results, this is due to the fact that at these ratios apart from reasons explained above, the piezoelectric beam becomes thicker in such a way that the thin beam theory can not give accurate results. Also the generated piezoelectric force is a function of applied voltage and the electromechanical properties of the piezoceramic material; therefore it

reaches to a ratio where an induced force is not enough to deform. The contour plots for displacement and force at the turning point (at maximum displacement) are shown in figures 4.21 and 4.22 respectively.

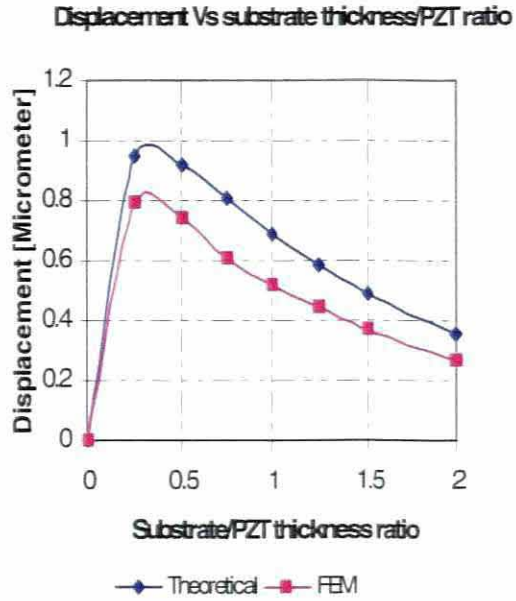


Figure 4.19: Displacement Vs thickness ratio: Theoretical results compared to numerical analysis, at 50V input voltage for brass substrate

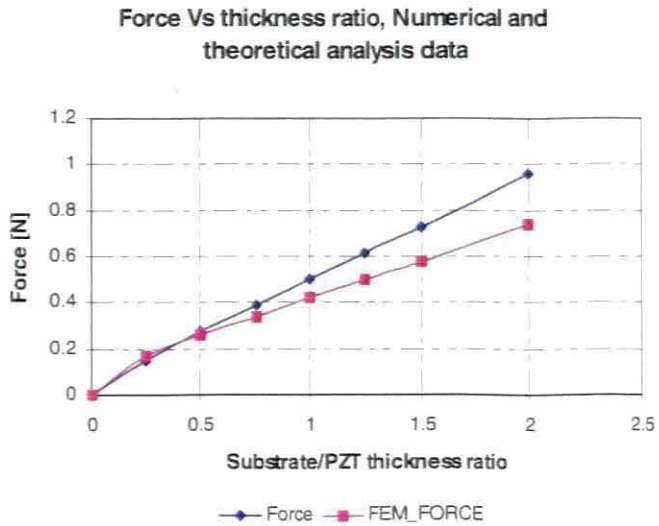


Figure 4.20: Force vs. thickness ratio: Theoretical results compared to numerical analysis at 50V input voltage for brass substrate



Figure 4.21: Contour plot of displacement in the X-direction, at 0.31 substrate/PZT thickness ratio



Figure 4.22: Contour plot of the actuator force in the X- direction at 0.31 thickness ratio

CHAPTER FIVE

Experimental Investigation

5.1 Introduction

The behaviour of the C-shape piezoelectric element as shown before is highly influenced by the material properties and size of the substrate.

The main purpose of the experimental investigation was to validate the previously shown influence of parameters such as substrate material and thickness on the performance of an actuator, namely displacement and force output under quasi-static conditions.

Displacement and force measurements were carried out for actuators made from three different substrate materials (i.e. aluminium, brass, and mild steel) and three different thicknesses for each material for, the voltage range of 25V to 175V.

5.2 Fabrication of a Unimorph C- Shape Actuator

During the investigation, individual unimorph C- shape actuators were produced consisting of three layers i.e. piezoceramic material (PZ26), an adhesive layer and a metallic substrate. Dimensions and specifications for the piezoceramic are as shown in table 1 in appendix A. nine prototypes of the laminated C- actuator were fabricated using mild steel, brass, and aluminium as the substrate material.

A C-shape piezoceramic layer was obtained from a piezoelectric tube of 20mm outside diameter, 18mm internal diameter and a width of 10mm cut along the width into two halves. The elements were pre-plated with silver electrodes both on the inner and outer surface (figure 5.1). Fabrication of the substrates was done by turning solid round bars to be able to conform inside the PZT ring. The bars were drilled to obtain tubes with different thicknesses (that is 0.31, 1.0, and 2.0mm). Finally the tubes were cut longitudinally into two halves (figure 5.2).



Figure 5.1: C-shape piezoceramic ring

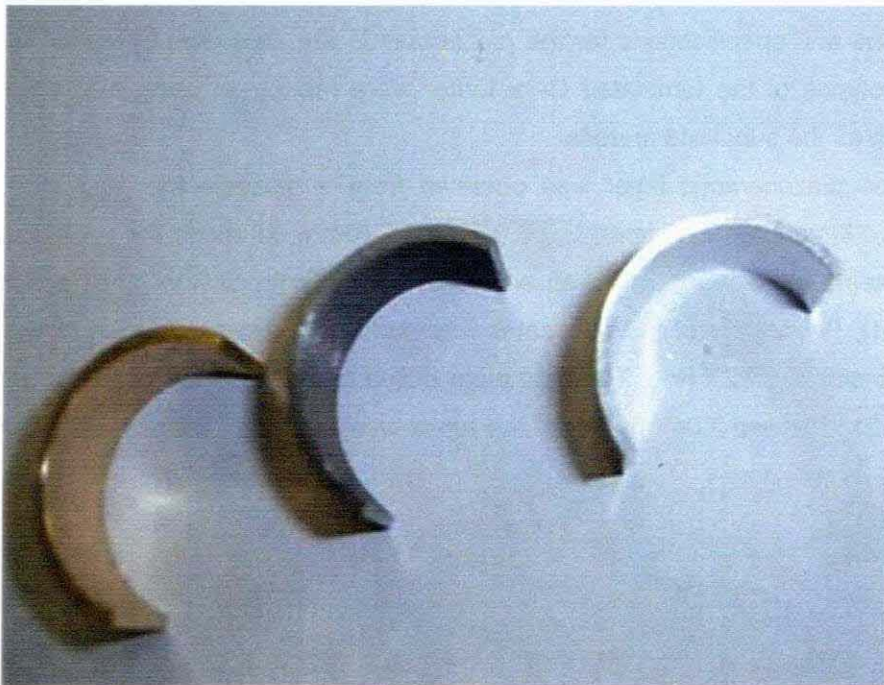


Figure 5.2: Substrate rings from Mild Steel, Aluminium and Brass

Wires were soldered on to the silver electrodes by using ordinary lead solder. Proper working temperature and solder time were maintained so as not to cause depoling of the piezoceramic material and degradation of the silver coating (electrodes). The fabrication of the actuator is shown in figures 5.3 and 5.4.

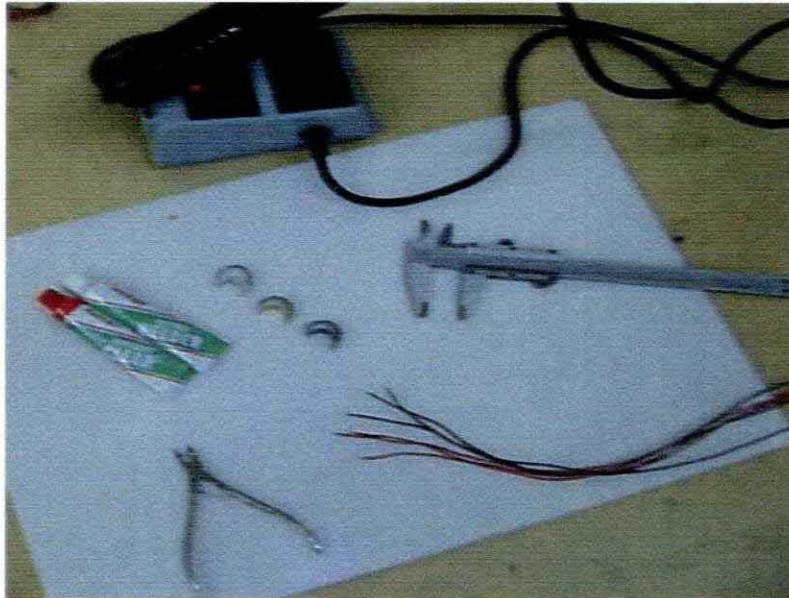


Figure 5.3: C-shape actuator components ready for assembly

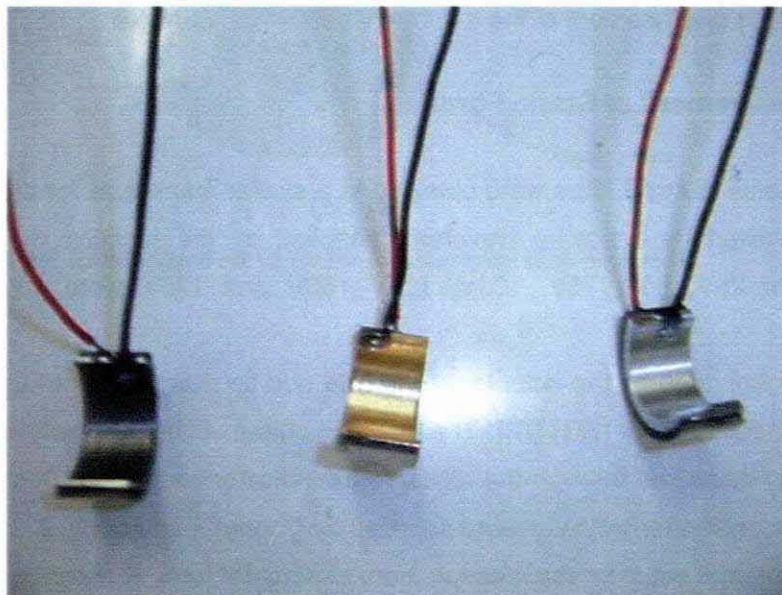


Figure 5.4: A set of assembled unimorph C-shape actuators with Aluminium, Brass and Mild steel substrates

A high strength Pratley quickset adhesive was used; resin and hardener of equal proportions mixed and applied to both surfaces to be bonded, that is the piezoceramic inner and substrate outer surfaces. The two surfaces were brought together and the bond was left to set and cure for 24 hours.

5.3 Experimental Procedure.

5.3.1 Measurements of the Static Displacement

Measurements of the static displacement of the actuator were obtained by using an OMEGA GP901 series digital gauging probe [72]. The displacement measurements were obtained directly in mm with the help of a high performance digital readout for linear encoders and digital gage probes - DR601 (Omega Engineering).

The measuring probe was brought into contact with the tip of the free end of the actuator. The actuator was excited by a square waveform produced by the function generator (Arbitrary Function Generator Model: AFG 310, Sony Tektronix). Voltages of 25V, 50V, 75V, 100V, 125V 150V and 175V were applied at a low cycle (0.05Hz) while attempting to measure the extension of the actuator.

The signal from the function generator was amplified by the piezo driver/amplifier – TRek Model PZD 700 Dual channel). The power supplied to the actuator was closely monitored through the TDS 224 four-channel digital real-time oscilloscope. The experimental setup for measuring the displacement of the actuator is shown in figure 5.5.

5.3.2 Measurement of Static Force

Measurements of static force were obtained in a similar manner as for displacement with the actuator excited by a square waveform supplied by the function generator (AFG 310). Voltages of 25V, 50V, 75V, 100V, 125V 150V and 175V were applied as previously described.

The force generated by the actuator at the free end tip was measured using a subminiature load cell (model: LCKD-1KG) [73]. The load cell output voltage proportional to actuator force was directly displayed through the digital force indicator/conditioner (model: DFI 7000 DM). The signal conditioner/indicator were supplied by Cooper Instruments & Systems [74].

The experimental setup for the measurement of actuator force is shown in the figure 5.6.

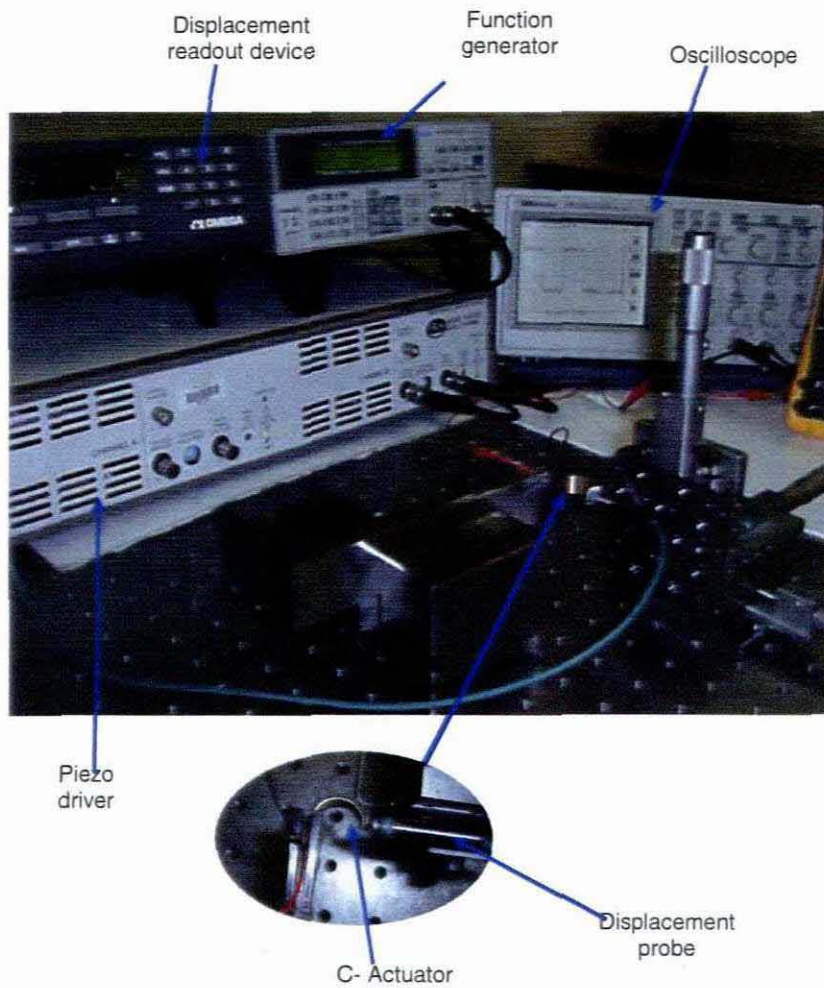


Figure 5.5: Experimental set up for the measurement of displacement.

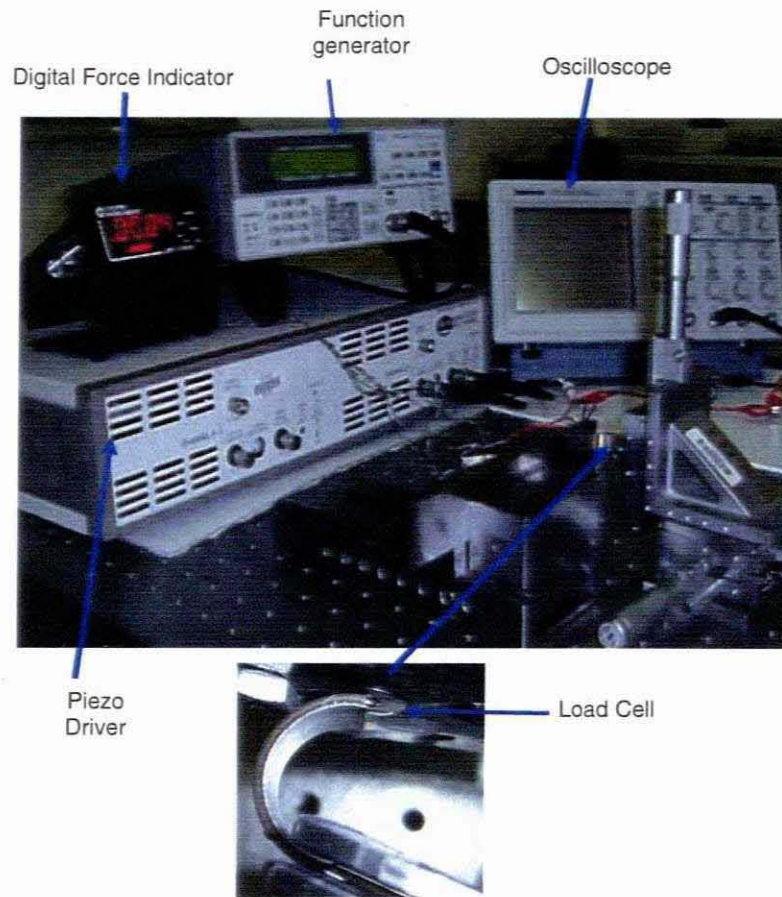


Figure 5.6: Experimental setup for the Measurement of static force

5.3.3 Displacement Measurement Results and Discussion

Actuators with thinner substrate give larger displacement than the thicker one, see figure 5.7. As far as the elastic properties of a substrate material are concerned, an actuator with a relative small value of Young's Modulus substrate material yields large displacements (figure 5.8). For all cases it is observed that displacement is increased with increase in applied voltage.

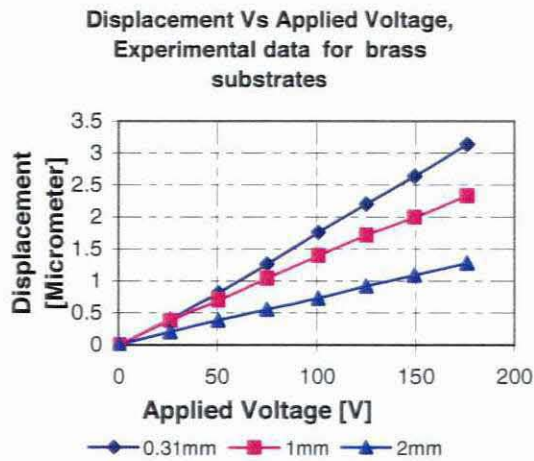


Figure 5.7: Displacement dependence on the applied voltage and on the substrate thickness

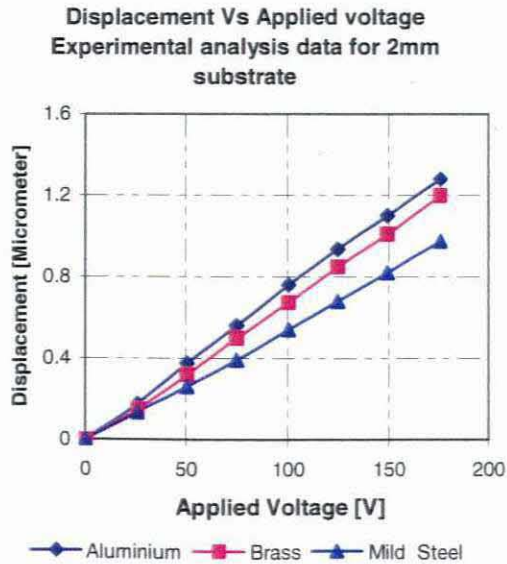


Figure 5.8: Dependence of actuator displacement on the applied voltage and on the elastic properties of the substrate material

A combination of elastic properties and geometry (thickness) contribute to the total actuator stiffness and thus influencing the displacement see table 5.1.

Figure 5.9 shows typical experimental results for the displacement of the free end of the actuator compared to those predicted by the finite element analysis and also for different thickness ratios as shown in figure 5.13.

Table 5.1: Total actuator stiffness for selected substrate materials and thickness

Substrate material	Substrate thickness	Actuator total stiffness[N/m]
Brass	0.31	1.87e+05
Brass	1.0	7.29e+05
Aluminium	2	2.44e+06
Brass	2	2.73e+06
Mild steel	2	4.39e+06

5.3.4 Force Measurement Results and Discussion

Larger forces are obtained from an actuator with thicker substrate (figure 5.10), as well as from substrates with larger Young's modulus of elasticity (figure 5.11). It is observed that the actuator output force is directly proportional to the applied voltage, and good agreement is shown between experimentally obtained force output and the predicted by the FE analysis (figure 5.12) and for different thickness ratios shown in figure 5.14.

Displacement Vs Applied voltage for the 1mm brass substrate

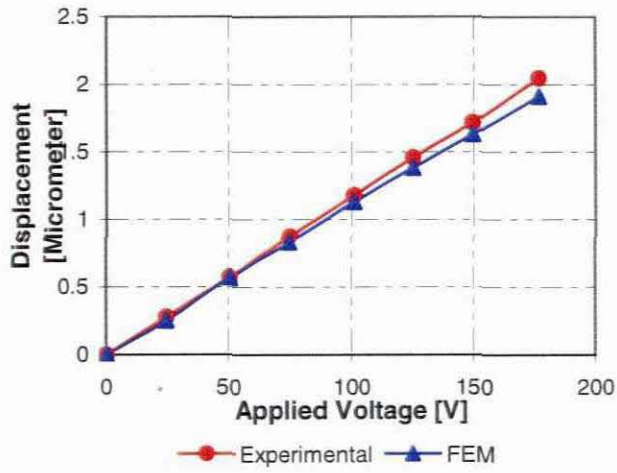


Figure 5.9: Experimental results compared to finite element analysis for displacement of an actuator made with a 1mm brass substrate.

Force Vs Applied Force, Experimental data for brass substrates

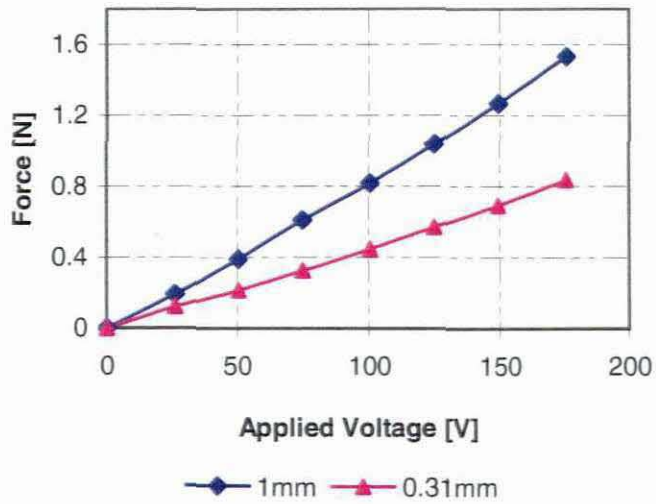


Figure 5.10: Dependence of force on the applied voltage for selected substrate layer thickness

Force Vs Applied Voltage, experimental data for 1mm substrates

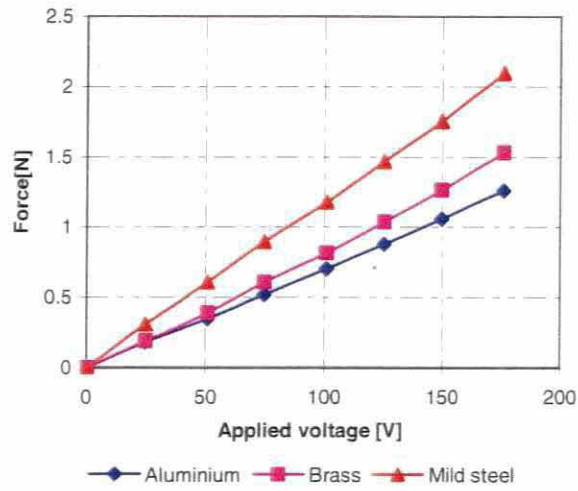


Figure 5.11: Dependence of force over applied voltage for selected substrate layer material

Force Vs Applied voltage, Experimental data for 1mm brass substrate

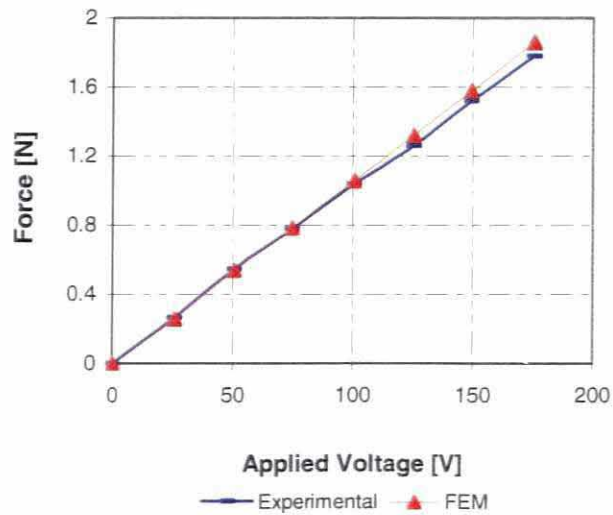


Figure 5.12: Comparison of experimental and predicted results of actuator force output for a 1mm brass substrate.

5.4 Conclusions

Nine different actuators have been analyzed for free displacement and blocked force conditions. Good agreement of predicted and experimental results was noted. It can be concluded therefore that, for a given PZT actuator material regardless of applied voltage, the free displacement and the blocked force are influenced by the actuator stiffness which is partly contributed by the substrate material elastic moduli and the geometry (in this case thickness).

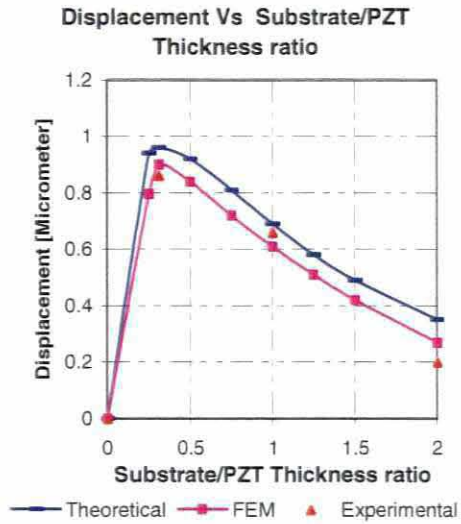


Figure 5.13: Results for Displacement for PZT/Brass thickness ratio. (1mm PZT thickness, 10mm width, at 50Volts)

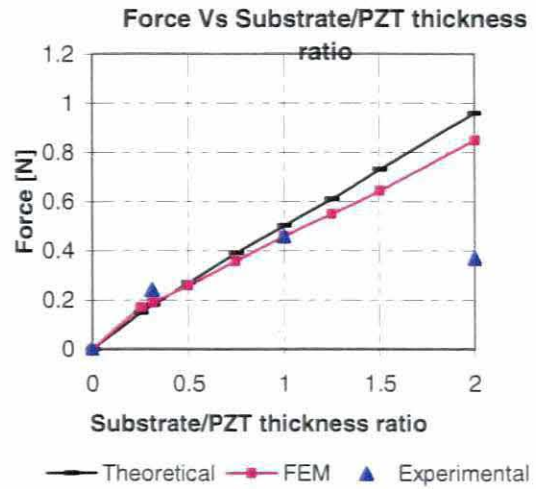


Figure 5.14: Results for the force for PZT/Brass thickness ratio. (1mm PZT thickness, 10mm width, at 50 Volts)

CHAPTER SIX

A Micro-Motor Comprised C-Shape Piezoceramic Actuators

6.1 Introduction

This chapter demonstrates how to use the information obtained from the previous case studies of optimizing the selection of the actuator material and geometry. The objective was to obtain an actuator, which can produce maximum displacement from the available PZ26 piezoceramic material. The information from figures 3.3 through 3.8 was used to determine the external radius, piezo-thickness and width and substrate material, while information from graphs 4.3, 4.8 and 4.16 to 4.18, was used to determine the appropriate thickness ratio, for the selected substrate material. Analytical models were used to compute the free displacement and blocked force of the micro-motor. The results were validated by the MSC Marc Finite Element Analysis commercial software.

In many applications piezoelectric 'patches' are bonded on to surfaces, which they are intended to control. In other instances, actuator end-tips are mechanically connected with the object they control. In this work a simple design for a stand-alone device comprising individual C-block actuators was proposed as shown in figure 6.1. The device is intended to work as an independent piezo-motor as a source of vibration or a vibration exciter.

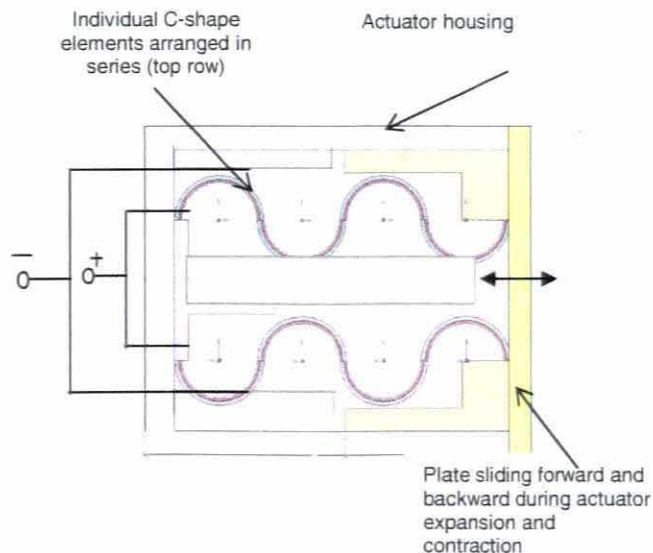


Figure 6.1: A section view of an actuating device showing part of C-element actuator arrays

Typical applications could be in microvibro-hoppers, for feeding devices in parts handling systems, as a motor for micro-shakers (declogging devices), or for portable micro-compacting machines.

6.2 C-Shape Actuators Connected in Series and Parallel Arrays

As mentioned earlier, adding individual actuators in series increases displacement proportional to their number without any increase in force, but if sets of actuators connected in series are put in parallel to each other and arranged to work as a team an increase in force is also obtained [58],[59]. The actuating device proposed in this work is made up of two parallel sets, each set comprising two individual actuators connected in series. Obviously, the number of actuators in series will determine the total displacement while the number of arrays in parallel will determine the total force.

The arrangement of actuators and the application of the electric field are in such a way that deflections of the end tips of individual elements sum up as shown in the figure 6.2.

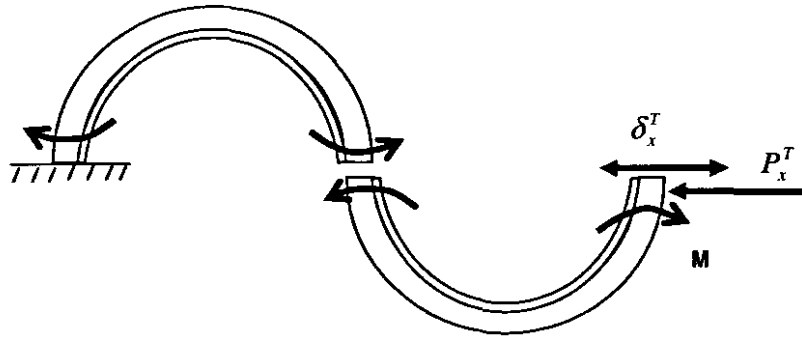


Figure 6.2: Summation of piezoelectric moment from individual actuator when joined in series

Since the force-displacement relationship is linear, the total displacement of any array is obtained by determining the energy stored into an individual element due to deformation. Applying Castigliano's 2nd theorem[62] the total displacement δ_x in the direction of applied load P_x for an individual element (see fig. 6.3) is obtained.

$$\delta_x = \frac{\partial U_c}{\partial P_x} \tag{6.1}$$

Where U_c is the complementary strain energy due to bending. The total complementary energy of an individual element at any angular position θ (figure 6.3) is obtained by the

$$U_c = \frac{1}{2D} \int_0^\pi M^2 R_{na} d\theta \tag{6.2}$$

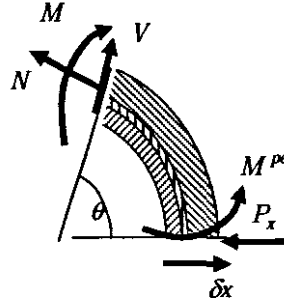


Figure 6.3: Internal forces and moment at a cross-section cut at an angle θ

The internal bending moment M , in this case is a sum of two moments; one being due to piezoelectric strain M^{pe} (equation 3.9) and the other is due to externally applied load - M^{px} . For q sets of parallel arrays, the externally applied load is equally distributed amongst the arrays making each array set to bear a load equal to $P^* = \frac{P_x}{q}$.

Thus

$$M = \pm(M^{pe} + M^{px}) = \pm\left(M^{pe} + \frac{P_x}{q} R_{na} \sin \theta\right) \quad (6.3)$$

Total complementary energy for the sets made up of 's' individual actuators in series and 'q' sets in parallel, is the product of complementary energy for individual elements and the number of actuators in series and the number of actuators in parallel

$$U_c = \frac{1}{2} qs \int_0^\pi \frac{(M^{pe} + \frac{P_x}{q} R_{na} \sin \theta)^2}{C} R_{na} d\theta \quad (6.4)$$

The displacement of the free end the tip of a single set of arrays, equation 6.1 becomes:

$$\delta_x = \frac{\partial}{\partial P_x} \left(\frac{1}{2} qs \int_0^\pi \frac{\left(M^{pe} + \frac{P_x}{q} R_{na} \sin \theta \right)^2}{D} \right) R_{na} d\theta \quad (6.5)$$

Substituting equation 3.9 for the piezoelectric moment into equation 6.5, integrating within the limits, and followed by partial differentiation with respect to externally applied load p_x , the displacement at the free end tips for an actuating device becomes:

$$\delta_x = \frac{s\pi P_x R_{na}^3}{2qD} - \frac{2sM^{pe} R_{na}^2}{D} \quad (6.6)$$

And the available force is:

$$P_x = \frac{2qD}{\pi s R_{na}^2} \delta x - \frac{4qM^{pe}}{\pi R_{na}} \quad (6.7)$$

If friction and the losses due to the weight are ignored, the total free displacement for the micro-motor comprised of 'q'arrays is obtained by setting the externally applied load in equation 6.6 to zero.

$$\delta_{free} = -\frac{2sM^{pe}R_{na}^2}{D} \quad (6.8)$$

The total blocked force for the free end tip i.e. at $\delta_x = 0$ is

$$F_b^{total} = \frac{4qM^{pe}}{\pi R_{na}} \quad (6.9)$$

Finding the ratio of the blocked force to the free displacement yields the actuator stiffness, in this case

$$k = \frac{F_b}{\delta_f} = \frac{2qD}{\pi s R_{na}^3} \quad (6.10)$$

6.3 Selection of Appropriate Substrate Material and Thickness

It was established in chapter 4, that larger displacements and force are obtained at the substrate/PZT thickness ratios between 0.25 and 0.35. A mild steel substrate was found to yield larger displacement than aluminium and brass. For the purpose of demonstration the thickness of 0.31mm mild steel substrate was selected, see table 6.1 for the material and geometry specification.

Number of actuators:

Parallel: 2

Series: 2

Predicted results at the applied voltage of 175V:

Displacement: $3.54 \times 2 = 70.18[\mu m]$ equation 6.8

Force: $0.877 \times 2 = 1.74[N]$ equation 6.9

Table 6.1: Material and dimensional specifications of the micro-motor basic unit

Material	External radius	Thickness [mm]	Width	Young's Modulus
Piezoceramic (PZ26)	10	1	10	76e+09
Bonding Material (Epoxy)		0.18	10	5.2e+09
Substrate (Mild Steel)		0.31	10	1.9e+11

6.4 Finite Element Simulation

The finite element analysis was conducted in order to compare with the theoretical results.

6.4.1 Creation of Finite Element Model

A similar procedure, used to create a finite element model for a single actuator demonstrated in chapter 4, was followed here with the exception that two individual actuators were joined in series at their end tips to form one array set. This was then followed by duplicating the array to form a model of two parallel sets as shown in figure 6.4.

6.4.2 Boundary Conditions

The translation and rotation in X and Y axes for the left hand side end tips for both arrays are constrained on the left, the other ends are left free to move. One independent node was created as a reference node for the rigid link body element (RBE3). The nodes from the two free end tips were tied to this node to enable them to produce the same displacement and force (figure 6.4).

For each element two electrodes were created, one on the inner surface of the piezoceramic layer for zero potential boundary condition(ground) and the other on the outer surface for non zero potential boundary condition(electrode).

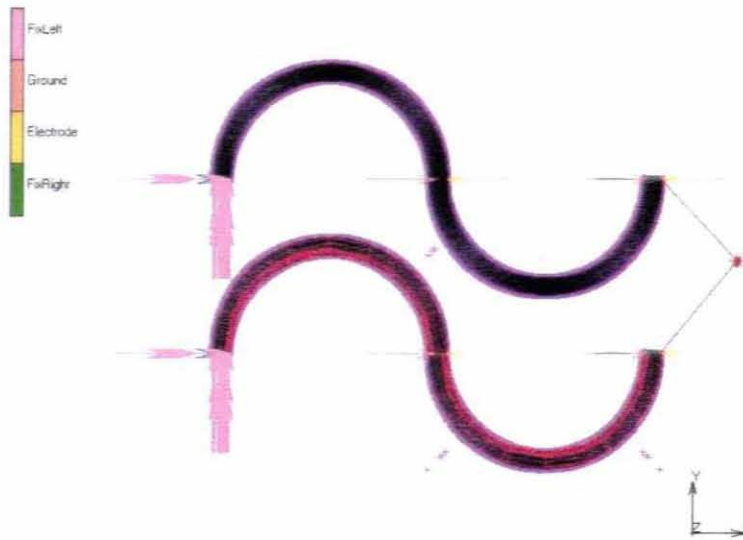


Figure 6.4: Parallel array and serial C -actuators and the applied boundary conditions

6.4.3 Load-Cases and Job Parameters

The main objective of the analysis is to obtain displacement and force of the micro-motor at a fixed input voltage under linear-elastic quasi-static conditions. The same element types 160 for piezoceramic material and element type 3 for non piezoceramic material were used (refer section 4.4.6).

6.4.4 Numerical Simulation Results.

As predicted, the simulation results show an increase of twice as much displacement for a two actuators in serial array and without increase in force compared to that of a single actuators (see figures 6.5, 6.6, 6.7, and 6.8. The force doubles when a parallel array is considered (figure 6.9, 6.19) while displacement remains unchanged.

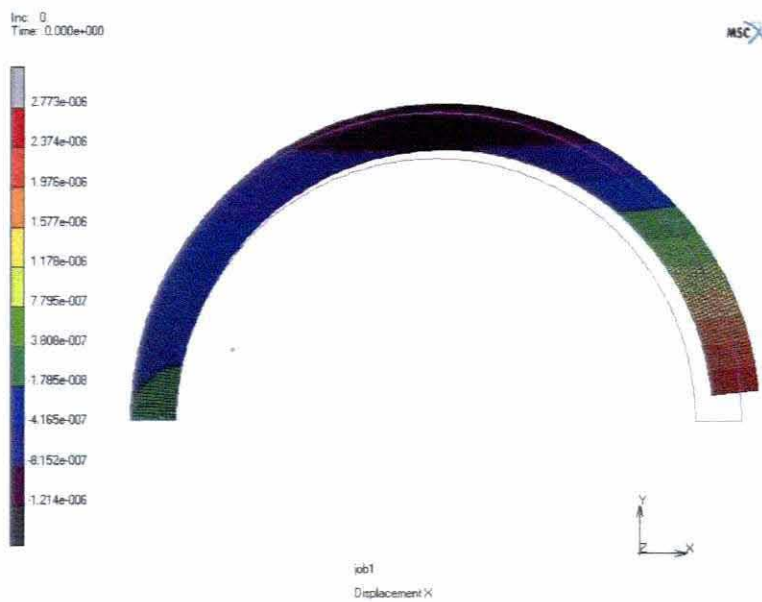


Figure 6.5: Displacement by a single actuator: 2.774 micrometer



Figure 6.6: Force generated by a single actuator: 0.504N

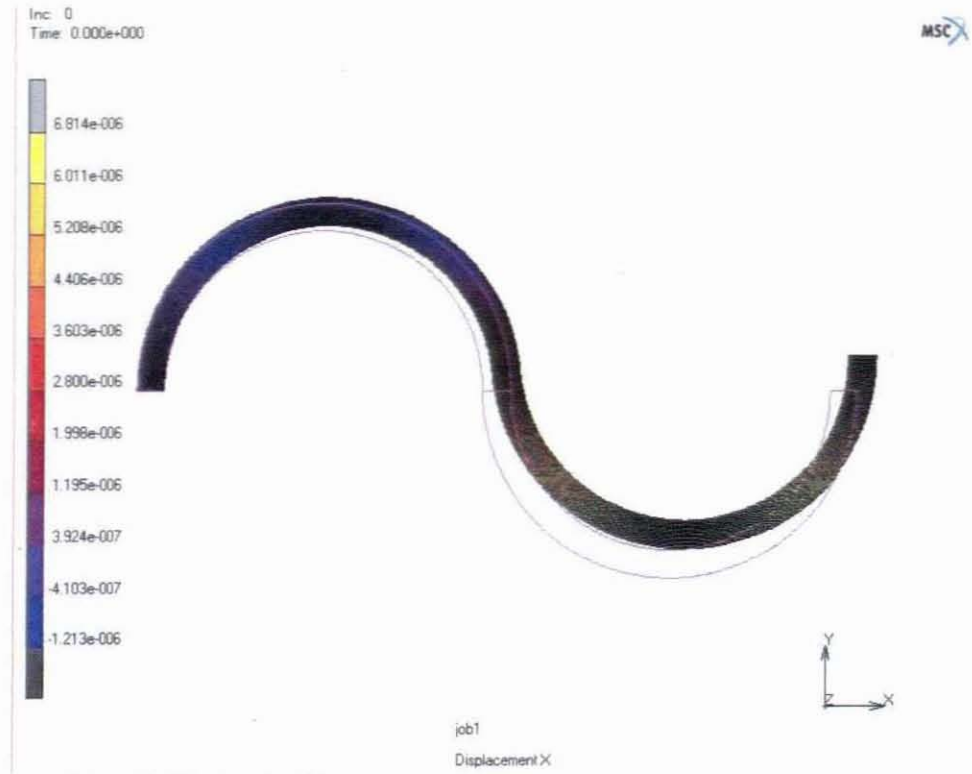


Figure 6.7: Displacement of two units in series: 5.548micrometer

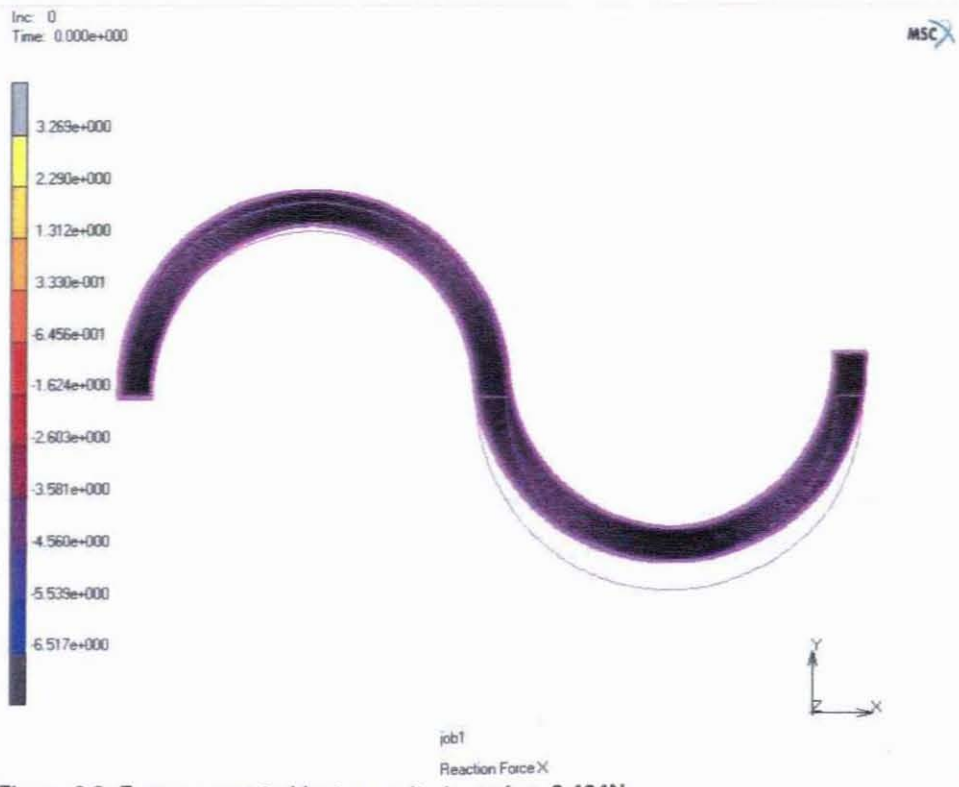


Figure 6.8: Force generated by two units in series: 0.404N

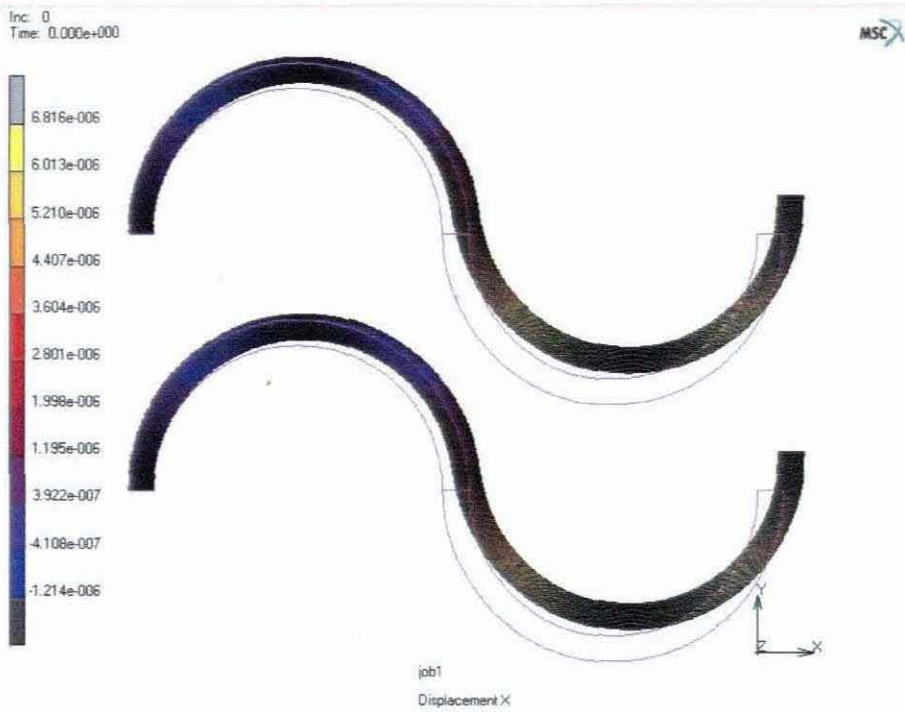


Figure 6.9: Displacement produced by two units in series and two units in parallel. Displacement = 5.53 micrometers.

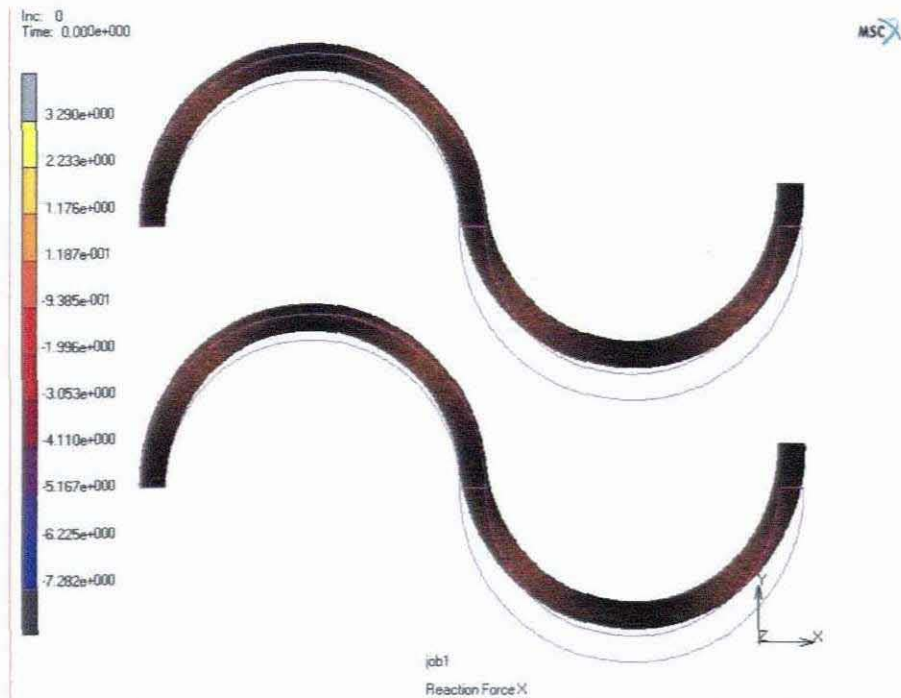


Figure 6.10: Two units in series and two units in parallel, Force = 0.8059N

CHAPTER SEVEN

Finite Element for Dynamic Analysis of an Individual C-Shape Piezoelectric Actuator

7.1 Introduction

Curved piezoelectric actuators are widely used in vibration control. Better understanding of their dynamic behaviour upon application of electric voltage can improve design [75] [76] [77]. Knowledge of the dynamic behaviour of a C shape actuator is critical for the effective operation and control on structures, to control vibration.

A Finite element model was developed, based on the Euler-Bernoulli theory, to investigate the dynamic behaviour of an individual C-shape piezoelectric actuator subjected to sinusoidal voltage. The main goal of this study was to develop and validate numerical analysis tools for curved shape piezoelectric actuators. Once validated for a simple configuration the results can ultimately be extended for more complicated geometries and be helpful in the optimization of the design of curved shape piezoelectric actuators. The dynamic solutions for a free/forced undamped piezoelectric actuator were obtained using a modal analysis method. For the verification of finite element formulation a MATLAB code, (see appendices B1-B5) was developed to aid in the computation of the fundamental frequency and the corresponding normal mode of a four elements model. The general purpose finite element software MSC Marc was used to simulate the first 3 natural frequencies and their respective mode shapes as well as locating the resonance points for three different substrate materials of three different substrate/PZT thickness ratios.

There is a wealth of dynamic analysis models developed by J. Moskalik and D. Brei [60] for this particular configuration, but the focus of their work has been the analytical (exact) approach. *The analytical approach is very challenging and involves a huge amount of mathematical work particularly when complicated boundary conditions are involved.* The finite element method, is a widely accepted and powerful tool for analyzing complex structures [78],[79][80]. Also finite element method lends itself to programming.

7.2 Finite Element Formulation

The C-shape piezoelectric actuator is obviously a curved shape. For simplicity and for computational economy, a flat (straight arc) element can be used to approximate a curved structure [71][82]. A straight arc element is assumed to undergo both extensional and bending deformations provided that the deformations are small. A straight arc element is obtained by superposing the standard two degrees of freedom (d.o.f) bar element to account

for axial displacement with the four d.o.f. beam element to account for lateral and rotational displacements [80] (figures 7.1a and 7.1b).

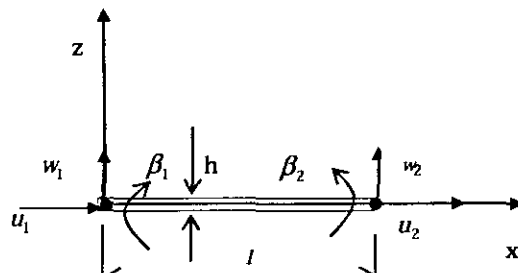


Figure 7.1a: Straight arc element subjected to both extensional and bending deformations

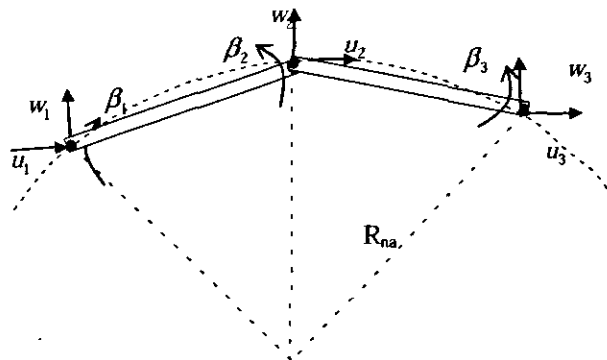


Figure 7.1b: Straight arc element assemblage used to model an arc

In the present formulation the following the assumptions made during the derivation of quasi-static models are also applied here i.e. that the piezoelectric actuator layers are perfectly bonded together (thus continuous strain across the bond is guaranteed, and also shear stresses in the interfaces are ignored. Material behaviour is limited within the linear elastic range (small displacements and strains). Also since the C shape actuator is a thin structure/beam therefore the Euler- Bernoulli model was considered for the finite analysis of the structure, that is, the effect of transverse shear forces is neglected, cross-sections remain plane and normal to the deformed longitudinal (neutral) axis, the rotational deformation is due to bending alone. [83] [84][85][86][87]

7.2.1 Kinematics

The model presented in this is based on the Euler-Bernoulli theory wherein a multilayered structure is reduced to kinematically equivalent single layer, thereby a 3D problem is reduced to an equivalent 1D problem [88][89]. The elements are bound with two nodes and they consist of the piezoelectric, bonding and substrate layers (figure 7.2), this means the laminate behaves as a "single" layer with "special" properties.

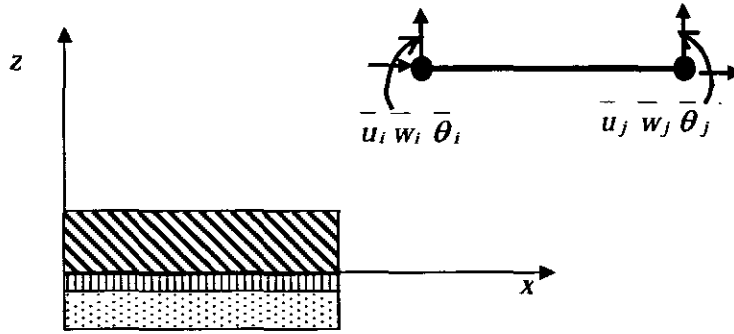


Figure 7. 2: The laminated beam (from bottom to top: substrate, bond and Piezoceramic layer) with the corresponding straight arc element

Each node has three degrees of freedom, that is axial, lateral and rotational displacements. The nodal displacements of the beam element in a local coordinate for an element are given by:

$$\{\delta\} = \{u_1, w_1, \theta_1, u_2, w_2, \theta_2\}^T \quad (7.1)$$

Where u_1, w_1, θ_1 are the respective approximate values of the tangential displacement, lateral displacement and rotation at node 1 while u_2, w_2, θ_2 are those at node 2 respectively.

The displacement vector $\{D\}$ at any point along the beam at any time may be expressed in terms of the spatial interpolation functions $[N_i]$ and their corresponding nodal degrees of freedom $\{\delta_i\}$ as follows:

$$\{D(x, t)\} = [[N_1(x)], [N_2(x)], [N_3(x)], [N_4(x)], [N_5(x)], [N_6(x)]] \{\delta_i(t)\}$$

If the characteristics of the chord may be represented by the corresponding straight arch element with the same cross section properties as those of the arc, the assumed displacement field equation would be:

$$u(x, t) = a_1(t) + a_2 x(t) \quad (7.2)$$

$$w(x, t) = a_3(t) + a_4 x(t) + a_5 x^2(t) + a_6 x^3(t) \quad (7.3)$$

This equation can also be written as:

$$u(x, t) = N_1(x)u_1(t) + N_2(x)u_2(t) \quad (7.4)$$

$$w(x, t) = N_3(x)w_1(t) + N_4(x)\theta_1(t) + N_5(x)w_2(t) + N_6(x)\theta_2(t) \quad (7.5)$$

Combining equations 7.4 and 7.5 we can write:

$$\begin{Bmatrix} u(x,t) \\ w(x,t) \end{Bmatrix} = \{D(x,t)\} = \begin{bmatrix} N_{u1}(x) & 0 & 0 & N_{u2}(x) & 0 & 0 \\ 0 & N_{w3}(x) & N_{w4}(x) & 0 & N_{w5}(x) & N_{w6}(x) \end{bmatrix} \begin{Bmatrix} u_1(t) \\ w_1(t) \\ \theta_1(t) \\ u_2(t) \\ w_2(t) \\ \theta_2(t) \end{Bmatrix} \quad (7.6)$$

7.2.2 Actuator Equations

The general linear piezoelectric actuator for the converse piezoelectric effect can be described in a stress form as follows:

$$\begin{aligned} \sigma &= [Q]\{\varepsilon\} - \{e\}^T \{E\} \\ \sigma &= [Q]\left(\{\varepsilon\} - [d]^T \{E\}\right) \end{aligned} \quad (\text{repeated equation 2.3})$$

Where:

$$\{e\} = [d][Q]$$

7.2.3 Strain Energy

The strain energy associated with the extension can be given by:

$$U_{ext} = \frac{1}{2} \int_v \{\sigma\}^T \{\varepsilon\} dv \quad (7.7)$$

From constitutive relationship we can write:

$$= \sum_{p=1}^n \frac{1}{2} \int_0^l \{\varepsilon_p\}^T Q_p \{\varepsilon_p\} A_p dx \quad (7.8)$$

Where $p=1, 2, \dots, n$ is the number of layers.

A = the cross-section area

Q = Young's modulus of elasticity

Equation 7.8 can also be written as:

$$U_{ext}(t) = \sum_{p=1}^n \frac{1}{2} \int_0^l [B_{ui}(x)]^T \{\delta_i(t)\} Q_p A_p [B_{ui}(x)] \{\delta_i(t)\} dx. \quad (7.9)$$

Where: $[B_u] = \left[\frac{\partial N_i(x)}{\partial x} \right]$ represent a matrix giving relationship between extensional displacement and strain.

The strain energy associated with the bending deformation can be given by:

$$U_{ben} = \sum_{p=1}^n \int_0^l \frac{M^2}{2Q_p I_p} dx \quad (7.10)$$

But from mechanics of materials, the bending moment is given by

$$M = QI \frac{d^2 w}{dx^2} \quad (7.11)$$

Where Q and I are the Young's modulus of the material and the second moment of area of a cross section about the neutral axis respectively.

Substituting equation 7.11 into equation 7.10 and after some rearrangement the instantaneous strain energy due to bending becomes

$$\begin{aligned} U_{ben}(t) &= \sum_{p=1}^n \int_0^l \left[\frac{d^2 w(t)}{dx^2} \right]^T \frac{Q_p I_p}{2} \left[\frac{d^2 w(t)}{dx^2} \right] dx \\ &= \sum_{p=1}^n \int_0^l [B_w(x)]^T \{\delta_i(t)\}^T \frac{Q_p I_p}{2} [B_w(x)] \{\delta_i(t)\} dx \end{aligned} \quad (7.12)$$

But $B_w = \left[\frac{\partial N_i(x)}{\partial x} \right]$ is the matrix describing the relationship between lateral displacement and the bending strain.

Strain energy related to piezoelectric induced strain can be calculated using the following equation:

$$U_{pe} = \int_{ve} \frac{1}{2} \{\sigma\}^T [Q]^{-1} \{\sigma\} dv \quad (7.13)$$

Substituting equation 2.3 into 7.13 we obtain:

$$\begin{aligned} U_{pe} &= \frac{1}{2} \int_{ve} \left\{ [Q_{pe}] \left[\{\epsilon\} - [d]^T \{E_z\} \right] \right\}^T [Q_{pe}]^{-1} \left\{ [Q_{pe}] \left[\{\epsilon\} - [d]^T \{E_z\} \right] \right\} dv \\ &= \frac{1}{2} Q_{pe} b t_p l \int_0^l [B(x)]^T \{\delta_i(t)\}^T [B(x)] \{\delta_i(t)\} dx - Q_{pe} b t_p \int_0^l [B(x)]^T \{\delta_i(t)\}^T d_{31} E_z dx + \\ &+ Q_{pe} b t_p \int_0^l E_z^2 d_{31}^2 dx \end{aligned} \quad (7.14)$$

The total strain energy for the actuator is now given by the summation of bending, extension and induced piezoelectric strains:

$$U = U_{ext} + U_{ben} + U_{pe}$$

$$U = \frac{1}{2} \{\delta(t)\}^T [k_e] \{\delta(t)\} - Q_p d_{31} E_z b t_p \int_0^l [B(x)]^T \{\delta(t)\}^T dx + Q b t_p \int_0^l E_z^2 d_{31}^2 dx \quad (7.15)$$

Where:

$[k_e]$ = Stiffness matrix of an element in a local coordinate system given by

$$[k_e] = \sum_{i=1}^n \int_0^l \left([B_w(x)]^T Q_p A_p [B_w(x)] + [B_w(x)]^T Q_p I_p [B_w(x)] \right) dx \quad (7.16)$$

The elemental stiffness in a global reference system becomes:

$$K_e = [\Psi]^T [k_e] [\Psi] \quad (7.17)$$

Where Ψ = Transformation matrix given by

$$\Psi = \begin{bmatrix} q_i & -r_i & 0 & 0 & 0 & 0 \\ r_i & q_i & 0 & 0 & 0 & 0 \\ 0 & 0 & 1 & 0 & 0 & 0 \\ 0 & 0 & 0 & q_i & -r_i & 0 \\ 0 & 0 & 0 & r_i & q_i & 0 \\ 0 & 0 & 0 & 0 & 0 & 1 \end{bmatrix} \quad (7.18)$$

But $q_i = \cos \beta_i$ and $r_i = \sin \beta_i$.

β_i is an angle defining orientation of the i^{th} element with respect to global coordinate system.

7.2.4 Kinetic Energy

The kinetic energy of an element is given by:

$$T(t) = \frac{1}{2} \sum_{p=1}^n \int_0^L \rho_p A_p \left[\left(\frac{\partial u_i(x,t)}{\partial t} \right)^2 + \left(\frac{\partial w_i(x,t)}{\partial t} \right)^2 \right] dx \quad (7.19)$$

Where

ρ_p is the mass density per unit length of the p^{th} layer

A_p The cross section area of the p^{th} layer.

Taking into consideration the assumption that there is a perfect bond between the layers, it implies that all points on the actuator cross-section will move with the same velocities in the respective directions. The kinetic energy of an element (equation 7.20) becomes:

$$T(t) = \frac{1}{2} \left\{ \dot{D} \right\}^T \int_0^L \rho_p A_p \left([N_{ui}(x)]^T [N_{ui}(x)] + [N_{wi}(x)]^T \left\{ \dot{D} \right\}^T [N_{wi}(x)] \right) dx \{ \delta \} \\ \{ \dot{D} \}^T [m_e] \{ \dot{D} \} \quad (7.20)$$

Where

$[m_e]$ = Is a local mass matrix of an element given by

$$[m_e] = \sum_{p=1}^n \int_0^L \rho_p A_p [N]^T [N] dx \quad (7.21)$$

N are shape functions (equation 7.6)

Similarly the elemental global mass matrix becomes:

$$[M_e] = [\Psi]^T [m_e] [\Psi] \quad (7.22)$$

The elemental mass matrix and stiffness are then combined to obtain the global mass and stiffness matrices $[M]$ and $[K]$ of the entire structure (actuator) while the boundary conditions are imposed.

$$[M] = \sum_{e=1}^{N_e} [\Psi]^T [M_e] [\Psi] \quad (7.23a)$$

$$[K] = \sum_{e=1}^{N_e} \Psi^T [K_e] [\Psi] \quad (7.23b)$$

Where N_e is the number of elements in the entire structure (actuator).

7.3 Equations of Motion

Equations of motion that govern the dynamic response of the structure can be derived by requiring the work of external forces to be equal to the work of internal, inertia and viscous damping forces for any small motion that satisfies both compatibility and essential boundary conditions (admissibility) [82]. Assuming no externally applied mechanical load for a single element the equation of motion becomes [90][91][92].

$$M_e \ddot{D} + C_{D_e} \dot{D} + K_e D = P_e \quad (7.24)$$

Where:

M_e and K_e are global mass and stiffness matrices of an element respectively.

\ddot{D} = A vector of nodal accelerations

\dot{D} = A vector of nodal velocities

D = A vector of nodal displacements

C_{D_e} = A matrix containing viscous damping terms.

P_e = Piezoelectric load vector given by

$$P_e = Q b t_{pe} d_{31} E_z \int_0^l [B]^T dx \quad (7.25a)$$

$$P_e = Q b t_{pe} d_{31} E \begin{Bmatrix} -1 & 0 & a & 1 & 0 & -a \end{Bmatrix}^T$$

$$= \begin{Bmatrix} -F & 0 & M & F & 0 & -M \end{Bmatrix}^T \quad (7.25b)$$

Where

$$F = \pm Q b d_{31} V \quad (7.26a)$$

$$M = \pm a Q b d_{31} V \quad (7.26b)$$

F and M are the induced actuator force and bending moment respectively.

a = *Moment arm* (a distance from the neutral axis to the midline of the piezoceramic layer)

t_{pe} represent the thickness of the piezoceramic layer

If the continuity at the inter-element nodes is imposed then the induced piezoelectric force and moments are assumed to be applied at the free end tip of the piezoelectric layer. This is due to the fact that there will be force cancellations at these nodes.

Equation 7.24 represents the dynamic behaviour of an element. If equations of motion of all elements are assembled and then followed by applying the appropriate boundary conditions it yields the equation of motion of the entire C-shape piezoelectric actuator.

Equation 7.24 can be rewritten into the forced vibration equation by assuming the displacements, forces, and actuator voltages are harmonic variables with different frequencies. If the right hand side is put equal to zero the equation is then reduced to the eigenvalue problem. From which eigenvalues ω_i and the eigenvectors (u_i , w_i and θ_i) can be determined.

7.4 Frequency Response Analysis

7.4.1 Modal Analysis Method

The amplitude – frequency response problem can be solved using the modal analysis method. In this method the expansion theorem is used where the displacements of masses are expressed as a linear combination of the normal modes of the system. Assuming that the system response is governed by ‘ m ’ modes of vibration, a set of ‘ m ’ uncoupled differential equations of second order are obtained. A solution of these equations is equivalent to the solutions of equations of ‘ m ’ single degrees of freedom [93][94].

The solution of equation 7.25 using modal analysis becomes

$$D(t) = X^{(1)} q_1(t) + X^{(2)} q_2(t) + \dots + X^{(n)} q_n(t) = \sum_{i=1}^n X^{(i)} q_i(t) \quad (7.27)$$

Where $X = X^{(1)}, X^{(2)}, \dots, X^{(n)}$ is the normal mode matrix and

$$q(t) = \begin{Bmatrix} q_1(t) \\ q_2(t) \\ \vdots \\ q_n(t) \end{Bmatrix} \text{ are the time-dependent generalized (modal) coordinates}$$

The nodal acceleration in terms of generalized coordinates becomes:

$$\ddot{D}(t) = X \ddot{q}(t) \quad (7.28)$$

Substituting equation 7.28 into equation 7.24 we obtain

$$MX \ddot{q}(t) + K X q(t) + C_D X \dot{q}(t) = P(t) \quad (7.29a)$$

Multiplying equation 7.29a by X^T both sides

$$X^T M X \ddot{q}(t) + X^T K X q(t) + X^T C_D X \dot{q}(t) = X^T P(t)$$

$$\overline{M} \ddot{q}(t) + \overline{K} q(t) + \overline{C}_D \dot{q}(t) = Q(t) \quad (7.29b)$$

Where:

$$\overline{M} = X^T M X = \text{the generalized modal mass matrix}$$

$$\overline{K} = X^T K X = \text{the generalized modal stiffness matrix}$$

$$\overline{C}_D = X^T C_D X = \text{the generalized modal damping matrix}$$

$$Q(t) = X^T P(t) = \text{the generalized forces}$$

Writing

$\overline{C}_d = 2\lambda_i \omega_i^2$, where λ_i is a modal damping factor, and if the modal vectors are normalized in such a way that

$$\overline{M} = X^{(i)T} M X^{(i)} = \begin{cases} 0 & \text{for } i \neq j \\ 1 & \text{for } i = j \end{cases} \equiv I = \text{diag}(1) \text{ where } I \text{ is the identity matrix,}$$

and

$$\overline{K} = X^{(i)T} K X^{(i)} = \begin{cases} 0 & \text{for } i \neq j \\ \omega_i^2 & \text{for } i = j \end{cases} = \text{diag}(\omega_i^2), \text{ where } \omega_i \text{ is the eigenfrequency of the}$$

i^{th} mode, then equation (7.29b) reduces to a set of decoupled equations of motion given by

$$q(t) + \omega^2 q(t) + 2\lambda \omega^2 \dot{q}(t) = Q(t) \quad (7.30)$$

Equation 7.31 is a non homogeneous differential equation which ordinary methods can now be used to solve for individual responses in the modal coordinate system.

The i^{th} decoupled equation of motion will be

$$q_i(t) + \omega_i^2 q_i(t) + 2\lambda_i \omega_i^2 \dot{q}_i(t) = Q_i(t) \quad (7.31)$$

7.4.2 Modal Solution

Equation 7.31 has the same form as those describing the dynamic response of a damped single degree of freedom harmonic oscillator whose complete solution is given by

$$q_i(t) = e^{-\lambda_i \omega_i t} \left\{ \cos \omega_{di} t + \frac{\lambda_i}{(1 - \lambda_i^2)^{0.5}} \sin \omega_{di} t \right\} q_i(0) + \left\{ \frac{1}{\omega_{di}} e^{-\lambda_i \omega_i t} \sin \omega_{di} t \right\} \dot{q}_i(0) + \frac{1}{\omega_{di}} \int_0^t Q_i(\tau) e^{-\lambda_i \omega_i (t - \tau)} \sin \omega_{di} (t - \tau) d\tau$$

(7.32)

$i = 1, 2, \dots, n$

Where $\omega_{di} = \omega_i \sqrt{1 - \lambda_i^2}$ is a damped frequency.

$q_i 0$, and φ_i are constants (generalized displacements and phase angles respectively) which must be defined from the modal initial conditions.

$$q_i 0 = \frac{Q_i 0}{\omega_i^2 \sqrt{\left[1 - \left(\frac{\Omega}{\omega_i}\right)^2\right]^2 + \left(2\lambda_i \frac{\Omega}{\omega_i}\right)^2}} \quad (7.33a)$$

$$\varphi_i = \tan^{-1} \left\{ \frac{2\lambda_i \frac{\Omega}{\omega_i}}{1 - \left(\frac{\Omega}{\omega_i}\right)^2} \right\} \quad (7.33b)$$

For $i = 1, 2, 3, \dots, n$, is the number of degrees of freedom

Ω = the driving frequency.

The modal solutions obtained from equation 7.32 are then transformed back to obtain the solutions in the physical coordinates by using relationship 7.28.

7.4.3 Eigenvalue Problem

In order to solve the equation of motion (equation 7.24) using the modal analysis method it is necessary first to solve the eigenvalue problem.

The natural frequencies ω_i and the respective modes of vibration $X^{(i)}$ of the piezoelectric actuator are obtained from the n^{th} order polynomial in ω^2 by using the equation 7.24 by assuming an undamped free vibration condition i.e. all external mechanical and electric excitations are assumed to be zero. This yields an eigenvalue problem of the form:

$$\det(-\omega^2 M + K) = 0 \quad (7.34)$$

The corresponding eigenvectors can be obtained by applying the following equation

$$(-\omega_i^2 M + K)X^{(i)} = 0, \text{ for } i = 1, 2, \dots, n \quad (7.35)$$

7.5 Numerical Examples

7.5.1 Computation of Eigenfrequency with the aid of MATLAB

In order to verify the validity of the finite element formulation the dynamic solution for a free/forced piezoelectric actuator under sinusoidal excitation was obtained using the modal analysis method. The curved actuator was approximated (divided) into 4 equal elements (figure 7.3). With the fixed-free boundary conditions, the local and global stiffness and mass

matrices for each element (equations 7.17, 7.18, 7.21, 7.22) and later for the whole structure (equations 7.23a, 7.23a) were determined and the details are shown in appendix C. The material and geometrical characteristics of a C-shape piezoelectric actuator used in the analysis are shown in table 1 in appendix A.

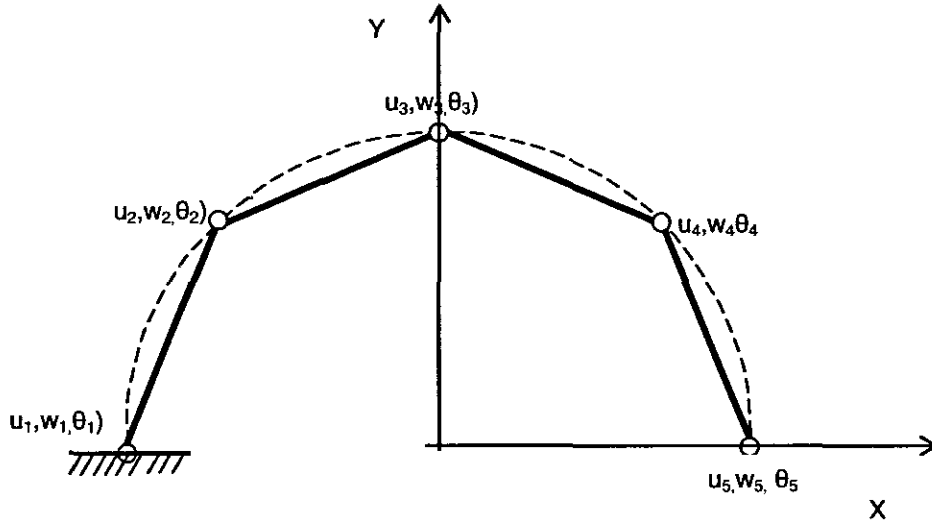


Figure 7.3: C-shape piezoelectric actuator approximated with four straight arc elements

The 3 lowest natural frequencies for the actuators with aluminium, brass and mild steel substrates each of three different thicknesses were computed with the aid of MATLAB code (appendix D). The results were compared to those calculated using the experimentally validated formula (equation 7.35) obtained from reference [61]. The results show good agreement as indicated in figures (7.4a, 7.4b, and 7.4c) an error of approximately 1.4% is noted. Their corresponding frequency-amplitude response curves are shown in figures 7.5 through 7.7

$$\left(\omega_i^2 = \frac{D\lambda_i^2}{\rho R_{na}^4} \right) \quad (7.35)$$

Where

ω_i is the i^{th} natural frequency, D is the composite bending stiffness [Nm^2], $\lambda_i = i^{th}$ Non-dimensional natural frequency, ρ is the mass per length [kg/m] and R_{na} is the radius of neutral axis. [m]

Fundamental Frequency Vs Substrate/PZT Thickness ratio

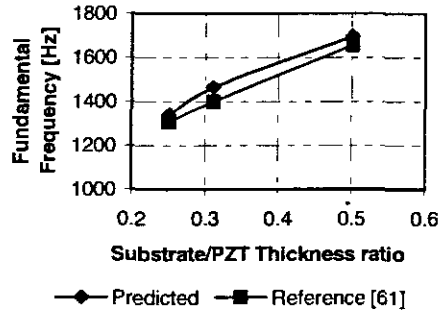


Figure 7.4a: Comparison of values of fundamental frequency for Mild Steel substrate.(Data taken from appendix D)

Fundamental frequency Vs Substrate/PZT Thickness ratio

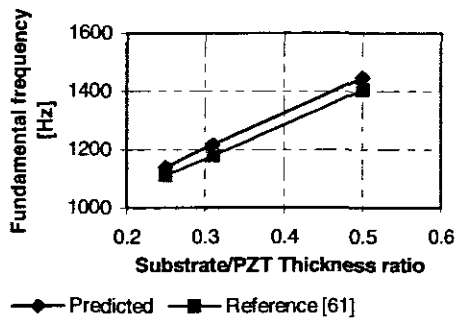


Figure 7.4b: Comparison of values of fundamental frequency for Brass Substrate (Data taken from appendix D)

Fundamental Frequency Vs Substrate/PZT thickness ratio

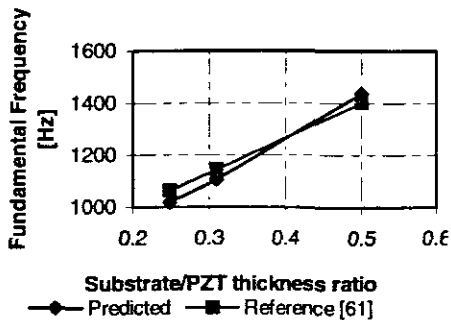


Figure7.4c: Comparison of values of fundamental frequency for Aluminium substrate. (Data taken from appendix D)

Fundamental Frequency Vs Substrate/PZT Thickness ratio

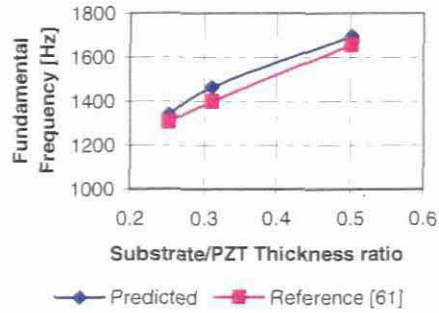


Figure 7.4a: Comparison of values of fundamental frequency for Mild Steel substrate.(Data taken from appendix D)

Fundamental frequency Vs Substrate/PZT Thickness ratio

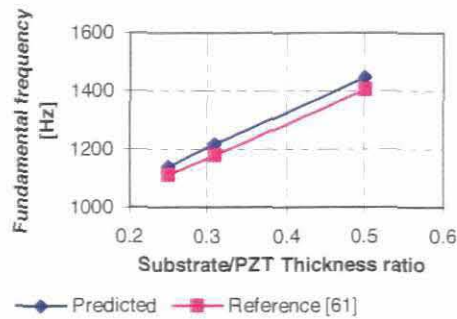


Figure 7.4b: Comparison of values of fundamental frequency for Brass substrate (Data taken from appendix D)

Fundamental Frequency Vs Substrate/PZT thickness ratio

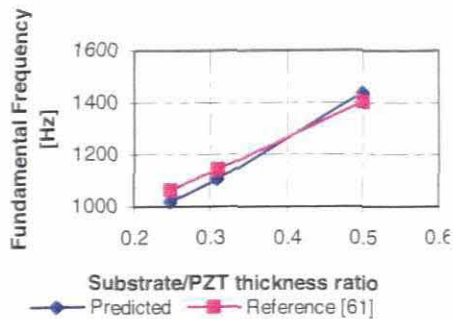


Figure7.4c: Comparison of values of fundamental frequency for Aluminium substrate. (Data taken from appendix D)

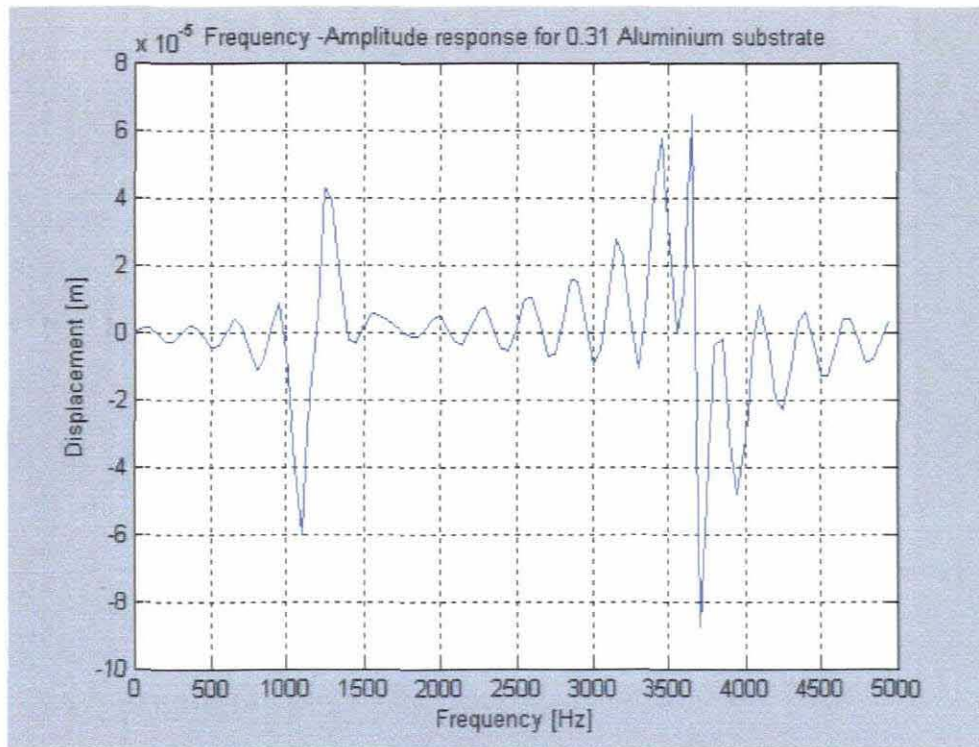


Figure 7.5: Frequency - response curves for aluminium substrate at an excitation voltage of 10V, damping Coefficient = 0.707

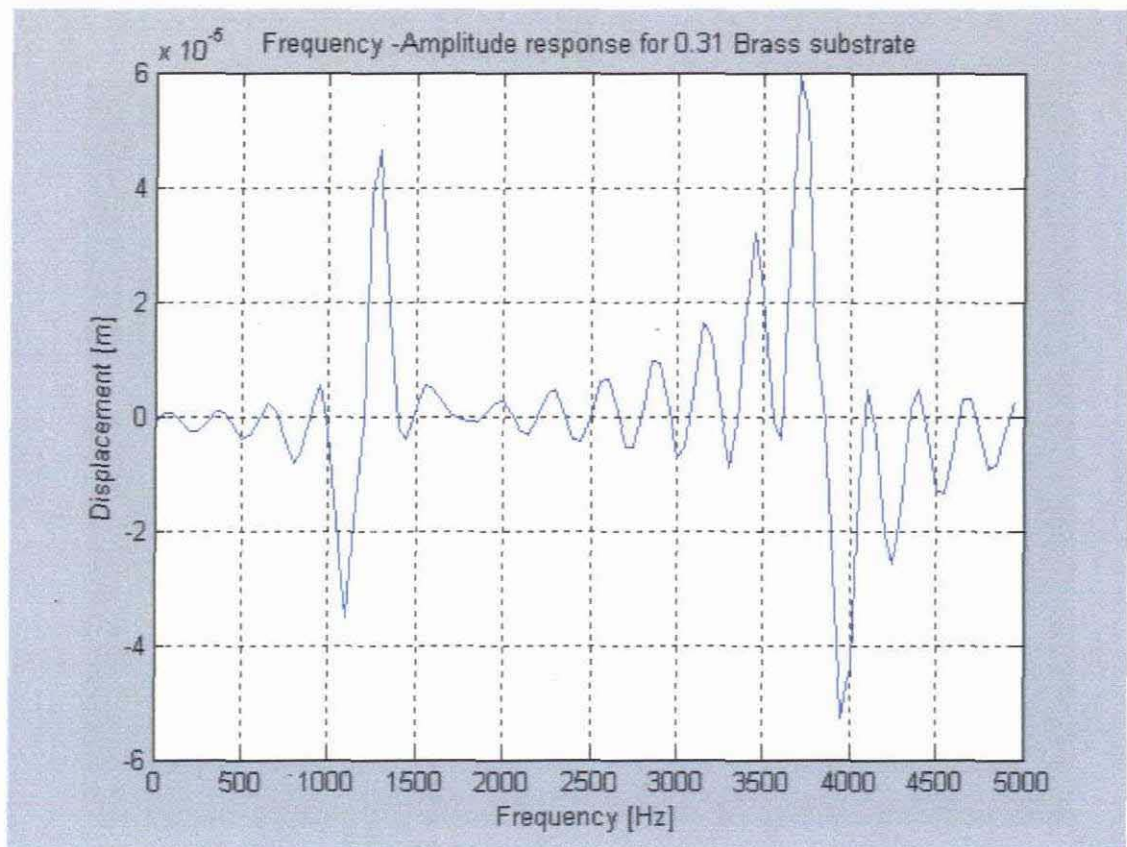


Figure 7.6: Frequency - response curves for brass substrate, (excitation voltage=10V, damping coefficient =0.7071)

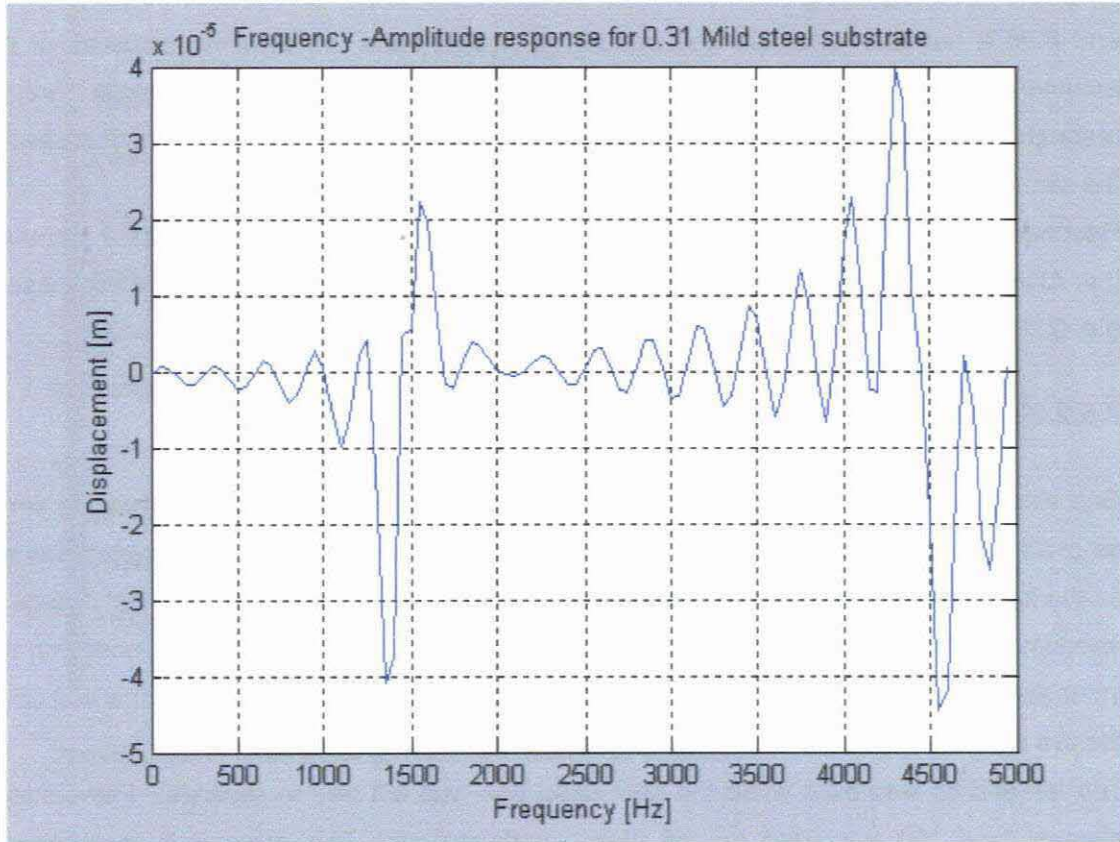


Figure 7.7: Frequency - response curves for a mild steel substrate (excitation voltage=10V, damping coefficient =0.7071)

7.5. 2 Dynamic Analysis Simulation Using MSC Marc.

7.5.2.1 Overview

A dynamic modal analysis was performed to obtain the resonance modes of the actuator, and then a harmonic analysis was performed to determine the dynamic response of the actuator to an alternating voltage. Displacements at a range of frequencies around resonance points were determined. The dimensions and material data for the models used in the simulation are as shown in tables 1 and 2 in appendix A.

Resonance points for the C-shape piezoelectric actuator for 3 different substrate materials (i.e. Aluminium, Brass and Mild Steel) were determined. For each material three thicknesses (i.e. 0.25mm, 0.31mm, and 0.5mm) were analysed.

7.5.2.2 Boundary Conditions

One electrode on one of the nodes of the inner surface of the piezoelectric ceramic to serve as ground terminal, while another node at the outer surface of piezoelectric ceramic was set as the live terminal. In the model, these electrodes are made by tying the potential degree of freedom of all nodes belonging to the respective surface to one node, that is all nodes on the inner surface are tied up to the ground terminal while the outer surface nodes are tied up to the live terminal.

The left end tip was fixed while the right hand one was left free to oscillate. Plane stress element type 160 was used for the piezoelectric material. This element is mechanically equivalent to element 3 which was used for the substrate materials. This element type has three degrees of freedom; the first two are for the X_ and Y_ displacement, and the third is for the electric potential.

7.5.2.3 Modal Analysis:

Load cases and piezoelectric dynamic modal parameters set to search for eigenfrequencies were as follows:

The LANCZOS method was used, whereas a number of frequencies were set to 3. The frequencies obtained are shown in figures 7.8 to 7.10.

7.5.2.4 Harmonic Analysis

For the harmonic analysis, the same model built for modal analysis was used. A new load case was set to suit harmonic boundary conditions. The frequency range was selected to be around the first 2 natural frequencies, i.e. from 1 kHz and 5 kHz into 50 steps.

Inc: 0.1
Time: 0.000e+000
Freq: 1.053e+003



Figure 7.8: First Mode shape for a 0.25mm Aluminium substrate

Inc: 0.2
Time: 0.000e+000
Freq: 3.276e+003

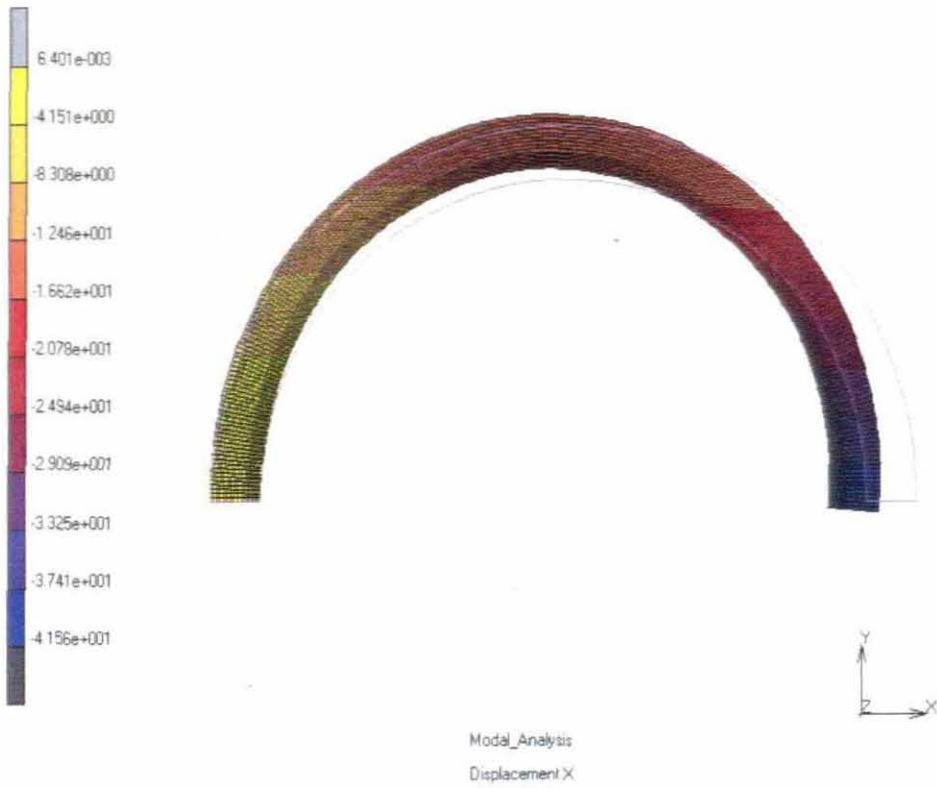


Figure 7.9: Second Mode shape for a 0.25mm Aluminium substrate

Inc: 0:3
Time: 0.000e+000
Freq: 1.095e+004



Figure 7.10: The third mode shape for a 0.25mm Aluminium substrate

7.6: Discussion of results

Finite element models based on Euler Bernoulli beam theory were used to perform the dynamic analysis of C-shape actuator consisting of a three layer unimorph laminated beam (Piezoceramic layer, adhesive layer and metallic substrate) where the only deformation impetus was an actuation strain induced in the piezoelectric layer.

The Effect of thickness and substrate material on the displacement and on the operating bandwidth is shown in figures 7.8 to 7.10 and in appendix D. The results show that an increase of both substrate/PZT thickness ratio and the elastic modulus of the substrate contribute to raise the fundamental frequency of the C-shape actuator. This implies that with appropriate combination of the thickness ratio and the elastic properties of the actuator it can be possible to determine the location of the fundamental frequency and thus set the range over which the actuator can operate before reaching resonance frequency. From the results obtained it can also be concluded that an actuator with a mild steel substrate can operate at higher frequencies compared to aluminium and brass substrates of the same thickness.

It can also be noted that, in this study the C- actuator was approximated using one dimensional element and more importantly only 4 finite elements (Straight arc) were used. The results reported in section 7.5.1 indicate that the predicted results and results calculated using equation (7.35) from reference [61] give an error of approximately 1.4%. This is apparent that if the number of elements is increased much more accurate results could have been obtained. In view of this, it can be concluded that the simplicity of the model can reduce the computational time remarkably.

CHAPTER EIGHT

CONCLUSIONS AND RECOMMENDATIONS

8.1 Conclusions

An investigation on the force, displacement and high bandwidth from a C shape actuator were the main focus of this research.

In chapter three, theoretical models were used to optimize the performance of the C shape actuator by investigating the effect of the piezoceramic layer thickness, the external radius and the piezoceramic width.

In addition to the above the electromechanical properties of the piezoceramic material are of paramount importance in determining the performance of the actuator. Therefore for a fixed thickness and elastic properties of the substrate, the external radius, the thickness and the width of the piezoceramic layer affects the actuator performance in different ways.

Results show that by increasing the external radius of the actuator, the displacement of the free end tip increases while the force decreases. The results also reveal that by increasing piezo-layer thickness the displacement is reduced while the force is increased. The explanation for this is that thickness affects stiffness and the flexibility of the actuator. While force requires stiff material, displacement requires flexible material.

The influence of the substrate to the performance of the actuator (especially in flexural mode) has not been given adequate attention by previous research work. In the present work the procedure was as follows:

Keeping the piezoceramic layer constant (in terms of size and electromechanical properties), by changing the substrate thickness, the study reveals that; there is a specific substrate/PZT thickness ratio which gives the maximum displacement and relatively small force. Higher ratios (> 0.30) give large force and relatively small displacement.

Three different substrate materials were compared, that is, aluminium, brass and mild steel. It shows that for the substrate/PZT thickness ratios up to 0.6 the substrate with higher Young's modulus yields increasing displacement while beyond this ratio the situation is reversed.

The analysis of what has been defined as the coefficient of unimorph actuator showed that it depends on the thickness ratio between the substrate and PZT layers. The equation to describe the dependence of the c_{ua} on the substrate/PZT ratio was also formulated.

In this study it has also been established that there is a similarity between the c_{ua} -to-substrate/PZT thickness ratio relationship (section 4.2.3) to that of the free displacement-to-substrate/PZT thickness ratio (section 4.2.1). However it is not apparent that the ratio between the moment arm and the composite bending stiffness (c_{ua}) can be used to determine the optimum value of displacement.

Experiments were carried out using actuators of three different substrate materials, each with three different thicknesses. Measurements of free displacement and blocked force under quasi-static conditions were obtained.

Finite Element Analysis software MSC Marc was used to simulate the free displacement and blocked force of the above described actuators and good agreement of the predicted and the experimentally obtained values was noted.

Due to the fact that piezoceramic materials are weak in tension, when designing a unimorph piezoceramic actuator, it is preferred that the piezoceramic layer be located on one side of the neutral axis, thus the equation to aid in the selection of the appropriate size and elastic properties of material has been derived accordingly.

A protocol for the selection of suitable size and elastic properties of the substrate material has been suggested, depending on whether the requirement is large force or large displacement or a reasonable compromise between them.

For demonstration purposes, data obtained from the analysis were used in the design of a simple micro-motor comprising of two individual actuators in series forming a set and two sets in parallel. Finite element simulation of the arrangement was performed and the results were found to agree well with the predicted values.

The Finite Element model that was developed, based on the Euler-Bernoulli beam theory to investigate the dynamic behaviour of an individual C-shape piezoelectric actuator, yielded results pertaining to the natural frequencies and the corresponding normal modes which agree well with the model developed using the general purpose finite element software- MSC Marc. The results also show that increasing the substrate/PZT thickness ratio and the elastic modulus of the substrate, contributes to an increase of the fundamental frequency of the actuator. The results for the natural frequencies were also compared to those calculated using equation 7.35 from reference [61]. Good agreement was noted.

Research Contribution to the existing knowledge

The following are what can be termed as original contributions from the research work presented in this thesis.

- The optimum displacement, force and bandwidth from the C shape actuator, by examining the influence of substrate geometry and material properties, resulted in what is the most important contribution from this work. The role of substrate material to actuator performance had not been given adequate attention in past research works. However through the present work,
 - The choice of the suitable geometry (radius, thickness and width) of the piezoceramic layer is provided.
 - The substrate/PZT thickness ratio which gives maximum displacement for the C shape actuator has been identified.

- Graphical data to assist a designer in selecting suitable substrate/thickness ratio and substrate material was established.
- An analysis to determine the safe location of the neutral axis of the actuator was formulated.
- Further, an expression for the coefficient of unimorph actuator c_{ua} for the C shape piezocomposite actuator was presented. It gives a description of the factors influencing this coefficient as well as attempting to associate this coefficient with the performance of the C shape actuator.
- Finally, a simple Finite Element tool for the dynamic analysis used in identifying the eigenfrequencies and the corresponding eigenmodes of the C shape actuator was developed. This was accompanied with the MATLAB code to aid in the computation.

A fixed free boundary condition model which was divided into only four-one dimensional finite elements (straight arc type) was used to approximate the C shape piezocomposite actuator. Although a minimum number of elements were used, an accuracy of 1.4% was achieved. The accuracy may be based on the fact that the influence of the extensional, rotation and bending deformations to each other have been taken into account by the use of straight arc elements characteristics in contrast to the commonly used standard beam elements.

The model is simple and can save a remarkable amount of computation time since with the use of only four elements the number of unknowns (equations) is reduced to only twelve. The model can ultimately be extended so it could be used to analyse curved structures with much more complicated boundary conditions.

8.2 Recommendations for Future Work

The focus of this work was on the actuator function. It is recommended in future to conduct an investigation on the behaviour of an individual C-shape device which incorporates a sensor and actuator so that the device can be used simultaneously for monitoring and control.

REFERENCES

- 1 Srinivasan, A. V and McFarland, D. Michael, 2001, Cambridge : Cambridge University Press, "Smart structures Analysis and design"
- 2 Gandhi M.V and Thomson B.S, 1992, Michigan State University, "Smart materials and structures".
- 3 Christopher Niezrecki, Diann Brei, Sivakumar Balakrishanan and Andrew Moskalik, "Piezoelectric actuation": State of the art, The shock and vibration digest, (July 2001) Vol.33, No. 4, 269 –280
- 4 Conway, N.J.; Sang-Gook Kim "Large-strain, piezoelectric, in-plane micro-actuator" Proceedings of the IEEE International Conference on Micro Electro Mechanical Systems (MEMS), 17th IEEE International Conference on Micro Electro Mechanical Systems (MEMS): Maastricht MEMS 2004 Technical Digest, 2004, p 454-457.
- 5 E.V. Ardelean, D.G. Cole and R.L. Clark, High Performance "V-stack" Piezoelectric Actuator. Journal of Intelligent Material Systems and Structures. 2004; 15: 879-889.
- 6 <http://en.wikipedia.org/wiki/Piezoelectricity#History>
- 7 Jaffe Bernard, Crook R William and Jaffe Hans, 1971, Academic Press London and New York, "Piezoelectric Ceramics"
- 8 Solescki R, Conant R. J, 2003, New York, Oxford University Press,"Advanced Mechanics of Materials".
- 9 http://www.efunda.com/materials/piezo/piezo_math/math_index.cfm, accessed in April 2006
- 10 Wang H, Newnham RE, Cross LE & Pan WY (1991) Piezoelectric properties of PLZT ceramics at different remanent polarization levels. IEEE Seventh International Symposium on Applications of Ferroelectrics, IEEE, New York, NY, USA, 422-425.

- 11 Lynch CS (1996) The effect of uniaxial stress on the electro-mechanical response of 8/65/35 PLZT. *Acta Materialia* 44 (10): 4137-4148.
- 12 Dausch DE (1997) Ferroelectric polarization fatigue in PZT-based RAINBOWs and bulk ceramics. *Journal of American Ceramic Society* 80 (9): 2355-2360.
- 13 Zhang QM & Zhao J (1999) Electromechanical properties of lead zirconate titanate piezoceramics under the influence of mechanical stresses. *IEEE Transactions on Ultrasonics, Ferroelectrics and Frequency Control* 46 (6): 1518-1526.
- 14 Ounaies Z, Mossi K, Smith R & Bernd J (2001) Low-field and high-field characterization of THUNDER actuators. *Proc. International Society for Optical Engineering, SPIE, USA, 4333: 399-407.*
- 15 Zhou D, Kamlah M & Munz D (2005) Effects of uniaxial pre-stress on the ferroelectric hysteretic response of soft PZT. *Journal of the European Ceramic Society* 25: 425-432.
- 16 Zhao J, Zhang QM & Mueller V (1998) Uniaxial stress dependence of electromechanical and dielectric properties of 0.9PMN-0.1PT electroceramics. *Proc. International Symposium on Applications of Ferroelectrics, ISAF'98, IEEE, Piscataway, NJ, USA, 361-364.*
- 17 Yang G, Liu S-F, Ren W & Mukherjee BK (2000) Uniaxial stress dependence of the piezoelectric properties of lead zirconate titanate ceramics. *Proc. International Symposium on Applications of Ferroelectrics, ISAF 2000, IEEE, Piscataway, NJ, USA, 1: 431-434.*
- 18 Crawley, E. F., 1994, "Intelligent Structures for Aerospace: A Technology Overview and Assessment", *AIAA Journal*, 32(8), pp 1689-1699, August 1994.
- 19 A A., Hagood, Nesbitt W. 1997 Piezoelectric fiber composites with interdigitated 164 electrodes, *Journal of Intelligent Material Systems and Structures*, 8(11) pp. 903- 919
- 20 Kawai H., "The Piezoelectricity of Poly(vinylidene Fluoride)," *Jpn. J. Appl. Phys.*,

Vol. 8, (1969) pp. 975-976

- 21 Ramsay J.V and Mugridge, E.G.V (1962), "Barium Titanate Ceramics for fine-movement control", *Journal of scientific Instruments*, Vol. 39, pp 636-637.
- 22 Chonan, S. Jiang Z.W and Koseki, M (1996), "Soft handling gripper piezoceramic Bimorph strips", *Smart materials and structures* Vol. 5, (407 – 414).
- 23 Chandran S. ; Kugel V. D. ; Cross L. E. and Regelbrugge Marc E., CRESCENT: A novel piezoelectric bending actuator, *Proc. SPIE* Vol. 3041, p. 461-469, 06/1997
- 24 Haertling, G.H. (1994b), "Rainbow ceramics- A new type of ultra- high displacement actuator", *American Ceramic Society Bulletin*, Vol.73, No. 1, 93-96.
- 25 Pearce, D.H. Button, T.W. , "Alternative processing routes for RAINBOW-type piezoelectric devices", *International Symposium on Applications of Ferroelectrics, ISAF 98, IEEE, Piscataway, NJ, USA, 547-549.*
- 26 Baron B. W., Li. G and Haertling, G.H. (1996), "Temperature dependent of Characteristics of Cerambow Actuators"; *ISAF 96, Proceedings of the Tenth IEEE International Symposium on Applications of Ferroelectrics, IEEE vol.1 pp 305-308.*
- 27 Mulling J, Usher Dessent T. B, Palmer J, Franzon P, Grant E, Kingon A, "Load characterization of high displacement piezoelectric actuators with various end conditions", *Sensors and Actuators A* 94(2001) 19-24 (www.elsevier.com).
- 28 FACE® INTERNATIONAL CORPORATION THUNDER® WHITE PAPER, <http://www.faceinternational.com/>, accessed April 2006.
- 29 K.J. Yoon, K.H. Park, S.K. Lee, N. S. Goo and H.C. Park, "Analytical design model for a piezo-composite unimorph actuator and its verification using lightweight piezo-composite curved actuators" –*LIPCA, Smart materials and structures* Vol. 13 (2004), 459- 467.

- 30 J. X. Gao and L. Cheng, "Modeling of high performance piezoelectric actuator assembly for active and passive vibration control", *Journal of Smart materials and structures*, 13 (2004), pp384-392.
- 31 Li X.; Vartuli J.S.; Milius D.L.; Aksay I.A.; Shih W.Y.; Shih W-H. Electromechanical Properties of a Ceramic d_{31} - Gradient Flextensional Actuator. *Journal of the American Ceramic Society*, Volume 84, Number 5, May 2001, pp. 996-1003(8).
- 32 YOON Chang-Bun ; LEE Sung-Mi ; LEE Seung-Ho ; KIM Hyoun H-E (2005), PZN-PZT flextensional actuator by co-extrusion process, *Sensors and actuators. A*, Vol. 119 pp 221-227)
- 33 Chang-Bun Yoon, Seung-Ho Lee, Sung-Mi Lee and Hyoun-Ee Kim,(2006), Multilayer bender-type PZT-PZN actuator by co-extrusion process, *Journal of the European Ceramic Society*, Volume 26, Issue 12 , 2006, Pages 2345-2348
- 34 Wu, C.C.M., Lewis D. Kahn M. and Chase M. (1999), "High Authority Telescopic actuators", *Proceedings of SPIE- The International society For Optical Engineering* Vol. 3674, 121 – 219
- 35 Paul W. Alexander, Diann Brei, "Piezoceramic Telescopic Actuator Quasi-Static Experimental Characterization", *Journal of Intelligent Material Systems Structures*, vol. 14, no. 10, October, 2003, p 643-656.
- 36 Onitsuka Katsuhiko, Dogan Aydin, Tressler James F, Xu Qichang; Yoshikawa Shoko, Newnham Robert E, "Metal-Metal-Ceramic Composite Transducer", the "Moonie" *Journal Of Intelligent Material Systems and Structures*. Vol. 6, no. 4, pp. 447-455. July 1995.
- 37 Dogan A, Uchino K, Newnham R.E, "Composite piezoelectric transducer with truncated conical endcaps" -"cymbal", *Ultrasonics, Ferroelectrics and Frequency Control*, IEEE Transactions, Volume: 44, Issue 3, May 1997, pp 597-605.
- 38 Dhananjay K Samak and Inderjit Chopra, Design of high force-high displacement actuator for helicopter rotors, *Smart Structure and Materials* Vol. 5 1996 pg 58 - 67.

- 39 Uchino Kenji, "Piezoelectric ultrasonic motors", *Smart Materials and Structure*. 7 (1998) 273–285.
- 40 Zhang QM & Zhao J (1999) "Electromechanical properties of lead zirconate titanate piezoceramics under the influence of mechanical stresses". *IEEE Transactions on Ultrasonics, Ferroelectrics and Frequency Control* 46 (6): 1518-1526.
- 41 Schwartz R W, Cross L E & Wang Q M, (2001) "Estimation of the effective d31 coefficients of the piezoelectric layer in rainbow actuators". *Journal of American Ceramic Society* 84 (11): 2563- 2569.
- 42 Li G, Furman E & Haertling GH (1997) "Stress-enhanced displacements in PLZT Rainbow actuators". *Journal of American Ceramic Society* 80 (6): 1382-1388.
- 43 Schwartz RW & Moon Y-W (2001) "Domain configuration and switching contributions to the enhanced performance of Rainbow actuators". *Proc. International Society for Optical Engineering, SPIE, USA, 4333: 408-417.*
- 44 Li X, Shih WY, Vartuli JS, Milius DL, Aksay IA & Shih W-H (2002) Effect of a transverse tensile stress on the electric-field-induced domain reorientation in soft PZT: in situ XRD study. *Journal of American Ceramic Society* 85 (4): 844-850.
- 45 Koch M, Harris N, Evans AGR, White NM & Brunnschweiler A (1998) A novel micromachined pump based on thick-film piezoelectric actuation. *Sensors and Actuators A* 70: 98-103.
- 46 Shepard JF Jr, Trolier-McKinstry S, Hendrickson MA & Zeto R (1996) Properties of PZT thin films as a function of in-plane biaxial stress. *Proc. International Symposium on Applications of Ferroelectrics, ISAF'96, IEEE, New York, NY, USA, 1: 161-165.*
- 47 Berlincourt D, Krueger HHA & Near C (2005), *Properties of Morgan ElectroCeramic ceramics*. Technical publication, Morgan Electro Ceramics Ltd,
- 48 <http://www.morganelectroceramics.com/pdfs/tp226.pdf>. Accessed in April 2006).

- 49 Sherrit S, Wiederick HD, Mukherjee BK & Haertling GH (1994) Dielectric, piezoelectric and hydrostatic properties of PLZT based RAINBOW ceramics. Proc. International Symposium on Applications of Ferroelectrics, ISAF'94, IEEE, New York, NY, USA, (390-393).
- 50 Furman E, Li G & Haertling GH (1994) Electromechanical properties of Rainbow devices, Proc. International Symposium on Applications of Ferroelectrics, ISAF'94, IEEE, New York, NY, USA, 146-149.
- 51 Li X, Shih WY & Aksay IA (1999) Electromechanical behaviour of PZT-brass unimorphs. Journal of American Ceramic Society 82 (7): 1733-1740.
- 52 Mossi KM, Selby GV & Bryant RG (1998) Thin-layer composite unimorph ferroelectric driver and sensor properties. Materials Letter 35 (1-2): 39-49.
- 53 Wise SA (1998) Displacement properties of RAINBOW and THUNDER piezoelectric actuators, Sensors and Actuators A 69: 33-38.
- 54 Shih WY, Shih W-H & Aksay IA (1997) Scaling analysis for the axial displacement and pressure of flextensional transducers. Journal of American Ceramic Society 80 (5): 1073-1078.
- 55 Stampleman, D.S. and A.H. von "Flotow microgravity isolation mounts based on piezoelectric films" in active and vibration control (ASME WAM, 1990) Vol. 8 pp. 57-67.
- 56 Bohannon, G.W, Schmidt V.H, Conant R.J, "Piezoelectric Polymer Actuators in a vibration isolation application" in Proc. SPIE no. 3987 pp 331-342(2000).
- 57 A.J. Moskalik and Diann Brei, Quasi- static behavior of individual C- block piezoelectric actuator, Journal of intelligent material Systems and structures Vol. 3 pg 577 – 587, (1997)
- 58 A.J. Moskalik and Diann Brei Force-deflection behavior of PE C- block actuator arrays, Smart structure and Materials Vol. 8, 1999, 531-543.
- 59 Aditi Chattopadhyay, Charles E Seeley and Lori Mitchell, "Design of smart flap using C- Block actuator hybrid optimization technique", Smart materials and

- structures vol. 6 (1997), 134- 144.
- 60 J. MOSKALIK and D. BREI, Analytical dynamic performance modeling for individual C-block, Journal of Vibration and Acoustics, 1999, 121, 221}230. actuators
- 61 J. MOSKALIK and D. BREI, Dynamic performance of C-block array architectures, Journal of sound and vibration (2001) 243 (2) pg 317-346
- 62 Budynas, Richard G., c1999, Boston, WCB/McGraw-Hill, "Advanced Strength and Applied stress Analysis", 2nd edition.
- 63 Isaac M Daniel and ORI ISHAI, Engineering mechanics of Composite Materials, 2006, New York : Oxford University Press.
- 64 http://www.piceramic.de/site/picomp_002.html
- 65 <http://www.morganelectroceramics.com/piezomaterials/pzmat9.html>
- 66 <http://www.staveleyndt.com/>.
- 67 *ConventorWare*, <http://www.coventor.com/coventorware/>, 2005.
- 68 Xiaoping Li, Wan Y. Shih, Ilhan A. Aksay and Wei-Heng Shih, Electromechanical behavior of PZT-Brass Unimorphs; Journal of American Ceramic Society 82(7) 1733 –40 (1999).
- 69 K.Y. Kim, K.H Park, H.C Park, N. S. Goo and K. J. Yoon, Performance evaluation of light weight piezo-composite actuators, Sensors and actuators A xxx (2005) xxx-xxx (www.sciencedirect.com)
- 70 MSC. Marc Mentat 2005r2 User guide Documentation.
- 71 MSC. Marc Mentat 2005r2 Volume A: Theory and User Information
- 72 <http://www.omega.com/pptst/GP901.html>.
- 73 <http://www.omega.com/Pressure/pdf/LCKD.pdf>

- 74 <http://cooperinst.thomasnet.com>
- 75 El Mostafa Sekouri, Yan-Ru Hu, Anh Dung Ngo, Modeling of a circular plate with piezoelectric actuators, *Mechatronics* 14 (2004) 1007–1020
- 76 You-Di Kuang, Guo-Qing Li¹ and Chuan-Yao Chen, Dynamic analysis of actuator-driven circular arch or ring using impedance elements, *Smart Mater. Struct.* 15 (2006) 869–876
- 77 Han J. M, Adriaens T. A, Willem L. de Koning and Reinder Banning, Modeling Piezoelectric Actuators *IEEE/ASME Transactions on Mechatronics*, VOL. 5, NO. 4, DECEMBER 2000 331.
- 78 Young-Hun Lim, Vasundara V Varadan and Vijay K Varadan, Closed loop finite element modeling of active structural damping in the frequency domain, *Smart Mater. Struct.* 6 (1997) 161–168.
- 79 S.X. Xu, T.S. Koko, Finite element analysis and design of actively controlled piezoelectric smart structures, *Finite Elements in Analysis and Design* 40 (2004) 241–262
- 80 K.M. Liew, X.Q. He, M.J. Tan, H.K. Lim, Dynamic analysis of laminated composite plates with piezoelectric sensor/actuator patches using the FSDT mesh-free method, *International journal of mechanical sciences* (2004), vol. 46, no.3, pp. 411-431.
- 81 Fumio Kikuchi, On the validity of the finite element analysis of circular arches represented by an assemblage of beam elements, *Journal of computer methods in applied mechanics and engineering* 5 (1975) 253-276.
- 82 Cooks D. R, Malkus D.S and Plesha M. E. ,1989, New York, John Wiley & Sons, "Concepts and applications of finite element analysis" pp 345
- 83 Wetherhold, Robert C, Singh, Aldraihem, Osama J. Tarunraj, Distributed control of laminated beams: Timoshenko theory vs. Euler-Bernoulli theory, *Journal of Intelligent Material Systems and Structures*, v 8, n 2, Feb, 1997, p 149-157

- 84 Lien-Wen Chen, Chung-Yi Lin, Ching-Cheng Wang, Dynamic stability analysis and control of a composite beam with piezoelectric layers, *Composite Structures* 56 (2002) 97–109.
- 85 Ellad B. Tadmor and Gábor Kósa, Electromechanical Coupling Correction for Piezoelectric Layered Beams, *Journal of Microelectromechanical Systems*, Vol.12, No. 6, December 2003, 899-906
- 86 Brij N Agrawal and Kirk E Treanor, Shape control of a beam using piezoelectric actuators, *Smart Materials. Structures.* 8 (1999) 729–740.
- 87 Christian N Della and Dongwei Shu, Vibration of beams with embedded piezoelectric sensors and actuators, *Smart Mater. Struct.* 15 (2006) 529–537
- 88 M. Arafa, A. Baz, Dynamics of active piezoelectric damping composites, *Composites: Part B* 31 (2000) 255–264
- 89 Paolo Gaudenzi, Rolando Carbonaro, Edoardo Benzi, Control of beam vibrations by means of piezoelectric devices: theory and experiments *Composite Structures* 50 (2000) 373-379
- 90 Chen Chang-qing, Wang Xiao-ming and Shen Ya-peng, "Finite Element Approach Of Vibration Control Using Self-Sensing Piezoelectric Actuators", *Journal of Computers & Structures* Vol. 60, No. 3, pp. 505-512, 1996
- 91 S. Narayanan , V. Balamurugan , Finite element modelling of piezolaminated smart structures for active vibration control with distributed sensors and actuators, *Journal of Sound and Vibration* 262 (2003) 529–562.
- 92 Rao, S. S, "Mechanical Vibrations", 2004, N. J., Upper Saddle River, Pearson Education
- 93 Daniel J. Inman, *Engineering vibration*, Englewood Cliffs, 1996 N.J, Prentice Hall

APPENDICES

APPENDIX A: MATERIAL SPECIFICATIONS

Table 1: Material Properties and Dimensions

Property and unit	PZT26	Aluminium	Brass	Mild Steel	Epoxy
External radius [mm]	10	8.82	8.82	8.82	9.0
Thickness [mm]	1	0.25, 0.31, 0.5,1.0,2.0	0.25, 0.31, 0.5,1.0, 2.0	0.25, 0.31, 0.5,1.0, 2.0	0.18
Length [mm]	10	10	10	10	10
Piezoelectric strain coefficient d_{31} [m/v]	-1.3e-12	0	0	0	0
Elastic modulus $\frac{N}{m^2}$	76e09	7.0e10	1.10e11	1.90e11	5.2e09
Density Kg/m^3	7.8e03	2.7e03	8.56e03	7.85e03	1.90e03
Maximum Voltage[VAC /mm]	200	-	-	-	-

Table 2: Electromechanical Properties of the PZ6

Properties	Value	Unit
S_{11}^E	$1.30e^{-11}$	$\frac{m^2}{N}$
S_{12}^E	$-4.35e^{-12}$	
$S_{13}^E = S_{23}^E$	$-7.05e^{-12}$	
$S_{44}^E = S_{55}^E$	$3.32e^{-11}$	
S_{66}^E	$3.47e^{-11}$	
d_{31}	$-1.28e^{-10}$	$\frac{C}{N}$
d_{33}	$3.28e^{-10}$	
d_{15}	$3.27e^{-10}$	
$\xi_{11}^{\sigma, r}$	1190	
$\xi_{22}^{\sigma, r}$	1190	
$\xi_{33}^{\sigma, r}$	1330	
Relative value to vacuum permittivity		
$\xi_o = 8.85 \times 10^{-12} \frac{F}{m}$		

APPENDIX B: MATLAB CODES

Appendix B1: Matlab program to find the Dynamic Response of the C-Shape Actuator

```
%=====
% This program is used to find the response of the C-actuator
% under applied sinusoidal voltage using Modal analysis method
% Main Program: C_actuator
% Calls functions: submpea, stiff, mass. They must be saved in the same folder as the %
main program.
%
%Prepared by A.N. Mtawa: - Cape Peninsula University of Technology (South Africa).
%=====

clear all
global Q Rna R c1 c2 le q r mo b d31 V nelem rho
fprintf('\n\n');
fprintf('This program is used to find the response of the 3 layered C-shape piezocomposite
actuator \n');
fprintf(' under bipolar excitation using Modal analysis method \n');
fprintf(' Main Program: C-actuator \n' );
fprintf('Calls functions: submpea,stiff, mass \n');
fprintf('\n\n');
fprintf('\n enter the number of elements "nelem" ');
n=input('?');
nelem=n;
fprintf('\n enter the radii of the actuator layers "r" ');
r1=input('?');
r2=input('?');
r3=input('?');
r4=input('?');
r1=r1;
r2=r2;
r3=r3;
r4=r4;
R=[r1,r2,r3,r4]
fprintf('\n enter the elastic modulus of the actuator materials "Q" ');
Q1=input('?');
Q2=input('?');
Q3=input('?');
Q=[Q1,Q2,Q3]
```

```

fprintf('\n enter the densities of the actuator materials "rho" ');
rho1=input('?');
rho2=input('?');
rho3=input('?');
rho=[rho1,rho2,rho3]
fprintf('\n enter the piezoelectric coupling coefficients "d" ');
d1=input('?');
d2=input('?');
d3=input('?');
d31=[d1,d2,d3]
fprintf('\n enter the widths of the actuator layers "b" ')
b1=input('?');
b2=input('?');
b3=input('?');
b=[b1,b2,b3];
fprintf ('\n enter the voltage to be applied "V" ')
Voltage=input('?');
V=Voltage;
% Calling function: submpea.
submpea(r1,r2,r3,r4);
% Calling function: stiff
%Generating elemental stiffness matrices
k1= stiff(c1,c2,le,q,r);
k2= stiff(c1,c2,le,r,q);
k3= stiff(c1,c2,le,r,-q);
k4= stiff(c1,c2,le,q,-r);
% Calling function: mass
%Generating elemental mass matrices
m1= mass(mo,le,q,r);
m2= mass(mo,le,r,q);
m3= mass(mo,le,r,-q);
m4= mass(mo,le,q,-r);
%
% Assembling stiffness matrices for all elements (The whole structure/actuator)
ndof=3*(nelem+1); % ndof- number of degrees of freedom
k=zeros(ndof);
for i=1:6
    for j=1:6
        k(i,j)=k1(i,j);

```

```

    end
end
for i=1:6
    for j=1:6
        k(i+3,j+3)=k(i+3,j+3)+k2(i,j);
    end
end
for i=1:6
    for j=1:6
        k(i+6,j+6)=k(i+6,j+6)+k3(i,j);
    end
end
for i=1:6
    for j=1:6
        k(i+9,j+9)=k(i+9,j+9)+k4(i,j);
    end
end
%
% Assembling mass matrices for all elements (whole Structure/actuator)
%
m=zeros(ndof);
for i=1:6
    for j=1:6
        m(i,j)=m1(i,j);
    end
end
for i=1:6
    for j=1:6
        m(i+3,j+3)=m(i+3,j+3)+m2(i,j);
    end
end
for i=1:6
    for j=1:6
        m(i+6,j+6)=m(i+6,j+6)+m3(i,j);
    end
end
for i=1:6
    for j=1:6

```

```

    m(i+9,j+9)=m(i+9,j+9)+m4(i,j);
end
end
% Remove zero degrees of freedom for zero deflection
% and zero slope at the left end
%
m=m(4:ndof,4:ndof);
k=k(4:ndof,4:ndof);
m1=(m^-0.5);
m2=(m^0.5);
k1=m1*k*m1;
% Calculating the eigenfrequencies and corresponding eigenmodes
[X,w]=eig(k1);
[w,id]=sort(diag(w));
w=sqrt(w); %eigenfrequencies
X=X(:,id); %eigenvectors: normalized in respect mass
w=(diag(w))/6.28;
S=m1*X; % Transformation matrix
S1=X*m2;
% Initial conditions in physical coordinates
x0=ones(12,1)*10e-07; % initial displacement
x0_dot=zeros(12,1); %initial velocity
%Initial conditions in modal coordinates
r0=S1*x0;
r0_dot=S1*x0_dot;
% Computing the moment arm vector
a=(r3+r4)/2-Rna; %Moment arm
f=[-1, 0,a,1,0,-a];
%
% Computing load Vector (Moment & Force)
for i=1:3
Pe(i)=Q(i)*b(i)*d31(i)*V;
end
Pe=sum(Pe);
Pe=Pe*f;
%
% Nodal load vector at the actuator end tip
%
```

```

Fa=[zeros(9,1);Pe(4:6,:)];
%
% Computing piezoelectric harmonic force in physical coordinates
nstep=100;
t=2
fprintf('Enter the maximum driving frequency "wdr" ')
drfrq=input('?');
w0=drfrq
for i=1:nstep
wdr(i)=w0*(i-1)/nstep;      % A range of driving frequencies
F(1,i)=Fa(1)*sin(wdr(i)*t);
F(2,i)=Fa(2)*sin(wdr(i)*t);
F(3,i)=Fa(3)*sin(wdr(i)*t);
F(4,i)=Fa(4)*sin(wdr(i)*t);
F(5,i)=Fa(5)*sin(wdr(i)*t);
F(6,i)=Fa(6)*sin(wdr(i)*t);
F(7,i)=Fa(7)*sin(wdr(i)*t);
F(8,i)=Fa(8)*sin(wdr(i)*t);
F(9,i)=Fa(9)*sin(wdr(i)*t);
F(10,i)=Fa(10)*sin(wdr(i)*t);
F(11,i)=Fa(11)*sin(wdr(i)*t);
F(12,i)=Fa(12)*sin(wdr(i)*t);
end
% Transforming the piezoelectric harmonic force into modal coordinates
F1=X'*m1*F;
F10=F1(1,:);
F20=F1(2,:);
F30=F1(3,:);
F40=F1(4,:);
F50=F1(5,:);
F60=F1(6,:);
F70=F1(7,:);
F80=F1(8,:);
F90=F1(9,:);
F100=F1(10,:);
F110=F1(11,:);
F120=F1(12,:);
xi=0.0707;                % Damping coefficient

```

```

%Total solution in modal coordinates
%Displacement in modal coordinate system based on equation 7.32
for j=1:nstep
rp1(j)=sqrt(w(1,1)^2*r0(1)^2)/w(1,1)*sin(w(1,1)*t+pi/2)+F10(j)/...
    (sqrt((w(1,1)^2-wdr(j)^2)^2+(2*xi*w(1,1)*wdr(j))^2))*...
    cos(wdr(j)*t-atan((2*xi*w(1,1)*wdr(j))/(w(1,1)^2-wdr(j)^2)));
rp2(j)=sqrt(w(2,2)^2*r0(2)^2)/w(2,2)*sin(w(2,2)*t+pi/2)+F20(j)/...
    (sqrt((w(2,2)^2-wdr(j)^2)^2+(2*xi*w(2,2)*wdr(j))^2))*...
    cos(wdr(j)*t-atan((2*xi*w(2,2)*wdr(j))/(w(2,2)^2-wdr(j)^2)));
rp3(j)=sqrt(w(3,3)^2*r0(3)^2)/w(3,3)*sin(w(3,3)*t+pi/2)+F30(j)/...
    (sqrt((w(3,3)^2-wdr(j)^2)^2+(2*xi*w(3,3)*wdr(j))^2))*...
    cos(wdr(j)*t-atan((2*xi*w(3,3)*wdr(j))/(w(3,3)^2-wdr(j)^2)));
rp4(j)=sqrt(w(4,4)^2*r0(4)^2)/w(4,4)*sin(w(4,4)*t+pi/2)+F40(j)/...
    (sqrt((w(4,4)^2-wdr(j)^2)^2+(2*xi*w(4,4)*wdr(j))^2))*...
    cos(wdr(j)*t-atan((2*xi*w(4,4)*wdr(j))/(w(4,4)^2-wdr(j)^2)));
rp5(j)=sqrt(w(5,5)^2*r0(5)^2)/w(5,5)*sin(w(5,5)*t+pi/2)+F50(j)/...
    (sqrt((w(5,5)^2-wdr(j)^2)^2+(2*xi*w(5,5)*wdr(j))^2))*...
    cos(wdr(j)*t-atan((2*xi*w(5,5)*wdr(j))/(w(5,5)^2-wdr(j)^2)));
rp6(j)=sqrt(w(6,6)^2*r0(6)^2)/w(6,6)*sin(w(6,6)*t+pi/2)+F60(j)/...
    (sqrt((w(6,6)^2-wdr(j)^2)^2+(2*xi*w(6,6)*wdr(j))^2))*...
    cos(wdr(j)*t-atan((2*xi*w(6,6)*wdr(j))/(w(6,6)^2-wdr(j)^2)));
rp7(j)=sqrt(w(7,7)^2*r0(7)^2)/w(7,7)*sin(w(7,7)*t+pi/2)+F70(j)/...
    (sqrt((w(7,7)^2-wdr(j)^2)^2+(2*xi*w(7,7)*wdr(j))^2))*...
    cos(wdr(j)*t-atan((2*xi*w(1,1)*wdr(j))/(w(7,7)^2-wdr(j)^2)));
rp8(j)=sqrt(w(8,8)^2*r0(8)^2)/w(8,8)*sin(w(8,8)*t+pi/2)+F80(j)/...
    (sqrt((w(8,8)^2-wdr(j)^2)^2+(2*xi*w(8,8)*wdr(j))^2))*...
    cos(wdr(j)*t-atan((2*xi*w(1,1)*wdr(j))/(w(8,8)^2-wdr(j)^2)));
rp9(j)=sqrt(w(9,9)^2*r0(9)^2)/w(9,9)*sin(w(9,9)*t+pi/2)+F90(j)/...
    (sqrt((w(9,9)^2-wdr(j)^2)^2+(2*xi*w(9,9)*wdr(j))^2))*...
    cos(wdr(j)*t-atan((2*xi*w(1,1)*wdr(j))/(w(9,9)^2-wdr(j)^2)));
rp10(j)=sqrt(w(10,10)^2*r0(10)^2)/w(10,10)*sin(w(10,10)*t+pi/2)+F100(j)/...
    (sqrt((w(10,10)^2-wdr(j)^2)^2+(2*xi*w(10,10)*wdr(j))^2))*...
    cos(wdr(j)*t-atan((2*xi*w(10,10)*wdr(j))/(w(10,10)^2-wdr(j)^2)));
rp11(j)=sqrt(w(11,11)^2*r0(11)^2)/w(11,11)*sin(w(11,11)*t+pi/2)+F110(j)/...
    (sqrt((w(11,11)^2-wdr(j)^2)^2+(2*xi*w(11,11)*wdr(j))^2))*...
    cos(wdr(j)*t-atan((2*xi*w(11,11)*wdr(j))/(w(11,11)^2-wdr(j)^2)));
rp12(j)=sqrt(w(12,12)^2*r0(12)^2)/w(12,12)*sin(w(12,12)*t+pi/2)+F120(j)/...
    (sqrt((w(12,12)^2-wdr(j)^2)^2+(2*xi*w(12,12)*wdr(j))^2))*...

```

```

        cos(wdr(j)*t-atan((2*xi*w(12,12)*wdr(j))/(w(12,12)^2-wdr(j)^2)));
end
% Displacement vector
r=[rp1(1,:);rp2(1,:);rp3(1,:);rp4(1,:);rp5(1,:);rp6(1,:);rp7(1,:);...
    rp8(1,:);rp9(1,:);rp10(1,:);rp11(1,:);rp12(1,:)];
%
% Transformation of the total solution (displacement) into physical coordinates
x=m1*X*r;
x11=x(11,:);
% Interpretation of the results graphically (lateral displacement of the free end tip)
plot(wdr,x11)
ylabel('Displacement [m]')
xlabel('Frequency [Hz]')
title('Frequency -Amplitude response for 0.31 Aluminium substrate')
grid on

```

Appendix B2: Matlab Sub-Function Program to Calculate actuator performance parameters

```

%=====
% Function: submpea
% This program calculates the radius of neutral axis, blocked force,
% free displacement, composite bending stiffness;
% piezoelectric moment, stiffness and mass constants; sine and cosine of angles of
% orientation of the beam elements
%
% Prepared by A.N. Mtawa: - Cape Peninsula University of Technology (South Africa).
%=====
%
function [Rna,Disp,Pb,D,Mpe,Za,le,c1,c2,mo,q,r]=submpea(r1,r2,r3,r4)
global R Q Rna c1 c2 le q r mo b d31 V nelem rho
%
% Computing internal and external radii of layers
for i=1:3
Ra(i)=R(i+1)-R(i);
Rb(i)=R(i+1)^2-R(i)^2;
end
%
% Computing the radius of neutral axis – “Rna” (equation 3.10)
for i=1:3
A(i) =0.5*Q(i)*b(i)*Rb(i);
B(i)=Q(i)*b(i)*Ra(i);
end
Rna=sum(A)/sum(B)
%
% Computing the piezoelectric moment- “Mpe” (equation 3.9) and
% Composite bending stiffness (D)- equation 3.6),
%
for i=1:4
Z(i)=R(i)-Rna ;
end
for i=1:3
Za(1,i)=Z(i+1)^3-Z(i)^3;
Zb(1,i)=.5*(Z(i+1)+Z(i));
end

```

```

%
for i=1:3
    Mpe(i)= Q(i) *b(i)*d31(i)*V*Zb(i);
    D(i)=1/3 *Q(i) *b(i)*Za(i);
end
Mpe =sum(Mpe);
D=sum(D);
% Actuator blocked force (Pb) – equation 3.11
Pb=4*Mpe/(pi*Rna);
% Free displacement (Disp) – equation 3.12
Disp=(2*Mpe*Rna^2)/D ;
%
%Computing the stiffness constants c1,c2: (equations C.1 and C.2 respectively) in
% appendix C
%
%
th = [r2-r1,r3-r2,r4-r3];      % Thickness of layers
le=(pi*Rna)/nelem;          % Element length (equation C.3) in appendix C
for i=1:3
    c1(1,i)=(Q(i)*th(i)*b(i))/le;
    c2(1,i)=Q(i)*b(i)*Za(1,i)*(1/(3*le^3));
end
c1=sum(c1);
c2=sum(c2);
%
%Computing the sine and cosine of angles ('q','r')with
% which the beam makes with X-axis in a global coordinate system
%
theta=(0:pi/nelem:pi); % angle subtending elements
for i=1:nelem+1
    x(1,i) = Rna*(-1)*cos(theta(i));
y(1,i) = Rna*sin(theta(i));
end
for i=1:nelem;
q(1,i)=cos(atan((y(1,i+1)-y(1,i))/(x(1,i+1)-x(1,i))));
r(1,i)=sin(atan((y(1,i+1)-y(1,i))/(x(1,i+1)-x(1,i))));
end
q=q(1);

```

```

r=r(1);
% Computing the unit mass constant 'mo' (equation C. 4)- appendix C
%
for i=1:3
    mo(1,i)=rho(i)*th(i)*b(i)*le/420;
end
mo=sum(mo);

```

Appendix B3: Matlab Sub-Function Program to Compute Stiffness Matrices of a Straight Arc Element

```

%=====
% Function: stiff
% computes the local and global stiffness matrices
% Prepared by A.N. Mtawa: - Cape Peninsula University of Technology (South Africa).
%=====
function k= stiff(c1,c2,le,q,r)
%computing Stiffness matrix of an element (straight arc)
k=[c1, 0, 0, -c1, 0, 0;
    0, 12*c2, 6*le*c2, 0, -12*c2, 6*le*c2;
    0, 6*le*c2, 4*le^2*c2,0,-6*le*c2, 2*le^2*c2;
    -c1, 0, 0, c1,0, 0;
    0, -12*c2, -6*le*c2, 0, 12*c2, -6*le*c2;
    0, 6*le*c2, 2*le^2*c2,0, -6*le*c2, 4*le^2*c2];
%
%Computing global matrix
%Transformation matrix "Tr"
Tr =[q,r,0,0,0,0;
    -r,q,0,0,0,0;
    0,0,1,0,0,0;
    0,0,0,q,r,0;
    0,0,0,-r,q,0;
    0,0,0,0,0,1];
k = Tr*k*Tr;

```

Appendix B4: Matlab Sub-Function Program to Compute Mass Matrices of a Straight Arc Element

```

%=====
% Function: mass
% Computes the local and global mass matrices
% Prepared by A.N. Mtawa: - Cape Peninsula University of Technology (South Africa).
%=====
%
function m = mass(mo,le,q,r)
%Computing stiffness matrix of an element
m = mo*[140,0,0,70,0,0;
        0,156,22*le,0,54,-13*le;
        0,22*le,4*le^2,0,13*le,-3*le^2;
        70,0,0,140,0,0;
        0,54,13*le,0,156,-22*le;
        0,-13*le,-3*le^2,0,-22*le,4*le^2];
%Computing global matrix
% Transformation matrix "Tr"
Tr =[q,r,0,0,0,0;
     -r,q,0,0,0,0;
     0,0,1,0,0,0;
     0,0,0,q,r,0;
     0,0,0,-r,q,0;
     0,0,0,0,0,1];
m = Tr'*m*Tr;

```

APPENDIX: C: Stiffness and Mass Matrices

Appendix C1: Global stiffness matrix of an element with the boundary conditions taken into account

Element 1-2, $\beta_1 = 67.5^\circ$ $q=0.383$ $r= 0.924$ $L_e = 7.25e-3m$

u_2	w_2	θ_2	
$q^2 C_1 + 12C_2 r^2$	$qC_1 r - 12qC_2 r$	$6C_2 Lr$	u_2
$qC_1 r - 12qC_2 r$	$12q^2 C_2 + C_1 r^2$	$-6qC_2 L$	w_2
$6C_2 Lr$	$-6qC_2 L$	$4C_2 L^2$	θ_2

Element 2-3, $\beta_2 = 22.5^\circ$ $q=0.924$, $r= 0.383$ $L_e = 7.25e-3m$

u_2	w_2	θ_2	u_3	w_3	θ_3	
$q^2 C_1 + 12C_2 r^2$	$qC_1 r - 12qC_2 r^2$	$-6C_2 Lr$	$-q^2 C_1 - 12C_2 r^2$	$-qC_1 r + 12qC_2 r$	$-6C_2 Lr$	u_2
$qC_1 r - 12qC_2 r^2$	$12q^2 C_2 + C_1 r^2$	$6qC_2 L$	$-qC_1 r + 12qC_2 r$	$-12q^2 C_2 - C_1 r^2$	$6qC_2 L$	w_2
$-6C_2 Lr$	$6qC_2 L$	$4C_2 L^2$	$6C_2 Lr$	$-6qC_2 L$	$2C_2 L^2$	θ_2
$-q^2 C_1 - 12C_2 r^2$	$-qC_1 r + 12qC_2 r$	$6C_2 Lr$	$q^2 C_1 + 12C_2 r^2$	$qC_1 r - 12qC_2 r$	$6C_2 Lr$	u_3
$-qC_1 r + 12qC_2 r$	$-12q^2 C_2 - C_1 r^2$	$-6qC_2 L$	$qC_1 r - 12qC_2 r$	$12q^2 C_2 + C_1 r^2$	$-6qC_2 L$	w_3
$-6C_2 Lr$	$6qC_2 L$	$2C_2 L^2$	$6C_2 Lr$	$-6qC_2 L$	$4C_2 L^2$	θ_3

Element 3-4, $\beta_3 = -22.5^\circ$ $q=0.924$, $r = -0.383$ $L\theta = 7.25e-3m$

u_3	w_3	θ_3	u_4	w_4	θ_4	
$q^2 C_1 + 12C_2 r^2$	$qC_1 r - 12qC_2 r^2$	$-6C_2 Lr$	$-q^2 C_1 - 12C_2 r^2$	$-qC_1 r + 12qC_2 r$	$-6C_2 Lr$	u_3
$qC_1 r - 12qC_2 r^2$	$12q^2 C_2 + C_1 r^2$	$6qC_2 L$	$-qC_1 r + 12qC_2 r$	$-12q^2 C_2 - C_1 r^2$	$6qC_2 L$	w_3
$-6C_2 Lr$	$6qC_2 L$	$4C_2 L^2$	$6C_2 Lr$	$-6qC_2 L$	$2C_2 L^2$	θ_3
$-q^2 C_1 - 12C_2 r^2$	$-qC_1 r + 12qC_2 r$	$6C_2 Lr$	$q^2 C_1 + 12C_2 r^2$	$qC_1 r - 12qC_2 r$	$6C_2 Lr$	u_4
$-qC_1 r + 12qC_2 r$	$-12q^2 C_2 - C_1 r^2$	$-6qC_2 L$	$qC_1 r - 12qC_2 r$	$12q^2 C_2 + C_1 r^2$	$-6qC_2 L$	w_4
$-6C_2 Lr$	$6qC_2 L$	$2C_2 L^2$	$6C_2 Lr$	$-6qC_2 L$	$4C_2 L^2$	θ_4

Element 4-5, $\beta_4 = -67.5^\circ$ $q=0.383$, $r = -0.924$ $L_e = 7.25e-3m$

u_4	w_4	θ_4	u_5	w_5	θ_5	
$q^2 C_1 + 12C_2 r^2$	$qC_1 r - 12qC_2 r$	$-6C_2 Lr$	$-q^2 C_1 - 12C_2 r^2$	$-qC_1 r + 12qC_2 r$	$-6C_2 Lr$	u_4
$qC_1 r - 12qC_2 r^2$	$12q^2 C_2 + C_1 r^2$	$6qC_2 L$	$-qC_1 r + 12qC_2 r$	$-12q^2 C_2 - C_1 r^2$	$6qC_2 L$	w_4
$-6C_2 Lr$	$6qC_2 L$	$4C_2 L^2$	$6C_2 Lr$	$-6qC_2 L$	$2C_2 L^2$	θ_4
$-q^2 C_1 - 12C_2 r^2$	$-qC_1 r + 12qC_2 r$	$6C_2 Lr$	$q^2 C_1 + 12C_2 r^2$	$qC_1 r - 12qC_2 r$	$6C_2 Lr$	u_5
$-qC_1 r + 12qC_2 r$	$-12q^2 C_2 - C_1 r^2$	$-6qC_2 L$	$qC_1 r - 12qC_2 r$	$12q^2 C_2 + C_1 r^2$	$-6qC_2 L$	w_5
$-6C_2 Lr$	$6qC_2 L$	$2C_2 L^2$	$6C_2 Lr$	$-6qC_2 L$	$4C_2 L^2$	θ_5

Where:

$$C_1 = \sum_{p=1}^n \frac{A_p Q_p}{L_e} = \sum_{p=1}^n \frac{(Q_p t_p b)}{L_e} \quad (C.1)$$

$$C_2 = \sum_{p=1}^n \frac{Q_p I_p}{L_e^3} = \frac{1}{3L_e^3} \sum_{p=1}^n Q_p b (Z_p^3 - Z_{p-1}^3) \quad (C.2)$$

Z_p and Z_{p-1} are the distances from the neutral axis to the outer and inner surfaces of the p^{th} layer respectively.

L_e is length of the beam taken to be equal to the arch length, that is

$$L_e = \frac{\pi R_{nat}}{4} \quad (C.3)$$

$q_i = \cos(\beta_i)$, $r_i = \sin(\beta_i)$, β_i = is an angle the beam element makes with the X-global axis.

Appendix C2: Global consistent mass matrix of an element with the boundary conditions taken into account

Element 1-2, $\beta_1 = 67.5^\circ$ $q=0.383$ $r=0.924$ $Le = 7.25e-3m$

	u_2	w_2	θ_2	
×	$840q^2 + 156r^2$	$684qr$	$22Lr$	u_2
	$684qr$	$156q^2 + 840r^2$	$-22Lq$	w_2
	$22Lr$	$-22Lq$	$4L^2$	θ_2

Element 2-3, $\beta_2 = 22.5^\circ$ $q=0.924$, $r= 0.383$ $L_e = 7.25e-3m$

	u_2	w_2	θ_2	u_3	w_3	θ_3	
	$840q^2 + 156r^2$	$-684qr$	$22Lr$	$420q^2 - 54r^2$	$474qr$	$-13Lr$	u_2
	$-684qr$	$156q^2 + 840r^2$	$22Lq$	$-474qr$	$54q^2 - 420r^2$	$-13Lq$	w_2
\times	$22Lr$	$22Lq$	$4L^2$	$-13Lr$	$13Lq$	$-3L^2$	θ_2
	$420q^2 - 54r^2$	$-474qr$	$-13Lr$	$840q^2 + 156r^2$	$684qr$	$22Lr$	u_3
	$474qr$	$54q^2 - 420r^2$	$13Lq$	$684qr$	$156q^2 + 840r^2$	$-22Lq$	w_3
	$-13Lr$	$-13Lq$	$-3L^2$	$22Lr$	$-22Lq$	$4L^2$	θ_3

Element 3-4, $\beta_3 = -22.5^\circ$ $q=0.924$, $r = -0.383$ $Le = 7.25e-3m$

	u_3	w_3	θ_3	u_4	w_4	θ_4	
×	$840q^2 + 156r^2$	$-684qr$	$22Lr$	$420q^2 - 54r^2$	$474qr$	$-13Lr$	u_3
	$-684qr$	$156q^2 + 840r^2$	$22Lq$	$-474qr$	$54q^2 - 420r^2$	$-13Lq$	w_3
	$22Lr$	$22Lq$	$4L^2$	$-13Lr$	$13Lq$	$-3L^2$	θ_3
	$420q^2 - 54r^2$	$-474qr$	$-13Lr$	$840q^2 + 156r^2$	$684qr$	$22Lr$	u_4
	$474qr$	$54q^2 - 420r^2$	$13Lq$	$684qr$	$156q^2 + 840r^2$	$-22Lq$	w_4
	$-13Lr$	$-13Lq$	$-3L^2$	$22Lr$	$-22Lq$	$4L^2$	θ_4

Element 4-5, $\beta_4 = -67.5^\circ$ $q=0.383$, $r = -0.924$ $Le = 7.25e-3m$

	u_4	w_4	θ_4	u_5	w_5	θ_5	
×	$840q^2 + 156r^2$	$-684qr$	$22Lr$	$420q^2 - 54r^2$	$474qr$	$-13Lr$	u_4
	$-684qr$	$156q^2 + 840r^2$	$22Lq$	$-474qr$	$54q^2 - 420r^2$	$-13Lq$	w_4
	$22Lr$	$22Lq$	$4L^2$	$-13Lr$	$13Lq$	$-3L^2$	θ_4
	$420q^2 - 54r^2$	$-474qr$	$-13Lr$	$840q^2 + 156r^2$	$684qr$	$22Lr$	u_5
	$474qr$	$54q^2 - 420r^2$	$13Lq$	$684qr$	$156q^2 + 840r^2$	$-22Lq$	w_5
	$-13Lr$	$-13Lq$	$-3L^2$	$22Lr$	$-22Lq$	$4L^2$	θ_5

$$= \sum_{p=1}^n \frac{\rho_p A_p L_c}{420} = \sum_{p=1}^n \frac{\rho_p b t_p L_c}{420} = \frac{L_c b}{420} \sum_{p=1}^n \rho_p t_p \quad (C.4)$$

APPENDIX D: The Three Lowest Eigenfrequencies for Selected Substrate Material and Substrate/PZT

Thickness Ratios

Material	Thickness ratio	ρ [kg/m]	Radius of Neutral axis Rna [m]	Bending Stiffness [Nm ²]	Natural Frequency [Hz]								
					Predicted			MSC Marc			$\left(\omega_i^2 = \frac{D\lambda_i^2}{\rho R_{na}^4} \right)$ From reference [61]		
					I	II	III	I	II	III	I	II	III
Aluminium	0.25	8.817e-02	9.345e-03	0.1582	1019	3194	10024	1053	3239	10110	1063	3359	9964
	0.31	8979e-02	9.31e-03	0.1843	1107	3464	10822	1255	3587	10900	1145	3619	10730
	0.5	9.492e-02	9.204e-03	0.2787	1437	4494	13064	1366	4414	13208	1402	4429	13140
Brass	0.25	1.028e-01	9.28e-03	0.197	1140	3573	12083	1098	3517	12116	1113	3517	12040
	0.31	1.08e-01	9.23e-03	0.2312	1218	3813	12884	1271	3877	12906	1180	3754	12860
	0.5	1.242e-01	9.108e-03	0.3512	1447	4524	15238	1339	4444	15212	1405	4438	15200
Mild steel	0.25	1.009e-01	9.183e-03	0.256	1340	4195	14176	1254	4105	14206	1307	4130	14150
	0.31	1.056e-01	9.134e-03	0.299	1465	4582	15195	1446	4557	15152	1400	4423	15150
	0.5	1.204e-01	8.98e-03	0.448	1698	5312	17903	1543	5182	17957	1657	5236	17930